ULTRAVIOLET ROLL-TO-ROLL NANOIMPRINT LITHOGRAPHIC FABRICATION OF FLEXIBLE POLYMER MOULDS

JARRETT JONATHAN DUMOND

NATIONAL UNIVERSITY OF SINGAPORE

2014

ULTRAVIOLET ROLL-TO-ROLL NANOIMPRINT LITHOGRAPHIC FABRICATION OF FLEXIBLE POLYMER MOULDS

JARRETT JONATHAN DUMOND

(M.Sc., B.Sc. STANFORD UNIVERSITY)

A THESIS SUBMITTED

FOR THE DEGREE OF DOCTOR OF PHILOSOPHY

DEPARTMENT OF MECHANICAL ENGINEERING

NATIONAL UNIVERSITY OF SINGAPORE

2014

DECLARATION

I hereby declare that the thesis is my original work and it has been written by me in its entirety. I have duly acknowledged all the sources of information which have been used in the thesis.

This thesis has also not been submitted for any degree in any university previously.

Jarrett J. Dumond — 18/8/2014

Jarrett J. Dumond Date

Acknowledgement

Over the ten years that I have lived and worked in a research career in Singapore, I have met and worked with so many notable people with whom I owe a sincere debt of gratitude that surely I will not be able to list everyone. However I will make mention of those most important.

I would like to thank my beautiful wife Feng Chen, for her love and support during the research and writing phase of this thesis. Without her support, finishing this work would have been impossible.

I would also like to thank my mother and father, Anne and William Dumond, whom I now see rarely – only once or twice a year. If there is anything I have regretted throughout my long stay in this great country, it is not being able to visit you more often. Our weekly phone calls have been a great source of comfort and strength and words cannot express how much I appreciate your loving kindness and care through the years.

To my other close family, my brother Josh, and his wife Annie, little Ali and Tate Dumond, Uncle Dale, Uncle Tam, Aunt Mary & Uncle Fred. I would especially like to dedicate this work to my late grandparents, Grandma Alice, Grandpa Bennett, Grandpa Alf, and Grandma Cathie, who passed away while this thesis was in preparation.

My sincerest thanks go to Dr. Low Hong Yee for her mentorship and support through the years at IMRE and beyond. I would say there are few others who know me better both personally and professionally and even fewer whom I hold in such high regard. I wish you all success at teaching and research at SUTD, and wherever life takes you.

I would also like to express my appreciation to Dr. Jerry Fuh and Dr. Lee Heow Pueh for their advice and mentoring through the coursework and research phases of my candidacy. I look forward to more collaborative work with both of you in the future.

There are certain IMRE staff members who also helped greatly with various experiments and demonstration activities – Ms. June Ong for her assistance with XPS characterization work, Dr. Saman Safari Dinachali for assistance with various resin formulations, Ms. Man Shu Mei, Ms. Chew Ah Bian, and Mr. Lee Chang Sheng for their operational help with our UV roll-to-roll nanoimprinting system.

Finally, and above all, to the Almighty, unsearchable God to whom all man's knowledge and understanding is as nothing.

Table of Contents

Declaration i

Acknowledgement ii

Table of Contents iii

Summary vi

List of Tables viii

List of Figures x

1 Introduction 1

1.1 An Introduction to UV Roll-to-Roll Nanoimprint Lithography 1

1.1.1 Industrial Applications 12

1.1.2 Theoretical Models for Throughput & Mould Cavity Filling 16

1.1.3 Current State of the Technology 21

1.2 Resin Mould Replication via UV Roll-to-Roll Nanoimprinting 24

1.3 Problem Description 30

1.4 Scope & Objectives 36

1.5 Organization of the Thesis 38

2 Literature Review 41

2.1 Industrial Applications for Resin Moulds 41

2.2 UV Roll-to-Roll Nanoimprinting Equipment for Resin Mould Production 44

2.3 Roller & Roll-Mountable Moulds for Resin Mould Manufacturing 50

2.3.1 Sheet Mould Replication Techniques 51

2.3.2 Seamless Roller Mould Fabrication Techniques 59

2.3.3 Soft Material Approaches to Seamless Roller Mould Fabrication.......65

2.4 Concluding Remarks.......67

3 Fabrication of UV Roll-to-Roll Nanoimprinted Resin Moulds.......70

3.1 Materials & Methodology.......74

3.2 High Resolution Resin Mould Fabrication Results.......80

3.3 Usage of Resin Moulds in Batch Mode Thermal NIL.......86

3.4 Comparison of Imprint Fidelity Across Multiple Replication Cycles.......89

3.5 Concluding Remarks.......95

4 Surface Delivery and Covalent Bonding of Release Agents to Resin Mould Surfaces.......98

4.1 A Brief Theoretical Treatment on Work of Adhesion and Demoulding Failure in Nanoimprint Lithography.......98

4.2 Comparison of Surface Modification Methods to Improve Release Performance.......102

4.3 The Unique Properties of PDMS and h-PDMS.......105

4.4 Delivery of Reactive Release Agents via a Soluble h-PDMS/PDMS Composite Roll-Mountable Polymer Mould.......110

4.5 Materials & Methodology.......111

4.5.1 Master Mould Preparation and Replication into h-PDMS/ PDMS bi-layer Silicone Roll-mounted Moulds.......113

4.5.2 Exposure and Absorption of Silicone-based Reactive Release Agent by h-PDMS/ PDMS bi-layer Silicone Roll-mounted Moulds.......116

4.5.3 Transfer of mPDMS from h-PDMS/PDMS bi-layer Silicone Roll-mounted Moulds to Fabricated Resin Moulds During UV Roll-to-Roll Nanoimprinting.......118

4.5.4 Test Bed Resin Formulation for UV Roll-to-Roll Nanoimprint Fabrication of Resin Moulds and Blank Resin Films 120

4.5.5 Characterization Methods for Fabricated Resin Moulds and Blank Resin Films with Transferred mPDMS 121

4.6 Characterization of Modulus for Modified h-PDMS Formulation....125

4.7 mPDMS-exposed h-PDMS/PDMS Bi-layer Roll-Mounted Mould Results....................127

4.8 Resin Mould Fabrication Results Utilizing mPDMS-Exposed h-PDMS/PDMS Composite Roll-Mounted Moulds 131

4.9 XPS Characterization of mPDMS Transfer to UV Roll-to-Roll Nanoimprinted Resin Films 138

4.10 Advancing Water Contact Angle Characterization of mPDMS Transfer to UV Roll-to-Roll Nanoimprinted Resin Films 146

4.11 Concluding Remarks....................150

5 Conclusions & Future Work....................152

5.1 Contributions & Important Findings....................152

5.2 Current Challenges & Opportunities for Further Study....................157

5.3 Outlook & Concluding Remarks 160

Bibliography 163

Appendix A Theoretical Modeling of Solubility for Monomethacryloxypropyl-terminated Polydimethylsiloxane in PDMS....................178

Appendix B Detailed Process Steps & Parameters....................195

List of publications 198

Summary

As an emerging technology for the mass manufacture of micro- and nano-scale patterns on flexible substrates, UV roll-to-roll nanoimprinting is attracting interest due to its inherent advantages of low cost, high throughput, large area patterning. Of particular note is the field of resin mould replication, or the precise copying of master moulds and patterned templates into low cost polymeric working moulds for subsequent lithography on other surfaces of commercial interest. High speed fabrication of UV roll-to-roll nanoimprinted resin moulds is possible through the deposition, exposure and polymerization of liquid UV curable resin coated engineering plastics against a given master mould at high speed. Resin moulds represent a major technological breakthrough in dramatically improving the cost profile and availability of micro- and nano-patterned surfaces to the private sector. They can be produced at such high speed and low cost that they can be used once and disposed of or recycled economically. In the delivery of this thesis, the production of resin moulds and methods to control their surface chemistry and surface energy will be presented. High fidelity resin mould fabrication to 50 nm feature diameter, at up to 120 cm^2 area, and at 10 meters min^{-1} throughput will be demonstrated from nickel shim masters. As-fabricated UV roll-to-roll nanoimprinted acrylic resin moulds were furthermore segmented out and employed in a batch mode thermal nanoimprinting process. Results show high fidelity mixed nanostructures, an average height loss of 3.7% from the curing shrinkage of the resin mould, and negligible (< 0.5%) shrinkage from the PMMA thermal nanoimprint step. Resin moulds can also be produced from polymeric composite masters such as flexible h-PDMS/PDMS silicone-based templates that can be mounted in UV roll-to-roll nanoimprinting systems. By employing a modified formulation chemistry, h-PDMS/PDMS composite templates with a modulus of ~6 MPa can be produced which can withstand mounting tension onto cylinders without cracking. Both PDMS and h-PDMS are also known for their unique

ability to absorb significant quantities of small non-polar molecules such as organic solvents. In this work, the potential to absorb functional non-polar molecules such as reactive monomethacryloxypropyl polydimethylsiloxane (mPDMS) release agent into h-PDMS/PDMS composite templates for *in situ* transfer and anchoring to polymerizing resin mould surfaces during UV roll-to-roll nanoimprint fabrication is explored. It was found that the heavily cross-linked nature of h-PDMS renders it capable of absorbing mPDMS without a large swelling response for exposure times of 15 minutes, allowing for fabrication of resin moulds with useful sub-micron structures and mPDMS release agent anchored to their exposed surfaces. The latter characteristic allows for a degree of built-in control over the surface energy of newly fabricated resin mould surfaces. Contact angle measurements in concert with XPS measurements were used to characterize the degree of release agent transfer, decay rates over several imprint cycles, and the increase in hydrophobicity over control samples. mPDMS transfer decay was measured via XPS and fitted to a first order exponential that leveled off at about 38% of its initial value after 10 imprint cycles. From the Si/C ratio, even after 10 imprint cycles, the majority of detected Si on resin films was found to be associated with mPDMS. Advancing water contact angle measurements found a stable improvement of 20° for resin films with transferred mPDMS over release agent – free reference films.

List of Tables

Table 3.1 (pp. 75) Materials & equipment used to demonstrate high resolution resin mould fabrication via UV roll-to-roll nanoimprinting.

Table 3.2 (pp. 87) Process parameters for batch mode thermal NIL using segmented UV roll-to-roll nanoimprinted resin moulds.

Table 3.3 (pp. 94) Line height shrinkage calculations from AFM profile measurements for the nickel roll-mounted mould – resin mould replication step and for the full three stage cycle, i.e. nickel roll-mounted mould – resin mould – PMMA thermal imprint (height losses from nickel electroforming steps are assumed negligible and are not considered).

Table 4.1 (pp. 113) Dimensions & feature geometries of master moulds used for h-PDMS/PDMS roll-mounted mould replication.

Table 4.2 (pp. 115) h-PDMS formulation from literature with comparison to the present modified formulation for large area roll-mountable h-PDMS/PDMS moulds.

Table 4.3 (pp. 121) Test bed resin formulation for fabrication of resin moulds via UV roll-to-roll nanoimprinting.

Table 4.4 (pp. 141) XPS & advancing water contact angle measurements of mPDMS transfer to fabricated resin moulds vs. no. of imprint cycles.

Table A.1 (pp. 189) General parameters used in calculation of the solubility parameter for monomethacryloxypropyl-terminated polydimethylsiloxane (mPDMS) and the Gibbs free energy change of dissolution in PDMS.

Table A.2 (pp. 189) Group contributions to the cohesive energy, molar attraction constants and the hydrogen bonding energy for calculation of the total solubility parameter and Hansen partial solubility parameters for mPDMS.

Table A.3 (pp. 190) Total and partial solubility parameters for mPDMS and PDMS.

Table B.1 (pp. 195) Process steps used for UV roll-to-roll nanoimprinting of resin moulds in Chapter 3.

Table B.2 (pp. 195) Process parameters for batch mode thermal NIL using segmented UV roll-to-roll nanoimprinted resin moulds in Chapter 3.

Table B.3 (pp. 196) h-PDMS Formulation used in h-PDMS/PDMS bi-layer silicone mould fabrication for Chapter 4.

Table B.4 (pp. 196) Process steps used for fabrication of h-PDMS/PDMS bi-layer silicone mould and exposure to mPDMS for Chapter 4.

Table B.5 (pp. 197) Process steps used for UV roll-to-roll nanoimprinting of resin moulds using mPDMS exposed h-PDMS/PDMS roll-mounted moulds in Chapter 4.

List of Figures

Figure 1.1 (pp. 2) Schematic of the conventional imprinting process.

Figure 1.2 (pp. 7) Schematic of a typical continuous UV roll-to-roll nanoimprinting setup with UV lamp exposure unit.

Figure 1.3 (pp. 11) An overview photo of the SRS 300 UV roll-to-roll nanoimprinting system used in the present work and co-developed with Solves Innovative Technology.

Figure 1.4 (pp. 13) *At left*, SEM image showing an anti-reflective conical cylinder array fabricated from a proprietary UV curable resin (Mitsubishi 7700) on a flexible PET substrate.[42] Reprinted with permission. Copyright 2008, IOP Publishing Ltd.

Figure 1.5 (pp. 15) TFT fabrication by SAIL.[43] Reprinted with permission. Copyright 2010, AIP Publishing.

Figure 1.6 (pp. 16) Active matrix display produced exclusively by SAIL roll-to-roll processing, a type of multi-level UV roll-to-roll nanoimprinting utilizing transparent silicone moulds.[44] Reprinted with permission. Copyright 2010, Wiley Interscience.

Figure 1.7 (pp. 19) Schematic showing 1-dimensional viscoelastic flow of a thick resin coating into an infinitely long channel.

Figure 1.8 (pp. 21) Schematic showing 1-dimensional viscoelastic flow of a thin resin film.

Figure 1.9 (pp. 25) Schematic showing the construction of a resin mould produced by UV roll-to-roll nanoimprinting.

Figure 1.10 (pp. 29) Process flow schematic illustrating how UV roll-to-roll nanoimprinted resin moulds can be incorporated into various manufacturing schemes.

Figure 2.1 (pp. 43) Cross-sectional SEM images of UVNIL imprinted pillars (top diameter ~2.2 µm, height ~2.5 µm) on 2" sapphire wafers fabricated against a UV roll-to-roll nanoimprinted resin mould reel.[100] Reprinted with permission. Copyright 2013, SPST.

Figure 2.2 (pp. 45) Schematic diagram of the batch mode UVNIL system used by Hidetoshi *et al*. to produce 2" PSS LED wafers covered with conical light scattering structures.[100] Reprinted with permission. Copyright 2013, SPST.

Figure 2.3 (pp. 47) Photographs of various epoxysilicone grating patterns imprinted on a PET strip by UV roll-to-roll nanoimprinting. Reprinted with permission. Copyright 2008, Wiley-VCH Verlag.

Figure 2.4 (pp. 48) Schematic and photo of UV roll-to-roll and roll-to-plate nanoimprinting setups used by Ahn *et al.* for patterning both flexible substrates utilizing a gravure offset resin coating system and a tensioned ETFE belt mould supported by two rollers.[34] Also, 4-inch wide, 12-inch long, epoxysilicone grating pattern on flexible PET substrate fabricated by UV roll-to-roll nanoimprinting. Reprinted with permission. Copyright 2009, American Chemical Society.

Figure 2.5 (pp. 50) SEM overhead image of an inverted pyramid array nickel shim mould and imprinted pyramid array produced from the mould via UV roll-to-roll nanoimprinting in urethane acrylate photopolymer (50 μm pitch, 24 μm height).[31] Reprinted with permission. Copyright 2007, The Japan Society of Applied Physics.

Figure 2.6 (pp. 54) SEM cross-section of a 70 nm linewidth, 70 nm height, 140 nm pitch grating master mould in silicon. Inset shows the polyurethane acrylate (PUA) "rigiflex" replicated mould.[52] Reprinted with permission. Copyright 2006, Elsevier B.V.

Figure 2.7 (pp. 56) Schematic mould replication process for producing a nickel shim mould from an AAO master template.[114] Also, overhead and cross-section SEM micrographs of a ~35 nm diameter, 120 nm tall, high aspect ratio pillar nickel mould replicated from a nanoporous AAO master. Copyright 2006, The Japan Society of Applied Physics.

Figure 2.8 (pp. 57) Photo of a hierarchical nickel shim mould replicated from an AAO master covered with patterned photoresist.[21] Also, zoomed out SEM image showing the photoresist generated pattern and zoomed in image showing high density pillars replicated from the AAO master. Copyright 2007, Springer-Verlag.

Figure 2.9 (pp. 58) Scanning force microscopy (SFM) images of PS-*b*-PEO self-assembled films at different film thickness on patterned poly(butylene terephthalate) substrates replicated from faceted sapphire (pitch: ~130 nm, amplitude: ~15 nm).[19] Reprinted with permission. Copyright 2010, WILEY-VCH Verlag.

Figure 2.10 (pp. 60) Stepped rotating photolithography apparatus shown with rotation stage, roller and photomask plate for the production of seamless roller moulds applicable for use in UV roll-to-roll nanoimprinting.[15] Reprinted with permission. Copyright 2009, Elsevier B.V.

Figure 2.11 (pp. 62) Process schematic showing fabrication of a seamless roller mould by dip coating, e-beam writing and resist development.[106] Reprinted with permission. Copyright 2014, Elsevier B.V.

Figure 2.12 (pp. 62) SEM overhead views of various Cr nanodot patterns fabricated on an aluminum roller.[106] Reprinted with permission. Copyright 2014, Elsevier B.V.

Figure 2.13 (pp. 64) AFM scans of a ~1 μm wide trench formed by two-step inclination laser ablation of an iron film sputtered onto a fused silica cylinder.[13] Reprinted with permission. Copyright 2008, Springer Science+Business Media B.V.

Figure 2.14 (pp. 66) Procedure for fabricating a soft PDMS roller with an array of microlens cavities using a polymer sheet mould replicated from a rigid master.[46] Reprinted with permission. Copyright 2007, Elsevier B.V.

Figure 3.1 (pp. 76) Process schematic detailing the major steps in producing high resolution resin moulds via UV roll-to-roll nanoimprinting, followed by demonstration via batch mode thermal NIL.

Figure 3.2 (pp. 77) Photograph of SRS 300 UV roll-to-roll nanoimprinting system used for the present work. Also, photograph of a nickel sheet mould mounted via mechanical fixation onto a slot mount piece fitted into the imprint roller installed with the SRS 300.

Figure 3.3 (pp. 81) SEM overhead view of an inverse hard disk servo pattern on the nickel working mould. Also, SEM overhead view of UV roll-to-roll nanoimprinted resin mould copy of the nickel hard disk working mould showing high fidelity reverse tone replication.

Figure 3.4 (pp. 85) SEM cross-sections of UV roll-to-roll nanoimprinted resin mould hard disk servo pattern, as well as preamble and data track transition.

Figure 3.5 (pp. 88) SEM overhead view of UV roll-to-roll nanoimprinted 50 nm linewidth line and space resin mould. Also, SEM overhead view of high fidelity replication of the same 50 nm linewidth line and space pattern in PMMA produced by using the UV roll-to-roll nanoimprinted resin mould to pattern a 200 nm thick PMMA film on a 4” silicon wafer.

Figure 3.6 (pp. 90) AFM section analysis of hard disk gray code region and AFM height profiles for the nickel hard disk mould, UV roll-to-roll nanoimprinted resin mould, and batch mode thermal NIL imprint produced from the resin mould.

Figure 3.7 (pp. 92) Schematic showing a cross-section of the imprint stack under pressure across the UV roll-to-roll nanoimprinting system imprint roller. The brushed grinding finish of the stainless steel cylinder is partially transmitted through the nickel shim mould. The dispensed liquid resin conforms to this surface and is solidified with this contour upon UV curing, obtaining the resin mould surface waviness found in AFM section measurements.

Figure 3.8 (pp. 95) AFM height profiles showing the detailed line topology of the 50 nm linewidth, 100 nm pitch data track region of the nickel hard disk mould, the UV roll-to-roll nanoimprinted resin mould (reverse tone), and the batch mode thermal NIL imprint produced with the resin mould.

Figure 4.1 (pp. 101) Reversible material failure in a nanoimprint stack with a resin mould, resist, and substrate where the work of adhesion, $A_{12}(\gamma_{1V} + \gamma_{2V} - \gamma_{12})$ between the mould and the resist exceeds the formation surface energy of the resist (cohesive failure), or the separation surface energy of the resist/substrate interface $2A_1\gamma_{1V}$ (interfacial failure).

Figure 4.2 (pp. 108) Process schematic for fabrication of resin moulds via UV roll-to-roll nanoimprinting with incorporation of a custom h-PDMS/PDMS roll-mounted mould with embedded monomethacryloxypropyl-terminated polydimethylsiloxane (mPDMS) reactive release agent.

Figure 4.3 (pp. 109) Small scale h-PDMS/PDMS test mould fabricated against a silicon master, prior to trimming and mPDMS exposure. Also, XPS scans of a blank resin film cured against an h-PDMS/PDMS sheet showing the transfer silicon in the form of un-reacted dimethylsiloxane oligomers.

Figure 4.4 (pp. 112) Workflow schematic showing the fabrication of a silicone roll-mounted mould from a master, followed by absorption of a liquid, reactive silicone-based release agent. Resin moulds are fabricated by UV roll-to-roll nanoimprinting against the silicone mould with embedded release agent, allowing transfer of the release agent to the resin mould surface. Because the release agent is reactive (methacrylated), it participates in the resin mould polymerization reaction and is covalently bound at the surface of the resin mould. The anchored release agent assists with release in subsequent lithography step(s) utilizing the resin mould.

Figure 4.5 (pp. 118) mPDMS deposition scheme onto h-PDMS/PDMS composite moulds via pooling on the patterned h-PDMS face. Swelling of the PDMS backing layer immediately adjacent to the h-PDMS film occurs within about ~5 minutes of mPDMS exposure, causing a swelling mismatch and convex bending of the composite mould.

Figure 4.6 (pp. 120) Photographs of a large area 160 x 75 x 4 mm, 500 nm diameter AR 1 hole h-PDMS/PDMS composite mould mounted on the SRS 400 UV roll-to-roll

nanoimprinting system, post-mPDMS exposure, after the 1st imprint to remove residual mPDMS.

Figure 4.7 (pp. 126) Instron 5569 Universal Testing System with pneumatic side-action grips and a mounted 20 x 5 x 0.53 mm h-PDMS strip.

Figure 4.8 (pp. 127) Stress-strain plot and tabulated data for the modified h-PDMS formulation, measured across 7 20 x 5 x 0.53 mm h-PDMS strips.

Figure 4.9 (pp. 130) Macro-bending effect of mPDMS exposure on 20 mm x 10 mm x 3 mm, 250 nm linewidth AR 1 grating h-PDMS/PDMS test mould.

Figure 4.10 (pp. 132) Cross-section SEM micrographs of 250 nm linewidth, AR1 resin mould samples and original master silicon mould cross-section. Resin mould samples were fabricated using h-PDMS/PDMS moulds with and without mPDMS exposure.

Figure 4.11 (pp. 133) Cross-section and overhead SEM micrographs of 500 nm linewidth, AR 4 resin mould samples. Resin mould samples were fabricated using h-PDMS/PDMS moulds with and without mPDMS exposure.

Figure 4.12 (pp. 134) Cross-section and overhead SEM micrographs of 500 nm diameter, AR 4 pillar resin mould samples. Resin mould samples were fabricated using h-PDMS/PDMS moulds with and without mPDMS exposure.

Figure 4.13 (pp. 138) Large area 160 x 75 mm, 500 nm diameter AR1 pillar resin mould fabricated via UV roll-to-roll nanoimprinting from an mPDMS exposed h-PDMS/PDMS composite mould.

Figure 4.14 (pp. 140) Series of XPS survey scans showing the evolution of the O1s, C1s and Si2p peaks on resin films fabricated from an extracted, mPDMS-exposed h-PDMS/PDMS sheet. 1st, 5th, and 10th imprint cycles are shown along with a reference scan of a resin film cured against an unexposed mPDMS-free, extracted h-PDMS/PDMS sheet.

Figure 4.15 (pp. 142) Plot of the normalized Si2p peak CPS, as acquired via XPS surface analysis of sequentially fabricated UV roll-to-roll nanoimprinted resin film samples cured against an mPDMS-exposed, h-PDMS/PDMS sheet. The scatter plot was fitted to a single term exponential decay with an adjusted R-Square of 0.94.

Figure 4.16 (pp. 143) Plot of the Si2p/C1s ratio, as acquired via XPS surface analysis of sequentially fabricated UV roll-to-roll nanoimprinted resin film samples cured against an

mPDMS-exposed, h-PDMS/PDMS sheet. The scatter plot was fitted to a single term exponential decay that is intended to guide the eye.

Figure 4.17 (pp. 148) Plot of the advancing water contact angle on blank resin films with transferred mPDMS vs. increasing number of imprint cycles.

Figure 4.18 (pp. 149) Scatter plot of advancing water contact angle vs. release agent concentration in wt. % for mPDMS and HFMA impregnated resin films.

Figure A.1 (pp. 192) Bar chart of calculated Flory-Huggins interaction parameter (dimensionless) for various x-mers of monomethacryloxypropyl-terminated polydimethylsiloxane.

Figure A.2 (pp. 193) Bar chart of calculated Flory-Huggins free energy change of mixing in Joules for x-mers of monomethacryloxypropyl-terminated polydimethylsiloxane in PDMS.

Chapter 1. Introduction

1.1 An Introduction to UV Roll-to-Roll Nanoimprint Lithography

Before introducing the topic of UV curable resin mould fabrication via UV roll-to-roll nanoimprinting, it is helpful to introduce UV roll-to-roll nanoimprinting first as an emerging platform manufacturing technology. All forms of nanoimprint lithography (NIL) are surface patterning techniques, and can be thought of as methods by which the negative surface relief of a mould can be replicated by direct contact with a patterning media, where the patterning media is often supported on a carrying substrate. In its most conventional form, nanoimprint lithography is a batch process utilizing rigid moulds to transfer the negative profile of the mould into a thin resist film on a rigid substrate as shown in Figure 1.1.[1] Over the years, the definition of nanoimprint lithography has been expanded to include flexible as well as rigid mould materials, flexible or liquid as well as rigid patterning media and patterning media that is unsupported instead of conventional thin resist films supported on rigid substrates.

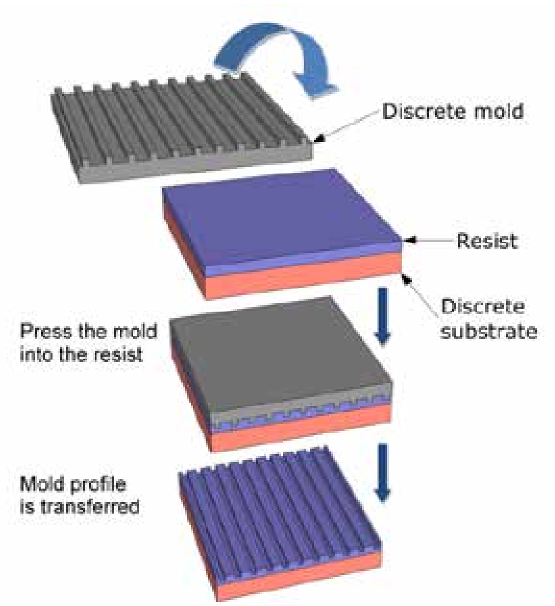

Figure 1.1 Schematic of the conventional imprinting process. Most imprinting techniques were originally developed as batch processes where patterns are fabricated on discrete substrates one at a time as shown. Batch mode imprinting is a contact lithography process in which a rigid mould is pressed into a resist film deposited on a discrete substrate in order to transfer the negative micro- or nano-scale profile of the mould into the resist.

Roll-to-roll, or continuous nanoimprinting introduces the concept of contact pattern replication using a roller- or roller-mounted mould.[2] Roller-mounted moulds are obtained by either wrapping a belt- or discrete flexible sheet mould around a blank roll. Flexible sheet moulds are generally the easiest and most economical to fabricate as they are discrete in nature and are compatible with various top-down patterning techniques, however mounting on a roll will leave a seam. The presence of a seam entails a fixed pattern yield loss relative to seamless patterning, which restricts compatible applications to those where the product is also discrete in nature. Roller mould cylinders are obtained by direct fabrication of mould features onto a roll. This is the only known way to achieve seamless replication of densely spaced features. Roller- and roller-mounted moulds can be obtained by both top-down and bottom-up approaches. Top-down methods include

beam writing techniques such as e-beam writing,[3-8] laser lithography,[9,10] interference lithography,[11,12] laser ablation,[13] and mask exposure techniques using UV or synchrotron x-ray radiation.[14-17] Bottom-up approaches include block copolymer self-assembly and growth of porous anodic alumina oxide on curved surfaces or on flexible sheets.[5,18-23] Roller- and roller-mounted moulds can also be replicated by contact patterning techniques such as electroforming, nanoimprinting, soft lithography, and casting.[9,24-29] Hereafter, Roller- and roller-mounted moulds will be referred to generally as "roller moulds" to refer to all mould types that are compatible with roll-to-roll nanoimprinting. "Belt mould" and "sheet mould" will be used to refer to roller-mounted moulds and "seamless roller mould" will be used to refer to roller moulds where features are directly written onto the roller.

Aside from the use of a roller mould, UV roll-to-roll nanoimprinting also relies on the deposition and curing of a low viscosity UV curable resin coating on a continuous, flexible substrate web feed. Broadly speaking there are four main components to the resin. First, a base monomer is required to form the majority of the cured polymer. Second, a reactive diluent is often used to adjust the viscosity of the formulation to a desired quantity. This component often also fills the role of a cross-linker, providing additional mechanical strength, or improved scratch and wear resistance. Third, a photo-initiator is added to initiate photo-polymerization leading to solidification of the resin. Finally, additives can be incorporated into the formulation to adjust the solid or liquid state resin properties. These additives will often include substances to customize the wetting or rheology of the resin to improve adhesion to the substrate web, and release agents used to reduce resin adhesion to the mould. The latter will be the subject of considerable attention in this work.

There are a large variety of resin polymerization chemistries available commercially or in the literature where organic synthesis from raw chemical compounds is possible. However, there are two major classes that are most commonly used, namely acrylated compounds that rely on free radical polymerization,[30-32] and UV curable epoxies, which rely on cationic polymerization.[33-35] Cationic polymerization occurs where a cationic (positively charged) initiator transfers charge to a monomer which can then react with another monomer in a chain growth polymerization process. Cationic curing epoxy resins are known as “living” polymer systems in the sense that polymerization can continue after the UV light irradiation source is turned off, especially for well purified formulations that are not contaminated with moisture or impurities. Cationic initiators are typically not reactive towards one another unlike free radical initiators and therefore obtain much longer lifetimes. This means that polymerization proceeds until all accessible monomers are consumed, therefore very little unreacted species remain, leaving near-100% solids. Unfortunately, epoxies take relatively longer time to cure and achieve their full mechanical properties. A complete cure can, however, be obtained more quickly by adding an annealing step. For UV roll-to-roll nanoimprinting however, the maximum achievable throughput with epoxy resins is generally around 1 meter min^{-1} as the curing (solidification) time is generally the rate limiting step. Although curing time is slower, UV curable epoxies do not suffer from oxygen inhibition, and therefore quickly establish dry, tack-free surfaces. This, along with low curing shrinkage, is perhaps the key characteristic that drives continued interest in applying these resins in a roll-to-roll manufacturing setting, given the difficulty in setting up a roll-to-roll line in a vacuum or in an inert atmosphere.

Acrylated compounds rely upon free radical polymerization in which the cured polymer forms by formation of a radical species on an initiator through UV excitation, which

attacks a neighboring monomer, leading to bond breakage (usually pi-bonds), rearrangement and transmission of the radical to the monomer. The monomer then attacks another monomer, leading to monomer addition, transmission of the radical to the 2nd monomer and so on as the chain propagates. Given the highly reactive nature of free radicals, polymerization rates are much faster compared to epoxies, with UV roll-to-roll nanoimprinting speeds of up to 10 meters per min^{-1} reported – or up to one order of magnitude faster.[32] At the same time, however, the high instability of free radicals leads to quenching via radical recombination, chain transfer, and termination events. As such, acrylate resins are not "living" polymerization systems and polymerization halts after UV irradiation is halted. Acrylates typically have superior impact resistance in comparison to epoxies, but are subject to the well-known problem of oxygen inhibition. Initiated radicals in the resin can form peroxy radicals with molecular oxygen, which are relatively more stable and thus have poor initiating capacity. In UV roll-to-roll nanoimprint lithography, this oxygen inhibition will generally result in undercured edges at both ends of the web width where the liquid resin front interfaces with the ambient – though the rest of the nanoimprint stack itself is sealed from oxygen when it is formed and so, while not a complete solution, an edge exclusion can be used and cut away post-fabrication. The fast curing property of acrylates also contributes to their comparatively larger shrinkage vs. epoxies (typically 3 – 15% by volume, whereas epoxies generally shrink 2 – 6%).[36,37] Some shrinkage is desirable for the purposes of promoting release, with the theoretical ideal shrinkage found to be slightly less than 2% by volume.[38] Aside from this beneficial characteristic, curing shrinkage is generally undesirable, as resins cure exothermically from the inside out such that the surface in contact with the mould will lose contact with it briefly while the resin is still tacky. Along with the shrinkage itself, this will lead to feature sidewall tapering and corner rounding effects which cannot easily be

compensated for in the mould design. However, for moderate shrinkage, predictable dimensional changes caused by shrinkage can be generally compensated for.

While there are various drawbacks to the use of acrylated compounds in UV roll-to-roll nanoimprinting, the large advantage in terms of curing speed is extremely difficult to ignore as the curing speed typically bottlenecks the overall throughput of the entire process. Furthermore the 1 meter min^{-1} typical throughput of epoxy resins is slow to the point of being insufficient to drive economies of scale for most applications. Therefore, our work has focused exclusively on UV curable acrylate resins for their commercialization potential and because their major disadvantages can generally be mitigated or compensated for in most cases.

Figure 1.2 shows a schematic drawing of a typical UV roll-to-roll nanoimprinting apparatus. A typical system always comprises a dispensing unit such as a slit die or an inkjet dispense array for the purpose of coating UV curable resin onto a transparent substrate. The coating thickness can be controlled directly by using a pair of flattening rollers or a doctor blade (shown), or indirectly by varying the dispense rate, the dispense head aperture diameter, the viscosity of the resin, and the substrate feed rate. Alternatively, the coating can be applied by transfer from a coating roller in a basin of liquid resin to the substrate as is the case with gravure coating, although this approach is less flexible in terms of thickness control. Currently, state-of-the-art inkjet dispensing arrays employ very sophisticated computer control in order to dispense resin on demand according to a map of the mould features, thus greatly improving residual layer uniformity.[39] More generally, it can be seen that the addition of a resin coating to the substrate does introduce additional process engineering requirements, such as ensuring uniform deposition and spreading, and sufficient adhesion of the coating to the substrate

web. However these complexities are offset by the added convenience and speed of room temperature and low pressure processing (typically 100 kPa spreading pressure). Figure 1.2 shows contact being made with the roller mould using two pressure rollers to assist with uniformly spreading of the resin.

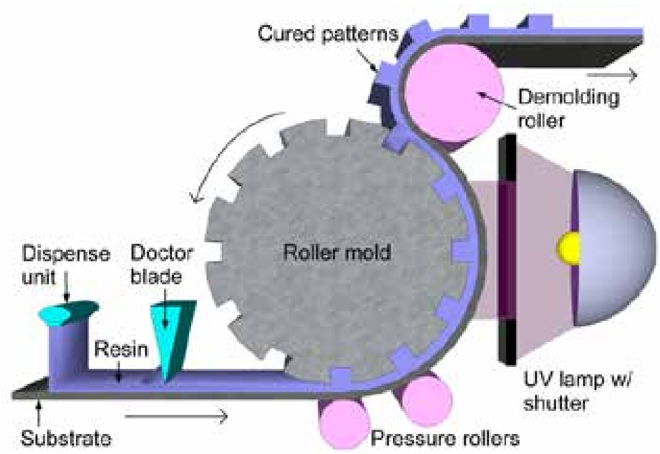

Figure 1.2 Schematic of a typical continuous UV roll-to-roll nanoimprinting setup with UV lamp exposure unit. A dispensing system is utilized to deposit a UV curable liquid resin either as a pattern of drops or as a continuous film (shown). Following deposition of the resin, a variety of thickness control measures can be employed, such as a doctor blade (shown). Multiple pressure rollers are often used to ensure uniform spreading of the resin and filling of the roller mould cavities prior to UV exposure. A demoulding roller is used to peel the cured patterns off the roller mould. There are many possible variations to this setup. However, this schematic shows some of the most commonly used elements.

Another standard component of UV roll-to-roll nanoimprinting systems is a UV source unit for illuminating the curing region where the roller mould and resin on the substrate web make contact after the resin has filled the cavities of the roller mould. The UV source is usually placed external to the rest of the UV roll-to-roll nanoimprinting system, between the stack forming (spreading) rollers and the separation rollers as shown in Figure 1.2. Alternatively, the source can also be placed inside the roller imprint drum if it is comprised of fused silica, quartz, polydimethylsiloxane (PDMS) or other UV

transparent materials.[40,41] The latter configuration allows for the use of non-transparent substrate web materials. The UV roll-to-roll nanoimprinting apparatus used in the present work (SRS 400, Solves Innovative Technology) relies on external UV sources placed between the gap created by the spreading and separation rollers. Selection of the UV light source depends on the required exposure wavelength range and photon flux density to fully cure a given volume of resin before it crosses the gap. The photon flux density plays a key role in terms of the overall throughput of a continuous UV roll-to-roll nanoimprinting process. At the early stages of resin polymerization, the rate of cure is typically governed by the volume density of excited radicals, which is directly influenced by the incident photon flux through the resin coating. The late stages of curing, particularly after solidification, are rate limited by the radical diffusion velocity. However, for UV roll-to-roll nanoimprinting, the resin solidification time is the most important throughput determining factor, as a contact-less secondary UV exposure to fully harden the patterned resin can be easily integrated into the line without confinement limitations imposed by the roller mould. Thus the nature of the UV source, along with the resin chemistry, often determines the throughput potential of the apparatus.

UV lamps (e.g. mercury arc lamps) are most commonly used in the field because their broadband emission spectra (typically between 250 – 500 nm) provides the widest compatibility with available photoinitiators. They produce high photon flux over a broad wavelength range but are very energy inefficient – most energy input is lost to heat, and only a fraction of the light emission is absorbed by the target photoinitiator. Heat dumping accessories, band pass filtering, and focusing optics to collimate the light are common. At low throughput, the broadband exposure is also useful as the deeper UV emission assists in fully hardening resin coatings. However, for exposure through plastic

web materials, this same deep UV emission can also yellow the plastic through a process of photo-aging.

Recently, UV LED arrays have emerged as an alternative UV source with a very tight emission profile (10 – 20 nm FWHM) and a selection of available peak emissions (e.g. 365 nm, 395 nm and 405 nm). Therefore, their conversion efficiency is significantly greater than comparable mercury arc UV lamps for well-matched photoinitiator absorption peaks, though the variety of photoinitiators that can be reliably excited is duly limited to the type of arrays available. For those photoinitiators that do have an overlapping absorption peak, however, the excitation rate is very high and therefore the curing speed for acrylate resins will approach the radical diffusion limit very quickly. For this reason, it is expected that high power UV LED arrays will enable throughputs in excess of 30 meters min^{-1} for acrylate resins.

A third potential UV source is a UV excimer laser. These UV sources produce the highest collimated photon flux with the narrowest wavelength range (less than 1 nm FWHM). However this is only accomplished over a comparatively small spot size, and with additional optics required to de-collimate the light, the apparatus tends to have a large footprint. As there are relatively few outstanding characteristics that do not overlap with the other available sources, UV excimer lasers are seldom used in the field.

A huge variety of substrate materials can be coated with UV resins. In addition, because UV roller imprinting is a room temperature and low pressure technique, soft mould materials with intrinsically low surface energy such as polydimethylsiloxane (PDMS) or ethylene tetrafluoroethylene (ETFE) can be used to pattern the resin, although more traditional nickel shim moulds are still widely used. The flexibility in terms of mould

and substrate materials makes UV roll-to-roll nanoimprinting a particularly versatile technique, with the well-known caveat that at least one of either the mould or the substrate must be transparent to UV light in order for the resin to be properly cured.

Separation of the roller mould from the cured resin imprint is assisted by a deflection roller and an applied web tension (typically 2 – 15 kg) on the web feed. In the present work, peel separation occurs as the applied web tension becomes progressively more vertical to the mould/resin/web stack as the web travels away from the roller imprint drum. The peel angle therefore relies on the web tension and the work of adhesion between the mould and substrate. An alternative arrangement is for the deflection roller to contact the imprint stack at the point of separation. Regardless of the arrangement used, the separation event is often a source of defects in the form of pull-outs, resin caking onto the mould, feature deformation or collapse due to slippage or non-vertical separation on peel and particle formation from collapsed structures leading to defects in subsequent imprint fields. High aspect ratio patterning of discrete structures (as opposed to line & space structures oriented parallel to the feed direction) are also challenging to fabricate due to the peel angle, slippage at the point of separation, vibrations or other sources of shear, and use of a high modulus mould that does not yield to the polymerized resin structures (e.g. nickel shim mould, fluoropolymer mould, other mould materials with modulus in excess of ~1 – 2 GPa). Therefore considerable attention is paid amongst the research community toward improving the release properties of the mould and the cured resin without negatively impacting the adhesion of the resin to the substrate web or the cohesive strength of the cured resin.

Figure 1.3 provides an overview photo of the SRS 300 UV roll-to-roll nanoimprinting system used by our group and co-developed with Solves Innovative Technology.

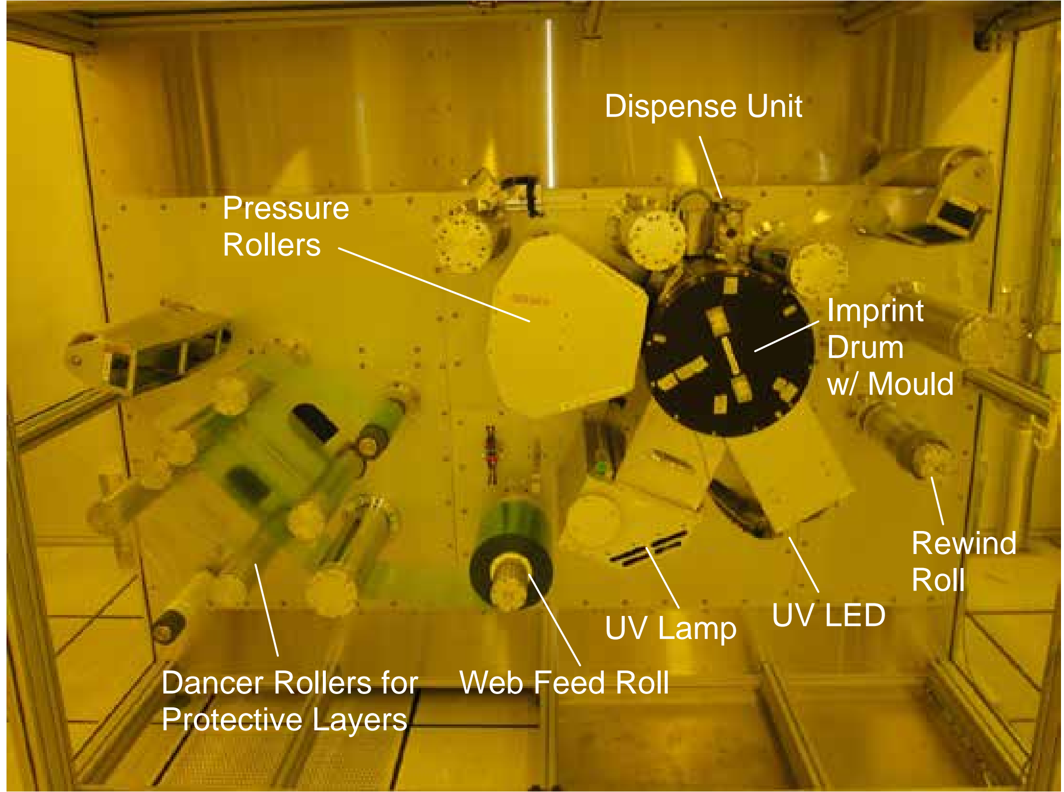

Figure 1.3 Is an overview photo of the SRS 300 UV roll-to-roll nanoimprinting system used in the present work and co-developed with Solves Innovative Technology. It is installed in a class 100 cleanroom, has a maximum throughput of 10 meters min^{-1}, and relies upon inkjet dispensing of UV curable liquid resins. UV mercury arc lamp and 395 nm UV LED sources are built-in to provide maximum photoinitiator compatibility and throughput.

This tool is a lab-scale system designed to handle a range of mould and web sizes from research scale to pilot production and played a crucial role in the development of the present work. It has a maximum throughput of 10 meters min^{-1}, which is among the highest known in the field as of this writing. It relies upon inkjet dispensing of UV curable liquid resins and has both UV mercury arc lamp and 395 nm UV LED sources for maximum photoinitiator compatibility and throughput. Additionally it has various features to improve process cleanliness such as dancer rollers to enable compatibility with web feedstock with protective cover layers and a deionizer bar with inert nitrogen jet

for the purpose of removing particles and contaminants. Aside from specializing in dispensing of low viscosity UV curable resins via inkjet dispense, this tool follows closely the model schematic presented in Figure 1.2 and many if not most of the above considerations discussed previously relating to the various components of a UV roll-to-roll system is applicable to the SRS 300. A more detailed discussion on process recipes and performance utilizing this apparatus in the context of resin mould fabrication follows in Chapter 3.

1.1.1 Industrial Applications

The earliest reports describing UV roll-to-roll nanoimprinting in the literature appeared in 2006, demonstrating the fabrication of lenticular lens arrays for the manipulation of image viewing.[30] Other reported applications include anti-reflective coatings and films,[42] flexible electronics and flexible display backplanes,[40,41,43,44] wire grid polarizers,[35] light enhancement coatings and films for displays,[30,31] microlens arrays,[45-47] and RGB color filters for LCDs.[48] Because a backing substrate is required, UV roll-to-roll nanoimprinting also has obvious application to lithography of the underlying substrate.[49] Perhaps the application which is closest to mass production are anti-reflective coatings and films which are unique in that they are fabricated from homogenous sub-micron moth-eye structures such as cones or pillars.[42] Because they are comprised of sub-micron structures, traditional lower-resolution roll-to-roll processing methods such as flexography or gravure printing cannot be employed. By contrast, the high resolution capability of UV roll-to-roll nanoimprinting is ideally suited for patterning of such structures, especially if the refractive index of the substrate web and the UV curable resin can be closely matched over the visible light spectrum.

Ting *et al.* reported on anti-reflective sub-wavelength structures fabricated with a UV roll-to-roll nanoimprinting tool.[42] They used a nickel electroformed mould with a SAM anti-stick coating (1H, 1H, 2H, 2H – perfluorooctyltrichlorosilane) to improve the releasing properties of the mould surface and prevent the cured resin from remaining attached to the mould upon separation. They also attempted to increase the covalent bonding density between the SAM and the mould by sputtering 20 nm SiO_x and 12 nm TiO_x onto the mould surface however this increases the sub-wavelength surface roughness on the mould which may lead to additional diffuse reflection. Figure 1.4 shows the imprinted result and measured values of reflectance and transmittance, respectively. The structures shown are a conical cylinder array, with spatial period of 400 nm, diameter of 200 nm and height of 350 nm. Although incomplete filling of the mould features was encountered, Ting was able to achieve reflectance below 2.45% and transmittances above 89.4% in the 450 – 700 nm visible spectrum. However, there is still room for improvement as the current industry target is less than 0.1% reflectance.

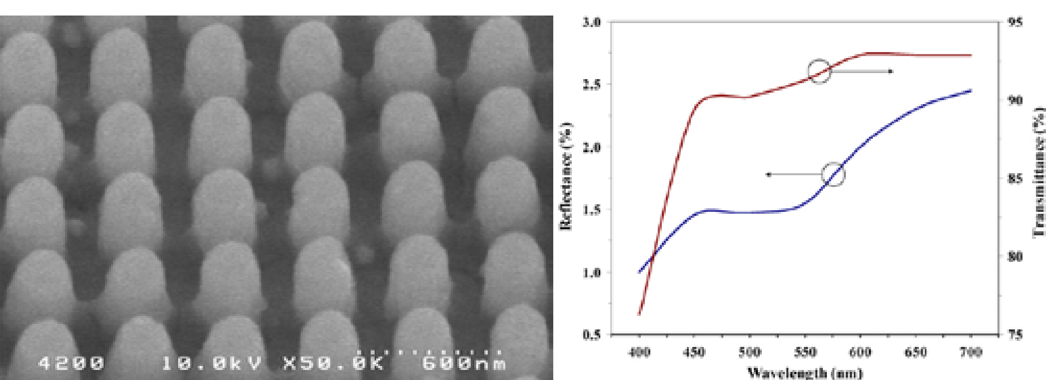

Figure 1.4 *At left*, SEM image showing an anti-reflective conical cylinder array fabricated from a proprietary UV curable resin (Mitsubishi 7700) on a flexible PET substrate.[42] The cones are each of 200 nm diameter, 350 nm height and 400 nm pitch. *At right*, reflectance and transmittance spectra over the visible spectrum for the fabricated anti-reflective film. The reflectance maximum is 2.45% at 700 nm. Reprinted with permission. Copyright 2008, IOP Publishing Ltd.

Another noteworthy effort in industrial application of UV roller imprint lithography was presented by Jackson *et al*. out of Hewlett Packard Laboratories in Palo Alto, CA.[23,54] They developed an innovative approach to roller imprinting called self-aligned imprint lithography (SAIL). Essentially their approach entails the use of a PDMS mould with multi-level features, or three-dimensional structuring with variations in feature depth as well as length and width across the mould (Figure 1.5). This PDMS mould is used to pattern an optical adhesive which is then polymerized using UV light that passes through the roller and the PDMS stamp. The SAIL process broadly targets flexible electronics and flexible display backplanes in particular for commercial production. Figure 1.6 shows an early active matrix display produced purely with SAIL roll-to-roll nanoimprinting. Such devices are generally comprised of multiple stacked functional layers which under conventional processing are aligned, exposed and etched layer-by-layer. This is a time-consuming, low throughput approach which SAIL addresses by incorporating all the layer information in a single imprinting step. The differing height levels of the imprint mask on top of the device layers and the polyimide substrate beneath define the in-plane dimensions of all the device layers simultaneously and the only alignment step that is required is the rough alignment required between the mould and the substrate during the UV roll-to-roll imprinting step. After imprinting the multi-level mask, the final device is defined through a series of etch steps. Multi-level masks are unique to imprint lithography and are not possible to achieve with conventional techniques such as photolithography and are therefore attracting interest from industry as a way to increase throughput and reduce cost.

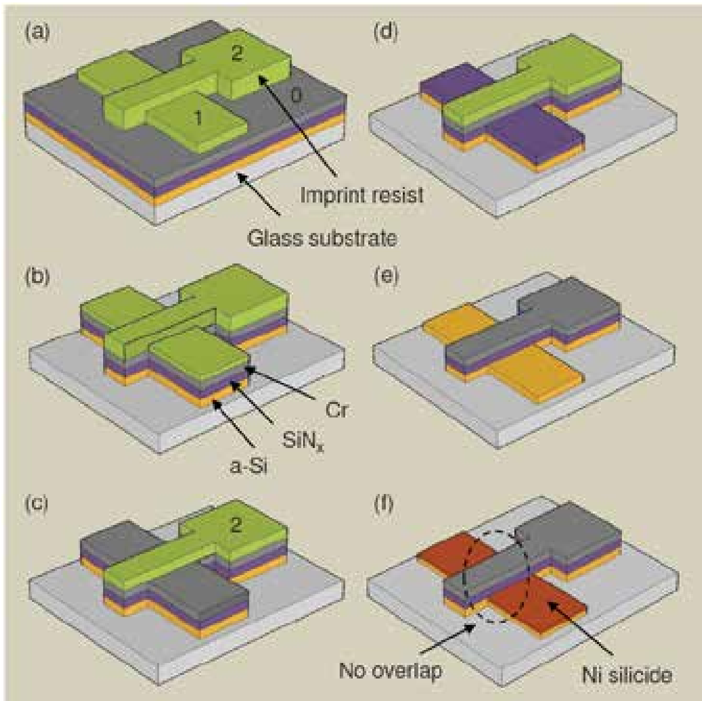

Figure 1.5 TFT fabrication by SAIL.[43] The SAIL process utilizes a multi-level master mould which has its negative relief profile replicated in a soft, intrinsically low surface energy polymer such as polydimethylsiloxane or tetrafluoroethylene-hexafluoropropylene copolymer. This soft polymer mould is then used to cure a photopolymer coating on top of a multilayer TFT stack as shown in a) after residual layer ashing. b) Electrical separation of TFTs by RIE. c) Thinning of the cured photopolymer to reveal level 2. d) Etching of the Cr layer in the source/drain area. e) Removal of cured photopolymer, followed by an anisotropic SiN_x etch. f) Blanket deposition of Ni, silicidation step and selective removal of Ni to expose the completed TFT. Reprinted with permission. Copyright 2010, AIP Publishing.

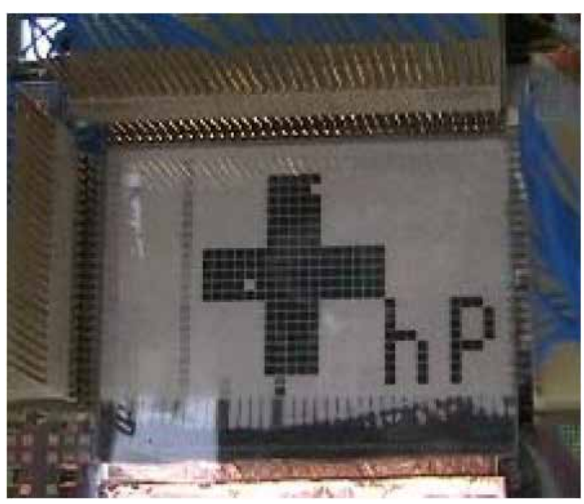

Figure 1.6 Active matrix display produced exclusively by SAIL roll-to-roll processing, a type of multi-level UV roll-to-roll nanoimprinting utilizing transparent silicone moulds.[44] Reprinted with permission. Copyright 2010, Wiley Interscience.

1.1.2 Theoretical Models for Throughput & Mould Cavity Filling

Mathematical models are of considerable utility in predicting, given a set of conditions and material properties, the speed of the rate limiting steps in a manufacturing process to get an idea of the throughput potential for a product application. For UV roll-to-roll nanoimprinting it is difficult to provide a general mathematical model for the throughput of a UV roll-to-roll nanoimprinting process through a mathematical description of the curing rate, because of its dependence on the precise nature of the resin chemistry, the UV source used, its position relative to the imprint stack as well as the stack geometry. Particularly with regard to the resin chemistry, it is difficult to provide mathematical expressions to generalize over all possibilities. However, it is possible and simpler to model the mould cavity filling time and use this value to estimate the maximum throughput potential of the process before the cavity filling time becomes the rate limiting step. In other words, this modeling approach would give the range of throughputs where the curing speed would be rate limiting before a differing physical

limit to the throughput is reached, while ignoring various other technical limitations that would be specific to the equipment used or materials selected. The cavity filling time is the amount of time required to fill a micro- or nano-feature on the mould with resin during the UV roll-to-roll nanoimprinting process. Filling time is dependent only on the viscosity and thickness of the resin coating, the size of the mould cavities to be filled, as well as the applied pressure. An engineer will generally have control over one or more of these parameters when designing a process. When the filling time is the throughput-limiting step, a feed rate which does not allow sufficient filling time will exhibit incomplete filling of the mould features and the imprint result will be poor.

There are two basic formulae, one which expresses the filling time in terms of the mould cavity geometry and the other which is in terms of the initial and final residual layer thicknesses. For thick resin coatings, the former case would be limiting while for thin coatings, the latter. The cut-off for cavity fill-limited or spreading-limited behaviour, respectively, is found for a 1 μm linewidth, aspect ratio 1 grating, a spreading roller contact width of 1 mm, and an applied force of 100 N (applied pressure of 100 kPa), to be for coating thicknesses of ~10 microns. For thick ($\gtrsim$ 10 μm), high viscosity resin coatings, the filling time for a discrete grating channel on a roller mould can be adequately described as a 1-dimensional squeezing flow of a viscoelastic material into an infinitely long channel cavity of height H and width W (see Figure 1.7). Certain additional assumptions are also required. First, it is assumed that the roller contact width L is much greater than H and W so that edge effects can be ignored. Second, the diameter of the roller is also assumed much greater than H and W such that the curvature of the roller does not affect the flow behaviour. Third, the pressure distribution is assumed to be uniform across the contact width L. Finally, it is assumed that the viscoelastic material is incompressible, and the flow is purely viscous with ideal adhesion of the resist

to the mould surfaces. The following equation for calculating the filling time, t_{fill} is obtained,[50,51]

$$t_{fill} = \frac{6\eta(T) \cdot H^2}{P(t) \cdot W^2} \tag{1.1}$$

where $\eta(T)$ is the web shear viscosity at the temperature, T, and $P(t)$ is the time dependent applied pressure. This model is not applicable to cases where L is very small such that the pressure distribution is strongly non-uniform and cases where more complex mould configurations such as discrete pillars, holes or irregular shaped features are employed. In addition, the elastic nature of the polymer web, local shear of the polymer, distortion of the stamp and complex filling are not considered.

For continuous imprinting at maximum throughput (ignoring curing speed), t_{fill} will be equal to the spreading roller contact width divided by V, the web feed rate, or

$$\frac{L}{V} \geq \frac{6\eta(T) \cdot H^2}{P(t) \cdot W^2} \tag{1.2}$$

and then solving for the feed rate,

$$V \leq \frac{P(t) \cdot L \cdot W^2}{6\eta(T) \cdot H^2} \tag{1.3}$$

in order to express the feed rate in terms of applied pressure, viscosity and geometric factors. Thus, a reduction in resin viscosity, or a reduction in channel aspect ratio will increase the maximum potential feed rate. Typical values for the UV curable resin viscosity can range on the order of 1 mPa·s to 10,000 mPa·s depending on the molecular weight of monomer components selected. Increasing the roller contact width L will also increase potential throughput. L can be calculated on a purely geometrical basis if the roller is assumed to be a perfect cylinder with either a pressure roller or flat stage underneath with a measured gap that is slightly narrower than the total thickness of the

substrate.[51] Increasing the applied pressure P will also tend to increase the roller contact width. In order to provide some reference values, assume a resin viscosity η of 1 Pa·s at constant temperature, a roller contact width of 1 mm, an applied pressure of 100 kPa and an aspect ratio of 1. This would yield a filling time on the order of 60 μs. The maximum potential throughput would then be ~1000 m min^{-1} before the filling time becomes rate limiting where UV exposure occurs immediately after emission from the spreading roller. The throughput scales linearly with viscosity, thus for 10 Pa·s the maximum potential throughput would be ~100 m min^{-1} and so on. Therefore at low viscosity there is considerable room for the curing speed to improve before throughput is bottlenecked by the rate of cavity filling, but at very high viscosity the cavity fill-rate limited throughput will eventually approach the curing-rate limited throughput for acrylates. At high aspect ratios (> 5), the cavity fill-rate becomes more important and can limit the throughput for resin viscosities of more than 1 Pa·s. For most practical applications, however, the throughput will never be cavity fill-rate limited.

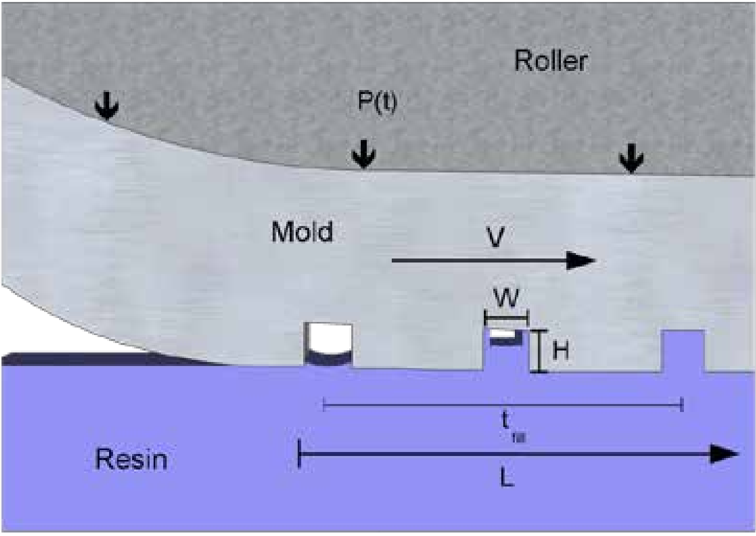

Figure 1.7 Schematic showing 1-dimensional viscoelastic flow of a thick resin coating into an infinitely long channel of width W and height H. The roller mould rotates with velocity V as the channel makes contact with the substrate and fills over time t_{fill}. The substrate and roller mould remain in contact across width L under applied pressure $P(t)$. The substrate material has shear viscosity $\eta(T)$.

For the spreading-limited case, for resin coating thicknesses < 10 μm (given the above described assumptions), we must consider how the resin is dispensed and spread on the supporting substrate. The simplest and most widely applicable treatment is to assume that the resin spreads as a uniform thin film across the substrate on contact with the spreading roller. As a thin coating the resin must spread between the substrate web and the spreading roller, thus this arrangement can be adequately described as a 1-dimensional squeezing flow of a thin resin coating of initial thickness h_o across the roller contact width L into an infinitely long channel cavity (see Figure 1.8). The following assumptions are made: first, that the spreading roller diameter is much greater than L such that the mould curvature does not affect the flow behaviour (the assembly is assumed approximately flat across length L). Second, the pressure distribution is assumed to be uniform across L. Third, that $L >> h(t)$ so that the hydrostatic pressure only has a lateral dependence. Finally, it is assumed that the flow is purely viscous, the resin is incompressible, and ideal adhesion of the resin to the mould surfaces. The following equation for t_{fill} is obtained,[52-54]

$$t_{fill} = \frac{\eta(T) \cdot L^4}{2F(t)} \left(\frac{1}{h_f^2} - \frac{1}{h_0^2} \right) \quad (1.4)$$

where $\eta(T)$ is the resin shear viscosity at the temperature, T, $F(t)$ is the time dependent applied force, h_o is the initial resin coating thickness, and h_f is the final, or residual layer thickness. Similar restrictions on the applicability of this model apply as with Eq. (1). Inputting typical values, 1 Pa·s resin viscosity, 1 mm contact width, 100 N applied force, initial film thickness of 10 μm and final film thickness of 9.5 μm (for perfect filling of a 1:1 duty cycle, 1 μm grating as above), a spreading time on the order of 5 μs is obtained. Note that for h_o of 1 μm and h_f of 0.5 μm, the spreading time increases drastically to ~15 ms, or a spreading-limited threshold of 4 m min^{-1} due to the increasing dominance of the

$\frac{1}{{h_f}^2} - \frac{1}{{h_o}^2}$ factor. Thus the transition from cavity fill-limited to spreading-limited behaviour occurs for resin coating thicknesses of less than 10 μm as described.

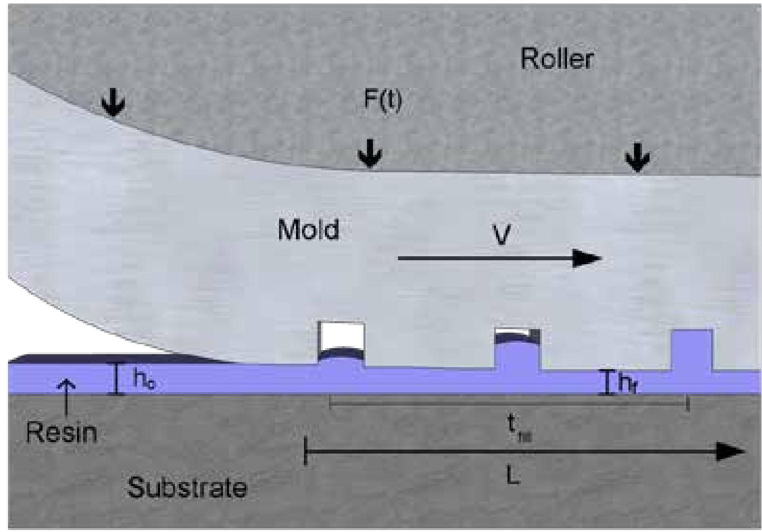

Figure 1.8 Schematic showing 1-dimensional viscoelastic flow of a thin resin film with initial and final thicknesses h_o and h_f, respectively. The roller mould applies a force $F(t)$ that squeezes the resin into an infinitely long channel over time t_{fill}.

In the present work, low viscosity resins are generally used, on the order of 10 mPa·s. Assuming this viscosity along with all other values the same as above, the spreading time is given as ~150 µs and the spreading-limited throughput is ~400 m min^{-1}. This throughput is well within typical values of ~10 m min^{-1} that our group has reported and as such our work is curing-speed limited.[32]

1.1.3 Current State of the Technology

From efforts to model some of the various physical limits to the throughput, it was found that UV roll-to-roll nanoimprinting is a high throughput, low cost process that is throughput-limited by the resin curing speed for resin viscosities <1 Pa·s or for coating

thicknesses >1 μm at reasonable process pressures of ~100 kPa. Thus as advances in resin chemistry continue to improve on the rate of cure the potential throughput for this technology will continue to improve within this window. UV roll-to-roll nanoimprinting is further advantaged by not requiring elevated temperature or large applied pressures to generate patterns, unlike with conventional thermal batch mode NIL.

That UV curable liquid resins undergo a liquid to solid phase change upon curing is another advantageous characteristic of this technology in that the liquid state of the resin has excellent transport properties at room temperature while the fully cured solid polymer will typically have a very high glass transition temperature or one that is above its decomposition temperature and thus fabricated features are typically more stable than those comprised of thermoplastic materials.. On this point, with comparison to thermal roll-to-roll nanoimprinting,[51,55,56] the high viscosity of thermoplastic web materials presents a major throughput bottleneck for direct embossing with a roller mould, as the pressure dwell time at the nip is very short. In contrast, we have shown that the filling time for low viscosity liquid resins is generally on the order of microseconds and is longer (and throughput limiting) only in extreme cases. Low viscosity liquid resins also enable the possibility of fabricating large features next to sub-micron and nanoscale features with reduced variations in film and residual layer thicknesses, a capability that is also difficult to achieve with thermoplastic films.[57]

UV roll-to-roll nanoimprinting has many advantages in terms of throughput and performance, but these advantages come at the expense of increased complexity and under some circumstances less flexibility compared to more conventional batch mode NIL or thermal roll-to-roll nanoimprinting techniques. Liquid resins require a solid substrate support for patterning, and this introduces all the attendant complexities and

problems associated with properly depositing and spreading the resin on the substrate. Ambient gases such as nitrogen, oxygen and water vapor have low solubility in UV resins, leading to a variety of difficulties with bubble trapping defects, especially for very low viscosity UV resins on the order of 10 mPa·s, low dispense volumes, thin residual layers or large features. Efforts have been made in the context of batch mode nanoimprinting to use light noble gases such as helium with higher solubility in order to dissolve trapped bubbles in the resin prior to curing.[58] More recently, refrigerant gases such as pentafluoropropane have been introduced.[59-62] These gases can be condensed at pressures as low as 10 kPa, converting trapped gas into a liquid that easily diffuses into the resin.[62] Adaptation or use of exotic gas environments in a UV roll-to-roll nanoimprinting line could greatly mitigate air trapping issues if the entire line is able to be enclosed and filled with either of these gas environments.

The low pressures utilized in UV roll-to-roll nanoimprinting also make it easier to protect the mould from accumulating damage due to imprinting particles and residues. However patterning a resin coating introduces the additional risk of caking the resin onto the mould. Yet the low pressure capability also enables the use of intrinsically low surface energy soft mould materials such as fluoropolymers and silicones without risk of feature distortion, which our group has encountered when using ETFE (and of course, PDMS) to imprint thermoplastic materials. These materials can greatly mitigate the risk of resin caking for reasonable mould feature densities and aspect ratios (e.g. 1:1 duty cycle and aspect ratios < 5). As previously mentioned, fluoropolymers and silicones in general do not require a self-assembled monolayer (SAM) anti-stick coating to enhance their release properties. This overcomes the temporary nature of conventional SAM coatings in the presence of the reactive chemistries found in UV curable resins.[63,64] Because of a lack of improvements in SAM robustness in recent years, intrinsically low surface energy

materials have drawn increasing attention from the research community. This trend is expected to continue while the throughput of UV roll-to-roll nanoimprinting is bottlenecked by the curing speed, which in turn is dependent on the volume density of radicals in the resin and efforts to increase the latter value to improve the former are likely to aggravate degradation issues with presently available anti-stick coatings.

Despite these drawbacks, the throughput advantages of UV roller imprinting are clear. The technique avoids time consuming thermal cycling, and large exposure area with high photon flux densities can be achieved to make inroads on the curing time bottleneck. Further exciting developments in the field, including more commercialized applications, are expected in the years to come.

1.2 Resin Mould Replication via UV Roll-to-Roll Nanoimprinting

One particular industrial use for UV roll-to-roll nanoimprinting that will comprise the majority of the present work is in the mass production of high resolution resin moulds for the purpose of enabling nanolithography at extremely low cost for myriad applications in nanofluidics, biomedicine, data storage media, and electronics. A resin mould is a type of polymer mould, however it is called a resin mould as a differentiating name since it comprises a bilayer: a cured resin layer which carries the mould pattern and a flexible backing film, usually a transparent plastic. A schematic diagram of a typical resin mould structure is given in Figure 1.9. The apparent structure of resin moulds is thus a direct employment of UV roll-to-roll nanoimprinting as resin mould replication of a mounted roller mould can proceed by forming a stack with a roller mounted mould, a liquid UV curable resin coating and a flexible backing substrate followed by UV exposure and

separation as previously described. Thus the conventionally known classes of feedstock materials can be utilized without any specialized equipment modifications or extra consumables so long as the roller mould feature density is reasonable and aspect ratios are low.

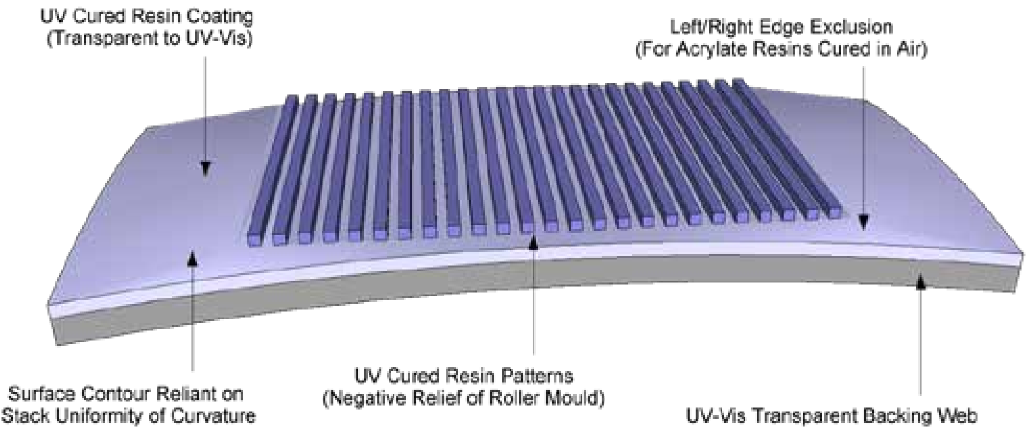

Figure 1.9 Schematic showing the construction of a resin mould produced by UV roll-to-roll nanoimprinting. This example is shown as a cut-out from a resin mould reel with a discontinuous, rectangular patterned field appropriate for use in a batch mode nanoimprinting process. The resin coating usually ranges from 100 nm – 100 µm thickness regime, while the backing web film typically ranges from 100 µm – 1 mm. In reel form, where a seamless roller mould is used to produce the resin mould pattern, the UV cured resin patterns would be continuous from left to right. All material layers must be at least partially transparent to UV-Visible light, depending on photoinitiator selected. An edge exclusion is shown which is standard for acrylate resins susceptible to oxygen inhibition. The flatness of the resin mould is controlled by the uniformity of curvature of the contacting surfaces.

The power of mass replication of nanoscale master moulds becomes apparent when considering the dominance of beam-writing and exposure-based technologies for production of sub-micron and nanofeatures. In particular photolithography and e-beam lithography have for many years dominated the commercial landscape for the top-down fabrication of arbitrary structures in resists. The chief advantage of these technologies over nanoimprinting techniques is that they are non-contacting replication methods. E-

beam writers are able to replicate patterns from a computer model, and photolithography steppers are able to replicate from a photomask through the manipulation of electrons or high energy photons, respectively. The avoidance of contact with the resist greatly reduces the opportunity and severity of defect generation from particles and residues, making it far easier to achieve commercially viable process yields. Moreover, solvent and plasma etching development will simply remove unwanted resist to expose the desired patterns. They do not rely on the flow or transport of resist from one location to another as does nanoimprinting where the resist must be transported to fill in the mould cavities. Where resist (or resin) transport is required, various defects can be generated such as underfilling, pull-outs, and residual layer non-uniformities formed by changes in feature size or density.[57] The formation of these defects is typically governed by the viscosity of the resist or the work of adhesion between the mould and the resist and between the resist and the substrate. These types of contact-related defects are foreign to e-beam lithography and photolithography and thus comprise their competitive advantage in the marketplace over most contact lithography methods, including all batch mode nanoimprinting techniques.

UV roll-to-roll nanoimprinting of resin moulds is an important iteration on conventional replication methods based on nanoimprint lithography because this technology can compete with e-beam lithography and photolithography on the basis of cost. While researchers developing batch mode thermal and UV nanoimprinting technologies sought to displace the use of photolithography by overcoming the diffraction limit plaguing the latter, the effort has thus far failed in great part because of the additional sources of defects inherent to all contact lithography techniques. Where UV roll-to-roll nanoimprinting of resin moulds can succeed while the other technologies have failed is in bringing the cost of nanolithography so low that new applications become economical

that were previously cost-prohibitive using e-beam or photolithography. This is accomplished by using roll-to-roll processing and a continuous production line to drive economies of scale well beyond what is possible with batch mode techniques. The fact that resin moulds can be manufactured using relatively inexpensive polymer materials should make it possible to overcome many of the above mentioned issues relating to random (probabilistic) defects simply by increasing the total number of replicated copies that can be produced per unit cost and thereby driving useful yields to commercially viable levels by that means even if the probability of defects is left to remain constant. Once the unit cost of nanolithography using resin moulds is low enough, it becomes economical to simply use the resin mould once, and dispose of it or recycle it, entirely circumventing the need to protect or clean the resin mould in a production environment.

Another advantage of manufacturing resin moulds via UV roll-to-roll nanoimprinting is the protection this method endows to the master mould. In all nanoimprinting techniques, typically the most costly and most technically challenging input is the master mould, where the cost generally increases with decreasing feature size and increasing feature density. The master mould must generally be obtained using some other top-down or bottom-up fabrication approach, as nanoimprinting techniques are based on replication of a base pattern and cannot be used to generate the base pattern itself. As fabrication of the master is expensive, considerable effort is spent to protect it from damage and it is usually not used directly to mass produce patterned surfaces for integration into commercial products. Similar considerations apply with photolithography where the photomask is often very expensive and protecting it from damage is imperative. Whereas the non-contact nature of photolithography is able to protect the photomask while copying the photomask pattern into photoresist on a wafer, resin mould replication via UV roll-to-roll nanoimprinting is able to convey protection to

the master mould by abstracting it from the mass production of patterned surfaces via substitution of intermediary copies.

A process flow schematic illustrating how resin moulds would be incorporated into various manufacturing schemes is provided in Figure 1.10, for both flat- and seamless roller master moulds. It can be seen from this schematic that final patterned surfaces produced with resin moulds is at least a copy-of-a-copy process, or a 3rd generation abstraction from the master mould. This is the case where the master is directly written to the roller mould utilized in UV roll-to-roll nanoimprinting of resin moulds (see Figure 1.2). Final patterned surfaces can also be 4th generation copies of a flat master mould piece, where the master is first replicated to a flexible sheet mould that is then wrapped around the imprint roller. Thus resin moulds are typically a 2nd or 3rd generation copy of the master. There are some benefits to abstracting the master mould multiple generations from the final product patterning step. For example, the specific technique chosen to replicate the master mould can be more selective to maximum fidelity at minimum risk of damage to the master without having to consider all of the materials and engineering requirements of the final products derived from it. For flat masters, good examples of high fidelity, low risk master replication technologies include nickel electroforming and casting replication techniques.[3,9,25,65,66] The materials, construction and properties of the abstracted resin mould can then be tuned to the required product specification, maximum throughput and low unit costs. Another benefit is the pyramiding effect. With more replication generations, more surfaces can be patterned before all replicated moulds are consumed and the master must be copied again. However, too many replication generations will result in significant fidelity loss, high defect density in the final patterned surfaces, and is very time consuming and laborious. Resin moulds as 3rd and 4th

generation copies of the master perhaps represent the current limit for what is technologically and economically feasible to employ in manufacturing processes.

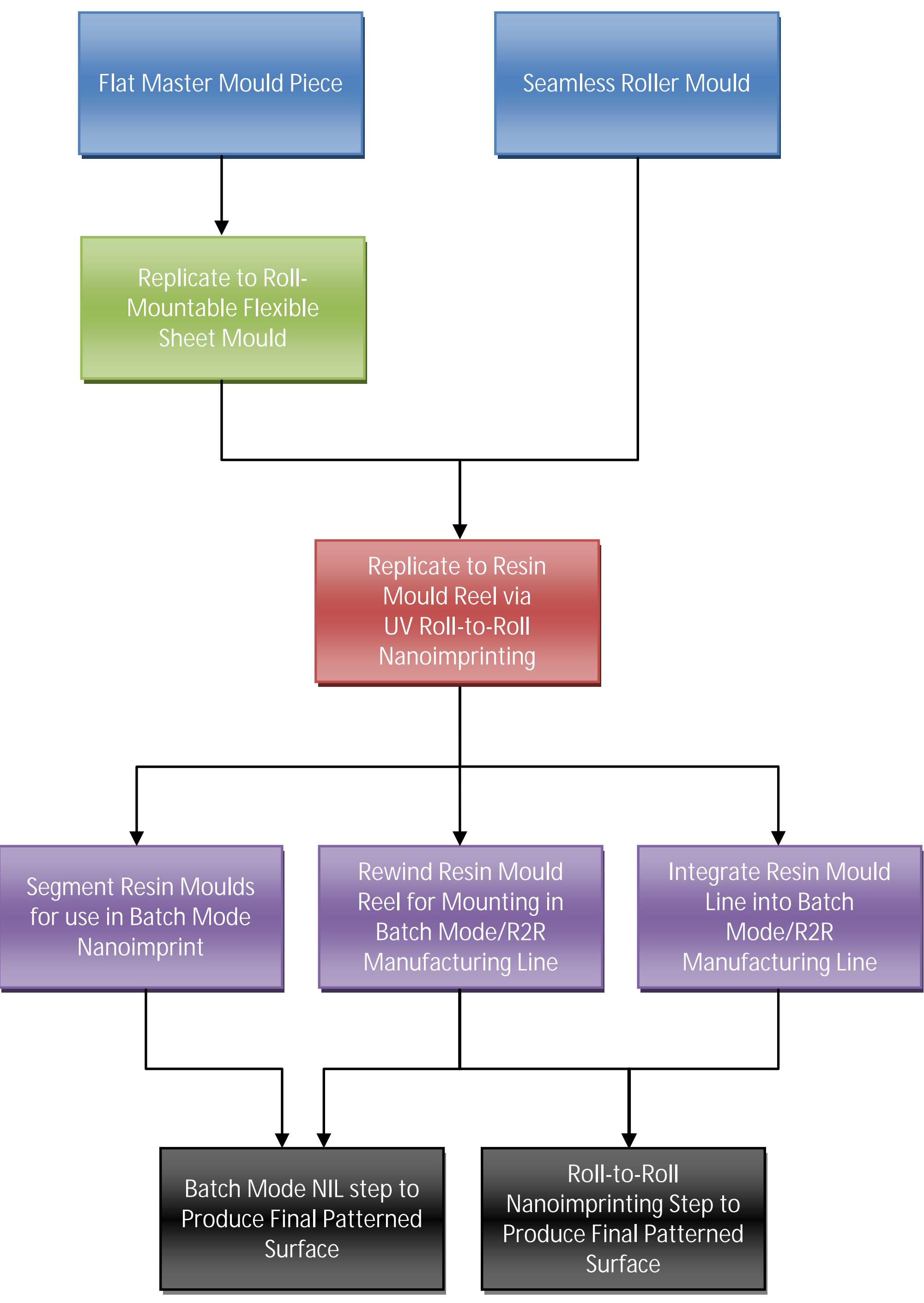

Figure 1.10 Process flow schematic illustrating how UV roll-to-roll nanoimprinted resin moulds can be incorporated into various manufacturing schemes. Final patterned surfaces shown at bottom typically go through certain additional processing steps for integration into actual devices.

In any case, once a resin mould is fabricated, it can be rewound into a reel, re-mounted and then utilized in a product manufacturing line that is also roll-to-roll based, or it can be cut-out and used in a batch mode nanoimprinting process, or the resin mould can be produced and utilized immediately in-line with the product manufacturing process. There are many possible end-use configurations by which resin moulds can be employed to obtain final patterned surfaces for integration into commercial devices and products. In the following chapters we will examine a few of these configurations as part of our study.

1.3 Problem Description

It should be noted that polymer mould replication by batch mode nanoimprinting techniques has been widely reported. This work will not cover in detail all of the available polymer mould materials reported in the literature, and readers are directed to a suitable review paper for these details.[67] We will instead address the two alternative classes of polymer materials in comparison to UV curable resin moulds. They are:

(1) Monolithic thermoplastic polymer mould materials

(2) Monolithic or multi-layer thermal curing polymer mould materials

The basic argument as to why UV curable resin moulds are preferred over the above alternatives is because of issues related to viscosity and thermal cycling. For monolithic thermoplastic mould materials, including fluorinated materials such as Teflon and ETFE, the high viscosity of these materials makes it very difficult to achieve high fidelity replication at sufficiently high throughput. Typical values for a plastic web viscosity can range on the order of 10 MPa·s near the glass transition temperature to 1 MPa·s and below as the melting temperature is approached. Even 1 MPa·s is many orders of

magnitude greater than even the highest viscosity UV curable resins. Thus, the ideal operating temperature for the best possible throughput in a thermal roller imprinting system is as close to the melting temperature as possible without exceeding the temperature at which significant creep or deformation of the web will occur under tension. Using Equation 1.1 as a guide to provide some reference values for typical thermal roll-to-roll filling times, assume a web viscosity η on the order of 1 MPa·s (accounting also for the likely high shear rate) at constant temperature, a roller contact width on the order of 1 mm, an applied pressure of 100 MPa and a feature aspect ratio of 1. This would yield a filling time on the order of 0.1 s. The maximum potential throughput would then only be on the order of 1 m min^{-1}. This corresponds well with the experimental throughput of 31 mm s^{-1} (1.86 m min^{-1}) reported by Fagan *et al*.[51] With the already extremely high pressure given and the relatively conservative viscosity (most thermoplastics will be in a molten state at viscosities below 100 kPa·s) there is little scope for significantly higher throughput for monolithic thermoplastic mould materials in a roll-to-roll nanoimprinting context, especially for feature aspect ratios >1. In order to increase the potential throughput without changes to the viscosity or the applied pressure, one would have to increase the pressure dwell time of the process by increasing the roller contact width beyond 1 mm. Yet the contact width at the nip with contacting cylinders is difficult to increase significantly without using unreasonably large diameter rollers.

The other great obstacle to scale-up for thermoplastic polymer moulds is thermal cycling. Because the imprinted polymer web field would have no maintenance pressure applied to it when emitted from the nip with the roller mould, the patterns would immediately succumb to viscoelastic recovery as the emitted web would still have a temperature exceeding the glass transition. Dumping heat from the imprint stack to get the stack temperature below the glass transition temperature of the thermoplastic web in time

before separation is difficult to accomplish in a roll-to-roll context. It is also not straightforward to maintain an adequate maintenance pressure to arrest viscoelastic recovery after the embossing nip. Batch mode nanoimprinting processes are generally able to apply a maintenance pressure to the imprint stack while cooling the stack to below the glass transition because the stack is not in motion. However this solution requires lengthy thermal cycling times and does not therefore improve throughput.

As for thermal curing materials (usually silicones), similar difficulties with thermal cycling arise in that typically these materials take too long to fully cure for roll-to-roll processing to be feasible.[66,68-70] Silicones such as Sylgard 184 PDMS, h-PDMS, and X-PDMS are usually heated for several hours at temperatures up to 100° C and for at least several minutes at temperatures up to 200° C. In either case the cure time is too long for roll-to-roll processing at commercially viable throughput.

Returning to the subject of UV cured resin moulds, while studies on performance and applications have been published in the literature using batch mode UV nanoimprinting as the chosen fabrication technique,[24,26,71] little has been reported and little is known regarding the performance of resin moulds fabricated by UV roll-to-roll nanoimprinting. Moreover, little has been reported on the performance of resin moulds in subsequent batch mode thermal nanoimprinting despite the fact that this application for resin moulds avoids further volumetric shrinkage. As mentioned previously, UV roll-to-roll nanoimprinted resin moulds are 2nd and 3rd generation copies of the master and undergo some degree of curing shrinkage. If the resin mould is used in a subsequent UV or thermal curing process in product production, then the structures produced will be subject to cumulative shrinkage,[72] particularly if the roller mounted mould was also fabricated using a UV or thermal curing material. To a certain extent, shrinkage can be

compensated for in the master mould design by increasing the protruding feature diameter, density and height for predictable shrinkages. However, certain effects of shrinkage such as sidewall tapering and rounding-off of feature corners cannot be compensated for in this manner. Thus it is of interest to confine the shrinkage to one or two generations and examine lithographic applications for resin moulds which have minimal or no volumetric shrinkage at high resolution.

Furthermore, as demand for higher feature resolution, density and aspect ratios continues to mount, it is critical to start looking at ways to manufacture resin moulds with built-in control over their surface chemistry. Surface chemistry is of crucial importance in determining the work of adhesion to separate the cured resin mould from the roller mounted mould in UV roll-to-roll nanoimprinting. The work of adhesion is given by the Dupré equation as the surface energy of the newly formed surfaces minus the energy of the interface

$$W_{12} = \gamma_1 + \gamma_2 - \gamma_{12} \tag{1.5}$$

where γ_1 and γ_2 are the surface energies on formation of the separated surfaces in vacuum (measured in mJ m^{-2}, also expressed as surface tension in mN m^{-1} for liquids), and γ_{12} is the interfacial energy due to the presence of an interface separating the two coexisting phases at equilibrium. In the present work, σ_1 and σ_2 can either constitute the cured resin mould and the roller mould during UV roll-to-roll nanoimprinting, or the cured resin mould and the resist (or resin) in a subsequent lithography step, respectively. With increasing mould feature density and aspect ratio, the work of adhesion at the interface can easily exceed the energy required to induce material failure of imprinted features on separation. This is particularly true for high density sub-micron structures with aspect ratios approximately greater than 2.

To offset high surface area, the surface energy of (ideally) both contacting surfaces must be reduced to promote clean release. When considering the use of resin moulds in subsequent lithography steps, it may be difficult or impossible to control the surface properties of the resist used to make the final pattern that will be integrated into a device due to product engineering or material constraints. Thus the requirement falls predominantly on the resin mould to obtain a surface energy that is as low as possible to promote clean release for general use in high density, high aspect ratio patterning.

Conventional methods of lowering the surface energy of cured resin surfaces involve liquid immersion deposition and vapour deposition of anti-stick self-assembled monolayer (SAM) coatings (typically after oxygen plasma treatment to hydroxylate the surface),[24,73-76] mixing release agents (typically fluorocarbon or silicone oligomers) into the resin formulation used to produce resin moulds,[29,72] or direct use of fluorinated monomers such as perfluoropolyethers (PFPE) and fluoro-silsesquioxanes in the UV curable resin.[77-82] Liquid immersion and vapour deposition of anti-stick coatings are generally not compatible with roll-to-roll processing. Liquid immersion or vapour modification of the process environment would greatly complicate the manufacturing line and both techniques require exposure times that are unacceptably long for the purposes of maintaining adequate throughput.

Fluorinated monomers such as PFPE and fluoro-silsesquioxanes are very expensive as they would comprise the majority of the resin (fluorinated compounds in general are costly to synthesize),[83,84] making per unit costs prohibitive.[85] These compounds also tend to have relatively long curing times that would serve to bottleneck the throughput in a roll-to-roll process.[85]

Mixing of reactive release agents into the resin formulation is commonly practiced in UV roll-to-roll nanoimprinting. In general however, the release agent concentration at the surface of the cured resin will only approximate the bulk concentration of release agent in the resin formulation. Achieving a high concentration of release agent in hydrocarbon-based resins is often difficult because the chemical composition of the bulk resin and the release agent are generally quite different. High performance release agents are generally composed of fluorinated or silicone-based compounds that have limited solubility in hydrocarbon-based resins. Furthermore, even if a high concentration of these compounds can be achieved, the resulting resin formulation will be far more costly. A more efficient approach would be to achieve a desirable surface property by delivering that property locally to the surface rather than attempting to achieve it indirectly by modifying the bulk resin formulation.

It should also be mentioned here that resin mould surfaces are not stable immediately after fabrication. Surface chain rearrangements and surface migration of low surface tension, unreacted monomers and oligomers will occur while the resin mould is exposed to air. Migration of unreacted surface release agents will also occur if they are added to the resin formulation. This migration effect will also reduce the surface energy of the resin mould significantly over time. However these molecules remain mobile and are not covalently bonded to the surface. They may not therefore remain at the interface to enhance release when the resin mould is used in subsequent lithography steps. Furthermore these unreacted release agent molecules are lost over multiple imprint cycles with the resin mould, degrading release performance and rendering it unpredictable beyond the first imprint cycle. It is much more desirable for a resin mould to have a stable, permanent reduction in surface energy.

Surface migration of release agents from the bulk of the cured resin is also very slow, occurring over several days. Relying on surface migration therefore presents difficulties in scaling up to mass production where a long waiting period prior to achieving optimal properties and placement into service is usually undesirable. There is thus a need to develop means to modify resin mould surfaces to reduce their surface energy with immediate effect but without reliance upon modifying the bulk composition of the resin itself. Ideally, this surface modification should be obtainable without adding extra processing steps or complicating the roll-to-roll resin mould production line. Further, the surface modification should be covalently bound to the resin mould surface to make the modification permanent such that utilization in subsequent lithographic step(s) will benefit from the reduced surface energy (and therefore enhanced release property) of the resin mould in a predictable and repeatable fashion.

1.4 Scope & Objectives

It is an objective of the present work to demonstrate the viability of batch mode thermal nanoimprinting for resin moulds as a lithographic application that avoids stacked or cumulative shrinkage as discussed previously. Stacked or cumulative shrinkage in height will be measured by AFM. A good measure of success would constitute a height loss of 2 – 5% from UV curing shrinkage of the resin mould and negligible (< 0.5%) height loss from the thermal nanoimprint step utilizing the resin mould. This would show that the total shrinkage is limited to the UV roll-to-roll nanoimprinting step to produce the resin mould. Process details and challenges specific to roll-to-roll fabrication of resin moulds will be discussed at length, particularly with respect to the curvature uniformity of the imprint roller.

For high density, high aspect ratio replication of resin moulds, a new method will be introduced to fabricate resin moulds via UV roll-to-roll nanoimprinting wherein reactive surface release agents are delivered via transfer from a bilayer h-PDMS/PDMS silicone roller mounted mould to the resin mould surface. Using a reactive, oligomeric dimethylsiloxane release agent that is highly soluble in silicones, in terms of objectives it will be shown that it is possible to sustainably transfer enough release agent molecules to resin mould surfaces to maintain a stable increase in surface hydrophobicity over several imprint cycles. A useful measure of success would entail monitoring successful transfer of monomethacryloxypropyl polydimethylsiloxane (mPDMS) over 10 imprint cycles via XPS and showing a reasonable percentage of the initial Si2p signal (the specific atomic peak associated with mPDMS) being transferred on the last resin film imprint cycle. Further, advancing water contact angle measurements will show how the surface chemistry, and therefore the surface energy, of the resin mould has been changed. An important objective is to show a sustainable imprint – to – imprint increase in the water contact angle over at least 10 imprint cycles, with an increase of at least 10° over release agent – free resin films. This method of transferring mPDMS release agent to resin moulds does not introduce any additional process steps to modify surface energy, unlike with liquid or vapour deposition of SAM anti-stick coatings. The modification of the resin mould surface occurs *in situ* during UV roll-to-roll nanoimprint fabrication as the resin mould surface is formed. Transferred mPDMS release agent molecules are able to participate in the resin polymerization reaction and are thus covalently bound to the surface of the resin mould, ensuring that the release agent will improve the release performance of the resin mould in subsequent lithography steps.

Using aforementioned release agent impregnated h-PDMS/PDMS moulds, large area roll-to-roll nanoimprinting of dense, 250 – 500 nm diameter pillar array and grating resin moulds up to an aspect ratio of 4 will be demonstrated. Linear shrinkage was closely monitored due to the swollen state of the bilayer silicone mould upon absorption of the release agent and contact with low molecular weight components of the resin.

1.5 Organization of the Thesis

This dissertation provides an in-depth study on resin mould fabrication via UV roll-to-roll nanoimprint lithography, including new production methods and demonstration of usage cases, and seeks to provide engineers and researchers a solid foundation in the scientific and engineering principles important to the field as well as a working understanding of the structure and performance characteristics of resin moulds. Chapter 1 introduces UV roll-to-roll nanoimprinting generally and provides a brief introduction to fabrication of resin moulds using this platform manufacturing technology. This chapter also seeks to distinguish the present work from other related work in the field and summarize the important findings covered in more detail in later chapters.

Chapter 2 focuses on the composition, design, production and industrial applications of resin moulds, including various UV roll-to-roll nanoimprinting equipment presented in the literature that are compatible with resin mould fabrication. A detailed review of roller mould fabrication techniques is also given, as this is a key intermediate step toward production of resin moulds. Both sheet mould fabrication and wrapping techniques as well as seamless roller mould production methods are covered.

Chapter 3 covers fabrication of high resolution UV roll-to-roll nanoimprinted resin moulds for use in batch mode thermal nanoimprinting, including materials & methodology, fabrication results and a comparison of imprint fidelity across all replicated pattern generations. Challenges specific to roll-to-roll fabrication of resin moulds are discussed at length, particularly with respect to the curvature uniformity of the imprint roller.

Chapter 4 presents a new method to fabricate resin moulds via UV roll-to-roll nanoimprinting wherein reactive surface release agents are delivered via transfer from a bilayer h-PDMS/PDMS silicone roller mounted mould to the resin mould surface. This method is designed for use with high density, high aspect ratio resin mould replication in order to introduce a stable and robust surface modification to fabricated resin moulds in order to reduce their surface energy vs. the freshly fabricated state and promote release in subsequent lithography steps. Fabricated samples are characterized by XPS and advancing water contact angle measurements and discussion and interpretation of results is provided.

Chapter 5 is the final chapter providing a summary of contributions and opportunities for further study. Various ways to further reduce the surface energy of fabricated resin moulds will be discussed. Improved resin formulations will be proposed that could de-swell the patterned h-PDMS mould layer in order to mitigate or eliminate resin mould shrinkage caused by swelling. Significant improvements in performance will be followed by lifetime studies over hundreds of imprint cycles to characterize the longevity of the release agent transfer.

Appendix A is provided as a supplement to Chapter 4 with a theoretical discussion on solubility of solvent-polymer systems along with supplemental theoretical calculations of the solubility of monomethacryloxypropyl-terminated polydimethylsiloxane (mPDMS) in solid PDMS. Similar calculations for related compounds of differing molecular weight are also provided for comparison.

Chapter 2. Literature Review

2.1 Industrial Applications for Resin Moulds

In the previous chapter, the structure and composition of resin moulds produced via UV roll-to-roll nanoimprinting was covered and the technology was distinguished from other known polymer soft mould fabrication techniques. In the current chapter various current and potential applications for resin moulds will be covered, followed by discussion on various UV roll-to-roll nanoimprinting equipment and roller mould production methods presented in the literature that are compatible with resin mould fabrication.

The mass production of large area resin moulds for low cost nanolithography is a compelling idea. Particularly with the tremendous growth in demand for commercial devices which require nanopatterned surfaces such as LEDs, solar cells, wire grid polarizers, nanophotonic devices, and wafer-supported optical component arrays.[86] Certain applications would benefit greatly from only a single lithography pass to texture, for example, the top surface of the device. Nanoimprinted anti-reflective layers for solar cells are a good example, and it has been shown that cells with anti-reflection exhibit improved power conversion efficiency over those without.[87]

Nanoimprinted photonic crystals, especially patterned sapphire substrates for LEDs (PSS LEDs) are an example of a single lithography pass to the base, or supporting substrate upon which the device is grown. This approach is considered one of the best ways to increase the overall quantum (light output) efficiency of the LED array and can also assist with uniformly diffusing the light output.[88,89]

Nanostructured glass materials, where a topcoat resist or functional layer can be imprinted or embossed with a soft polymer mould is another promising application for the purposes of controlling light transmission, collimating or focusing light, reflecting certain wavelengths of light, color filtering, or maintaining the cleanliness of the glass through the use of anti-wetting structures.[45,48,90-93] Functional glass is finding wide application in smartphones, displays, specialty lenses for scientific equipment and consumer eyewear, and self-cleaning cover glass for solar panels.

Finally, the flexibility of soft polymer moulds is finding application in patterning of non-planar or curved surfaces. Biomimetic structures,[94] curved gratings for rotary optical encoders,[95] optical fibers,[96] and contoured, porous anodic alumina oxide surfaces[97] are just a few of the possible opportunities through which UV roll-to-roll nanoimprinted resin moulds could be adapted to enable scale-up to commercial production.

At the time of writing, resin moulds have been specifically studied in the production of PSS LEDs for the purpose of improving the internal quantum efficiency by enabling lateral epitaxial patterned sapphire (LEPS),[98] as well as the external quantum efficiency via light extraction using light scattering structures or a photonic crystal lattice.[99-102] The conformal nature of flexible resin moulds allows full contact with the surface despite the warped nature of the multi-layered wafer. Moreover the low cost, high replication speeds enabled by UV roll-to-roll nanoimprinting are required to keep up with the tremendous production volumes of sapphire-based green, blue and white LED wafers currently (600,000 pcs per month).[103] Hidetoshi *et al.* successfully demonstrated low aspect ratio conical structures in sapphire with base diameter of ~2.6 μm and height of ~1.5 μm, etched from an imprinted pillar array produced with a UV roll-to-roll imprinted resin

mould Figure 2.1.[100,101] This structure roughening has recently been shown to double or triple the power conversion efficiency relative to smooth sapphire LEDs.[99]

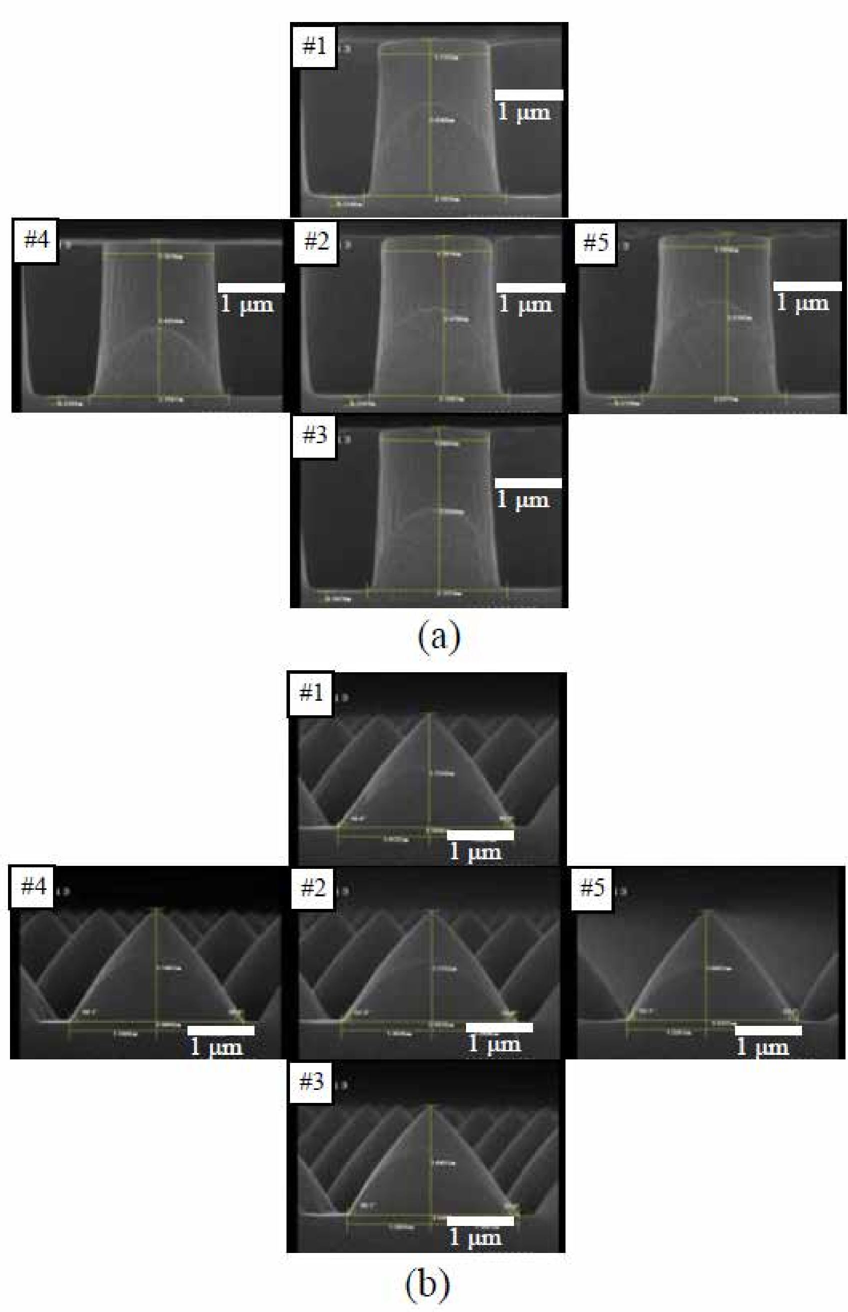

Figure 2.1a) Cross-sectional SEM images of UVNIL imprinted pillars (top diameter ~2.2 μm, height ~2.5 μm) on 2" sapphire wafers fabricated against a UV roll-to-roll nanoimprinted resin mould reel.[100] These pillars were etched to form b) conical light scattering structures with base diameter ~2.6 μm and height ~1.5 μm for PSS LEDs. Inset numbering indicates the imprinted feature and associated etched result. Reprinted with permission. Copyright 2013, SPST.

2.2 UV Roll-to-Roll Nanoimprinting Equipment for Resin Mould Production

The structure of fabricated resin moulds is heavily dependent on the nature of the apparatus and tools used to produce them. For UV roll-to-roll nanoimprinting, the resin dispense and spreading method as well as the viscosity of the UV curable resin will determine many important parameters such as the resin coating thickness, thickness uniformity and, in concert with the mould geometry and wetting characteristics, the propensity of the coating to trap air bubbles. The UV exposure method and the line throughput heavily influence the mechanical properties of the coating, including its cohesive strength and adherence to the substrate web. The position of the UV source, whether mounted opposite the web line or inside a transparent imprinting roller determines whether the web or the mould must be transparent to UV light. Finally, the diameter and positioning of the rollers in the roll-to-roll line are important in determining the range of web thicknesses that the apparatus can accept and thereby the thickness range of the backing polymer film comprising the resin mould.

Several combinations of UV roll-to-roll nanoimprinting equipment have been reported in the literature as part of exploratory studies.[30,31,33-35,100,101,104] This chapter will briefly cover known equipment arrangements that are compatible with production of resin moulds. As mentioned in the prior section, the most direct study of resin moulds outside of work published by our group was conducted by Hidetoshi *et al.* from Toshiba Machine Company.[100,101] Their apparatus, the CMT-400U, can handle up to 230 mm field width on 300 mm wide web of up to 200 μm thickness, and electrode-less UV lamp curing at 240 W cm^{-1} line intensity at up to 10 m min^{-1} throughput. Flexible nickel shims of <0.25 mm thickness were wrapped around an imprint roller to produce resin moulds. The

characteristics of the resin formulation and the orientation of UV exposure were not disclosed, however the system can handle viscosities in the range of 50 – 2000 mPa·s using gravure coating methods. Importantly, the fabricated resin mould reel was rewound and moved to a batch mode UVNIL system which was rigged to handle a continuous resin mould film reel (see Figure 2.2 for schematics) where the resin mould tape was used to imprint resist coated sapphire wafers. This was the first demonstration of resin moulds used in reel form to perform a batch mode nanoimprinting process as part of the production chain for PSS LEDs.

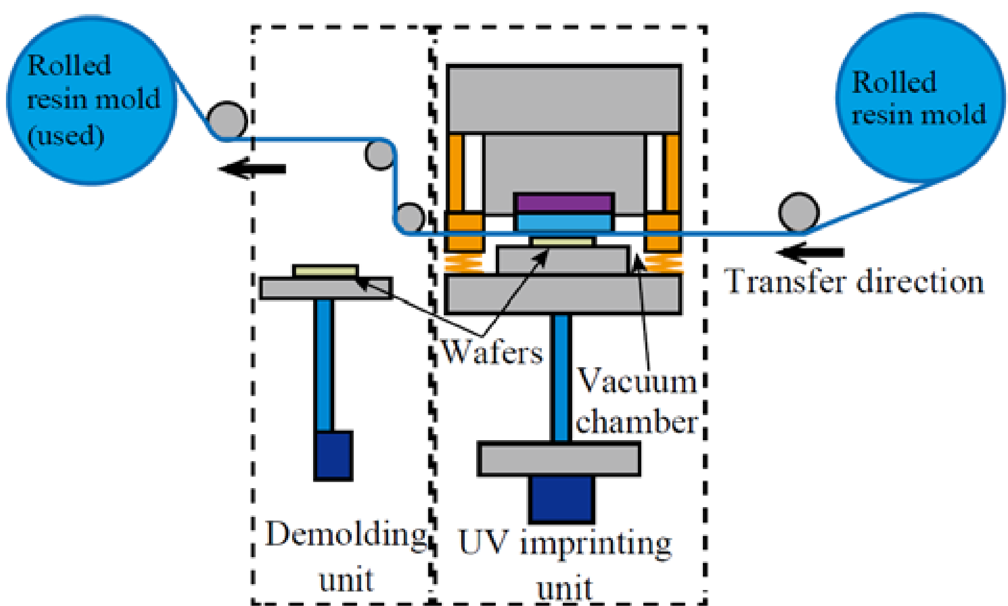

Figure 2.2 Schematic diagram of the batch mode UVNIL system used by Hidetoshi *et al.* to produce 2" PSS LED wafers covered with conical light scattering structures.[100] This was adapted to accept a UV roll-to-roll nanoimprinted resin mould reel. It therefore utilizes a flexure-based chuck to apply uniform pressure instead of pneumatic pressure delivery. Reprinted with permission. Copyright 2013, SPST.

Other UV roll-to-roll nanoimprinting studies in the literature did not specifically fabricate or mention resin moulds, however the apparatus used could be adapted to fabricate them. L. Jay Guo's group at the University of Michigan, Ann Arbor reported on UV roll-to-roll

nanoimprinting with ETFE fluoropolymer roller mounted sheet moulds.[33-35] They fabricated nanoscale line and space patterns (down to 70 nm linewidth and 100 nm period) from a UV-curable low viscosity liquid epoxysilicone resin coated on a PET substrate.[33] ETFE has a high modulus (1.2 GPa) at room temperature but can be softened at temperatures exceeding 200 ºC. Therefore, an ETFE mould can be replicated from an original Si or nickel master mould by a thermal NIL process, although this replication process requires high pressure which risks damaging the master from particles and residues over many replication cycles.[105] The benefit of using ETFE is that it has intrinsically good release properties (critical surface tension of 15.6 mN m^{-1}, cf. PDMS 19.6 mN m^{-1}).[33] Epoxysilicone resins were used to imprint patterns on PET substrates. Epoxysilicone is a cationic curing system whose characteristics were covered in Chapter 1. Their particular formulation required an adhesion promoter for high aspect ratio features on PET substrates in order to prevent pull-outs and caking onto the ETFE mould. Also, the maximum reported feed rate using this resin formulation was 1 m min^{-1}.

Figure 2.3 shows some of the best results achieved using a UV roller imprinting setup capable of patterning 10 mm wide PET strips. In particular, sub-100 nm linewidth gratings were fabricated and shown in cross-section.[33] In an earlier report they used a similar UV roller imprinting apparatus to fabricate wire grid polarizers on 10 mm wide PET strips.[35] More recently, Guo has unveiled a universal 6-inch roll-to-roll and roll-to-plate capable apparatus and demonstrated continuous imprinting of 300 nm linewidth and 700 nm period gratings on a wider 4-inch form factor (see Figure 2.4).[34] The new system utilizes a gravure offset coating system with doctor blade and an imprint module with dual backing rollers for tensioning the web against the roller mould for UV exposure in the gap through the web.

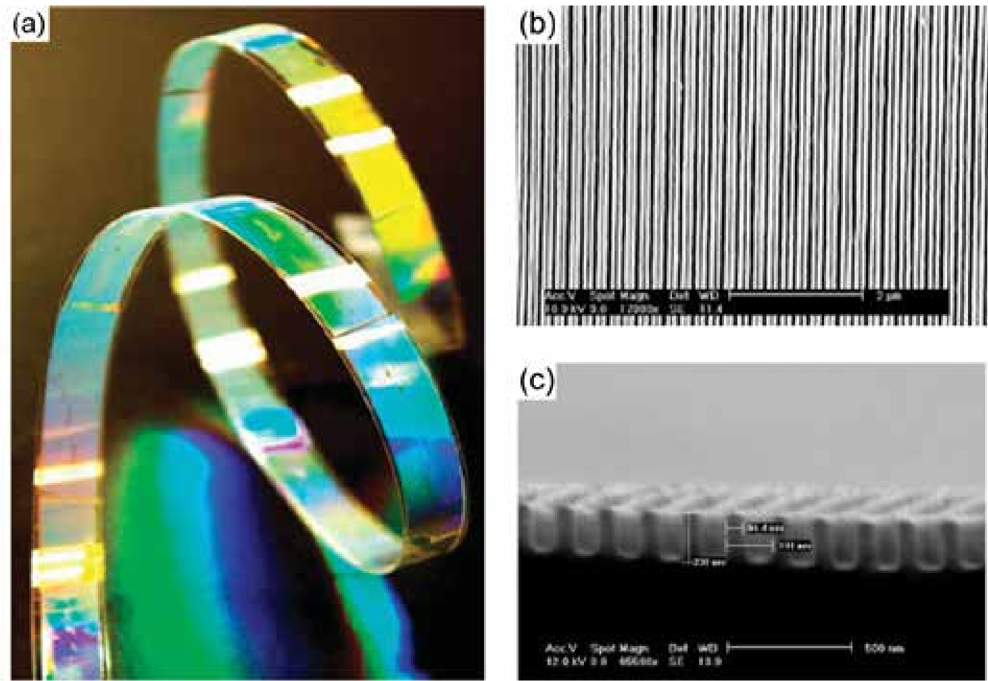

Figure 2.3a) Photograph of 700 nm period, 300 nm linewidth epoxysilicone grating pattern imprinted on a PET strip by UV roll-to-roll nanoimprinting and showing bright light diffraction.[33] b) 100 nm period, 70 nm linewidth epoxysilicone grating shown under SEM. c) SEM cross-section of 200 nm, 70 nm linewidth epoxysilicone grating. Reprinted with permission. Copyright 2008, Wiley-VCH Verlag.

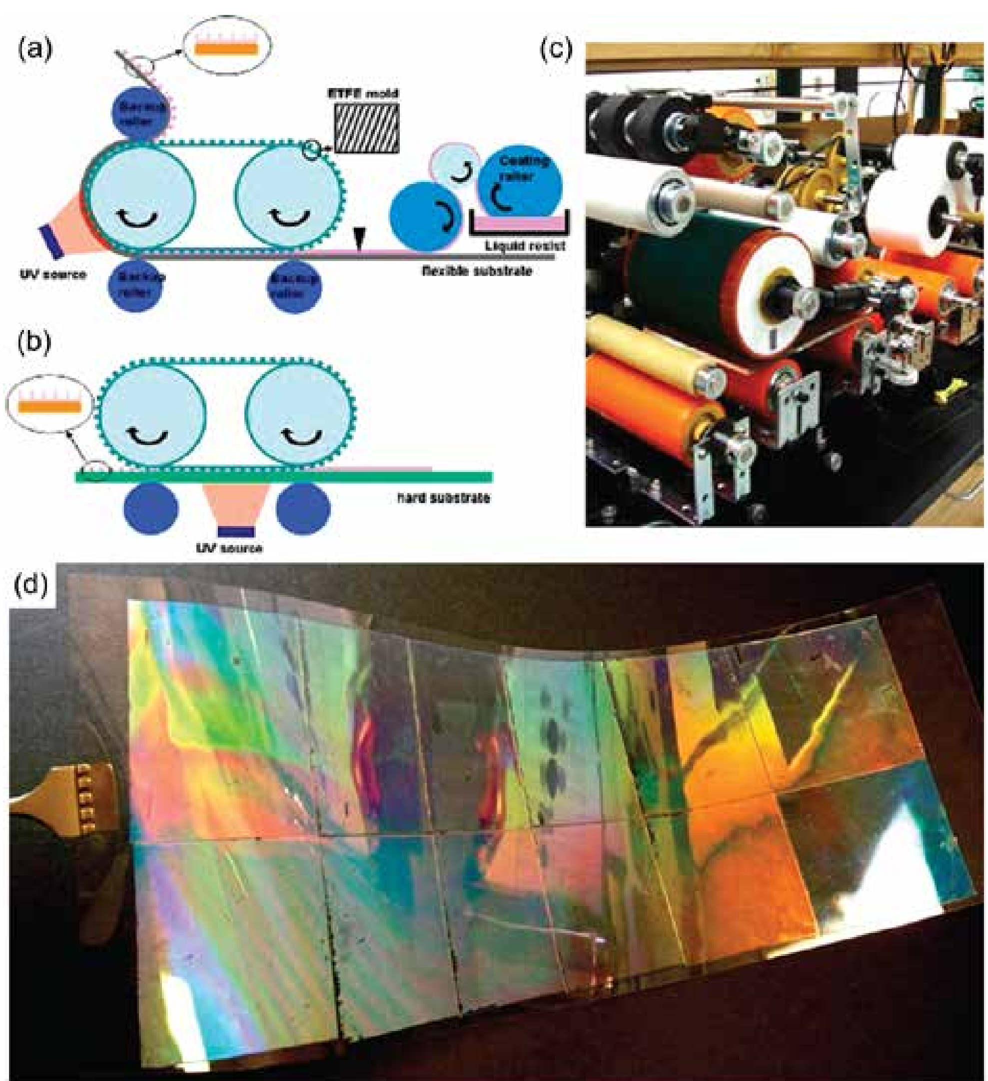

Figure 2.4a) Schematic of UV roll-to-roll and roll-to-plate nanoimprinting setups used by Ahn *et al.* for patterning both flexible substrates utilizing a gravure offset resin coating system and a tensioned ETFE belt mould supported by two rollers.[34] b) UV roll-to-plate schematic for rigid substrates. c) Photograph of 6-inch universal UV roll-to-roll and roll-to-plate nanoimprinting apparatus. d) 4-inch wide, 12-inch long, epoxysilicone grating pattern on flexible PET substrate fabricated by UV roll-to-roll nanoimprinting. This result is a close analogue to a flexible resin mould. The grating dimensions are 300 nm linewidth, 600 nm height and 700 nm pitch. Reprinted with permission. Copyright 2009, American Chemical Society.

Another investigation into UV roller imprinting was reported by Ahn *et al.*[30,31] Their setup is similar to that shown in Figure 1.2. It is equipped with a dispensing syringe that pools a UV-curable urethane acrylate photopolymer with a viscosity of 300 cP at 25 ºC

(cf. water 0.91 cP at 25 ºC). This resin also required an adhesion promoter to be coated on transparent PET web materials to prevent delamination, similar to Guo.

Their apparatus was furthermore equipped with a pair of spreading rollers to achieve a uniform coating of the photopolymer and to join the imprint stack with the roller mould, a UV lamp unit for exposing the gap between contacting rollers, and a demoulding roller which releases the fabricated optical film from the roll stamp. For the pressure rollers, a passive gap control system was used to fix the applied pressure at 90.6 N on contact with the web which is the principal factor determining the final thickness of the imprinted photopolymer film. A metal halide UV-lamp with a wavelength range of 265 – 420 nm and an irradiation intensity at the aperture plane of 200 mW cm^{-2} was used. A calculated feed rate of 0.785 m min^{-1} was selected in order to ensure a sufficient exposure dose of about 300 mJ cm^{-2}.[31]

Ahn *et al.* are among the few researchers to show both micro- and nano-scale features produced with the same UV roller imprinting apparatus, as well as multiple approaches to fabricating and mounting the roller mould. These approaches included direct mechanical micro-machining on an aluminum roll base with a two-axis CNC diamond machining system (NANOFORM 200) and nickel electroforming after micro-machining to form a flexible nickel sheet mould that can be wrapped around the roller.[31] They also performed mould replication with UV-curable silicone urethane acrylate photopolymer in order to form thin polymer sheet moulds which could also be wrapped around an aluminum base roller.[31] Thus, Ahn *et al*. reported large area UV roller imprinting of features with both seamed and seamless roller moulds. Figure 2.5 shows an SEM image of their UV roller imprinted pyramid pattern with pitch 50 µm and height 24 µm which can be used as a brightness enhancing optical film for LCD backlighting units. In this case the mould was

both micro-machined and replicated through nickel electroforming. The largest reported features were lenticular lens arrays with a sag height of 47 μm and radius of curvature of 223 μm which were micro-machined directly on the roller.[31] Such features are useful for increasing the viewing angle in projection displays. Other fabricated features include micro-lens arrays similar to earlier work reported by Chang *et al*.[45]

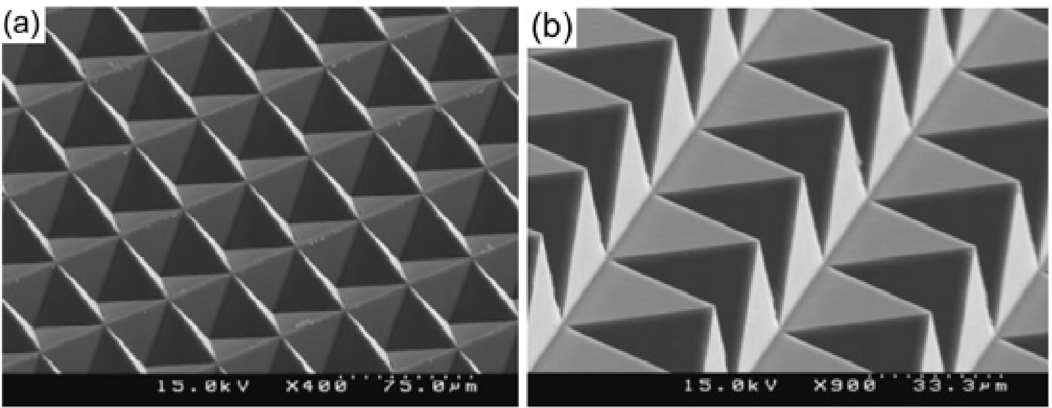

Figure 2.5a) SEM overhead image of an inverted pyramid array nickel shim mould and b) imprinted pyramid array produced from the mould via UV roll-to-roll nanoimprinting in urethane acrylate photopolymer (50 μm pitch, 24 μm height).[31] These structures could be useful as light extraction structures for LEDs and OLEDs. CNC diamond machining, followed by nickel electroforming, was used to produce the mould. Reprinted with permission. Copyright 2007, The Japan Society of Applied Physics.

2.3 Roller & Roll-Mountable Moulds for Resin Mould Manufacturing

In addition to the equipment design, the method of producing the roller or roll-mountable mould for use in UV roll-to-roll nanoimprinting is crucial to successful, high fidelity resin mould production. The roller or roll-mountable mould is a predecessor mould that is replicated via UV roll-to-roll nanoimprinting to produce resin moulds. It can be either a 1st generation master mould if it is a directly written seamless roll cylinder, or it can be a 2nd generation negative relief replica of a master mould written to a flat, rigid substrate

such as quartz or silicon. 2nd generation replica moulds are typically flexible sheet moulds suitable for wrapping around a smooth roller. It is also possible to fabricate the master directly on a flexible sheet, however this is not common because doing so can harm the long range order and the certainty of relative positioning of features that are located far afield, particularly where soft materials are used. For low resolution applications however, even 3rd generation roller moulds have been demonstrated.[46,47] In general though, high strength, high stiffness materials are used for the original master mould, whether supplied as a roll cylinder or as a flat, rigid piece.

The master mould, whether flat or in roll form, can be obtained by both top-down and bottom-up approaches. Top-down methods include beam writing techniques such as e-beam writing,[3-8,106-108] laser lithography,[9,10] interference lithography,[11,12] laser ablation,[13] and mask exposure techniques using UV or synchrotron x-ray radiation.[14-17] Bottom-up approaches include block copolymer self-assembly and growth of porous anodic alumina oxide on flat and curved surfaces.[5,18,19,21,22,109] Most master mould fabrication techniques are designed to pattern flat surfaces. This chapter will not cover in detail all of the techniques or considerations involved in selecting a fabrication approach for a flat master mould as there are myriad high quality texts on this subject available elsewhere. Direct fabrication of cylindrical master roller moulds will be covered later in section 2.3.2.

2.3.1 Sheet Mould Replication Techniques

Flexible sheet moulds suitable for mounting in UV roll-to-roll nanoimprinting systems can be replicated from an original master using a wide variety of techniques, each with its own strengths and weaknesses in terms of throughput and fidelity. In general, however, they can be wrapped easily around a single roller (or multiple rollers in the case of belt

moulds) using mechanical tensioning to minimize slippage. This is the approach used by Fagan *et al.* and Ahn *et al.* among others discussed earlier.[30,31,51] Commonly used sheet mould replication approaches include nickel electroforming,[9] casting,[46,47] and batch mode nanoimprinting (UV or thermal) in the case of polymer sheet moulds.[33,34]

Nickel electroforming produces high strength metallic moulds that are resistant to defect accumulation and the process does not damage the master mould pattern for low aspect ratio masters. This approach is also at a more advanced stage in terms of industrial development than other sheet mould fabrication techniques. Specialized equipment has already been produced to mount nickel electroformed moulds onto rollers and measure the wrapping alignment error and roll radius variation.[65] Furthermore, electroformed moulds can be replicated again by metal-on-metal electroforming so that the master does not need to be employed for all replication cycles. However, the technique suffers from resolution and aspect ratio limitations. Currently, it is difficult to achieve sub-85 nm patterns and aspect ratios greater than 3:1 over large areas, especially for densely spaced features.

Replication by casting is perhaps the simplest and most inexpensive master replication approach because no special equipment is required and because the replication process is typically achieved through polymerization chemistry. Casting techniques generally do not involve the application of pressure against the master mould and thus the risk of damage to the master is minimal so long as polymerized residues can be stripped. A wide variety of pre-polymer resins and polymer solutions can be used in casting, including low surface energy materials like PDMS and fluoropolymers such as Teflon.[66,110] A strong effort in casting replication was made by Hong Lee's group at Seoul National University using poly(urethaneacrylate) (PUA), a UV curable

material.[52,72,111] Moulds fabricated from PUA are called "rigiflex" moulds because they are rigid enough for sub-100 nm imprint patterning and yet flexible enough for conformal contact with the resist and substrate stack. The anti-sticking surface property of their PUA formulation has also been shown to induce de-wetting of low viscosity UV curable resists at room temperature, which could enable residue-layer free roller imprinting.[112]

Figure 2.6 shows the master mould with inset showing the PUA rigiflex mould replicated from it.[52] The master mould is composed of a 70 nm linewidth, 120 nm height, 140 nm pitch grating. However the rigiflex mould exhibits rounded corners and line height of only 90 nm, due to insufficient penetration of the PUA resin into the master mould features as well as an unknown degree of shrinkage. For resin mould production, cumulative shrinkage is the main drawback of producing roll-mounted sheet moulds from a master using thermal curable or UV curable resin casting approaches. This approach will require replicating a resin mould to produce more resin moulds, resulting in a large overall shrinkage, especially if acrylate resins are used throughout. In the present work we employed nickel electroforming to produce roll-mountable nickel shim moulds to minimize shrinkage from the 2nd generation replication of the master mould. Using a low viscosity resin and adequate pressure in a UV roll-to-roll nanoimprinting process, improved fidelity at higher resolution over the abovementioned results was achieved with 3rd generation resin moulds. This will be covered in more detail in Chapter 3.

Replication by batch mode thermal nanoimprinting can significantly improve replication quality on the nanoscale as compared to casting because thermoplastic polymers can be used, which are not subject to curing shrinkage (see also Chapter 3). The application of pressure also works to force the material to conform closely to the master mould features. To replicate resin moulds from thermoplastic polymers, a high modulus, high glass

transition (T_g) material that is inert to the polymerization chemistry used to replicate resin moulds against it is required. The high modulus, high T_g characteristic is helpful to maximize the glassy character of the thermoplastic for the purposes of retaining fidelity to the master for a long period of time with minimal viscoelastic recovery. Fluoropolymers generally fit all these requirements, which is why materials such as ETFE and Teflon are often selected for this application.[33,34,113] Replication by imprinting can also yield some unique structures through partial filling of features on the master as demonstrated by Chang *et al.*[45] For example, Chang was able to fabricate a micro-lens array mould in a polycarbonate sheet by partially filling a silicon master consisting of cylindrical holes. This result could be reproduced with inert fluoropolymers.

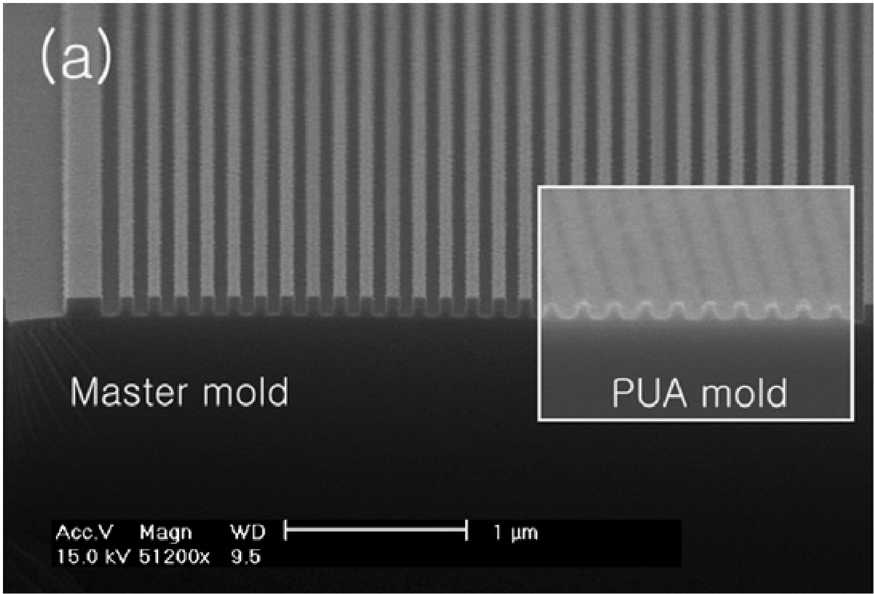

Figure 2.6 SEM cross-section of a 70 nm linewidth, 70 nm height, 140 nm pitch grating master mould in silicon. Inset shows the polyurethane acrylate (PUA) "rigiflex" replicated mould.[52] Rigiflex moulds can be used as roller-mounted sheet moulds in the roll-to-roll manufacture of resin moulds. Reprinted with permission. Copyright 2006, Elsevier B.V.

The chief weakness of master mould replication via batch mode thermal nanoimprinting of thermoplastics is the high pressure that is generally required (at least 10 bars for most

thermoplastics). High pressures place the master at risk to cracking if comprised of a brittle material, as well as damage from hard particles and residues.

Aside from conventional top-down fabrication and replication approaches for production of roll-mountable sheet moulds, there are self-assembly techniques that allow for bottom-up fabrication of sheet moulds with nanoscale resolution. One of the chief advantages of self-assembly approaches is cost. Sheet moulds are inexpensive to produce with most self-assembly techniques relative to top-down methods. However, self assembly is usually limited in terms of the types of structures that can be fabricated and obtaining defect free, long range ordering of structures is difficult. Those structures that can be produced by self-assembly methods, however, can usually access the nanoscale with ease.

The first approach, and the most widely used, is the growth of porous anodic alumina oxide (AAO) nanoimprint masters and flexible sheet mould replication strategies thereof.[20,97,114,115] Well-aligned cylindrical AAO pores can be grown with control over the interpore distance, pore diameter and length by tuning anodization parameters such as voltage, temperature, electrolyte solution composition, and anodization time.[97,116] Nanoscale pores can thus be accessed easily and at extremely high density and aspect ratio. However, anodized alumina surfaces tend to have relatively high surface energy (critical surface tension of ~170 mN m^{-1})[117] and are thus less attractive for use as a roll-mounted sheet mould in the production of resin moulds via UV roll-to-roll nanoimprinting. Instead, nanoporous AAO moulds can be used as inexpensive masters for replication against flexible polymers or electroformed metal sheets with lower surface energy or reduced surface roughness as shown schematically in Figure 2.7.[20,114,115] Importantly, AAO nanopores can be grown over very large area and can even be

integrated into a hierarchical mould where the nanopores cover microstructures produced via top-down methods as shown in Figure 2.8.[21] Such structures can find application in the production of anti-reflection films and coatings, photonic crystals, and nanostructured electrodes for solar cells. They are thus relevant to production scale UV roll-to-roll nanoimprinting for these applications and there is much room for further developments on this topic.

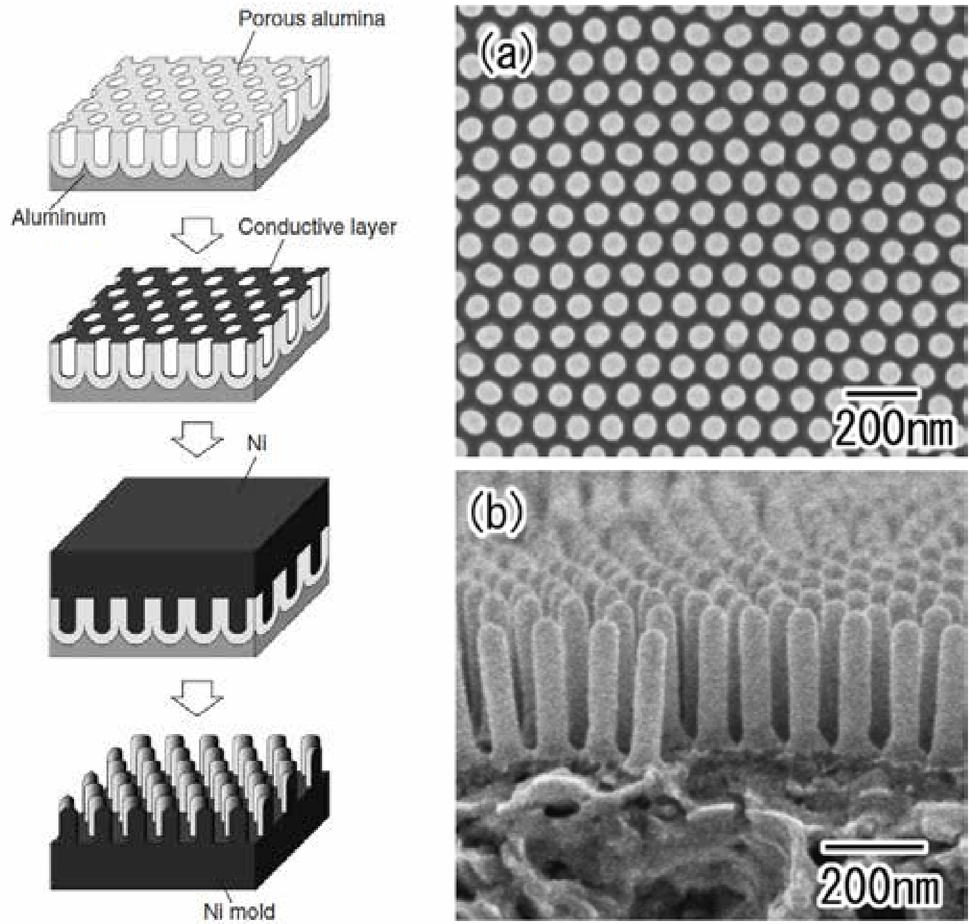

lication process for producing a nickel shim a) Overhead SEM image and b) cross-section spect ratio pillar nickel mould replicated from a nanoporous AAO master. This process could be applied to produce large area, nanostructured resin moulds via UV roll-to-roll nanoimprinting. Reprinted with permission. Copyright 2006, The Japan Society of Applied Physics.

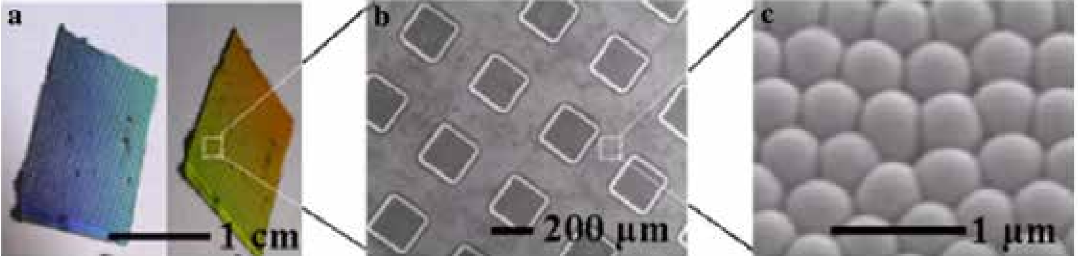

Figure 2.8a) Photo of a hierarchical nickel shim mould replicated from an AAO master covered with patterned photoresist.[21] b) Zoomed out SEM image showing the photoresist generated pattern. c) Zoomed in image showing high density pillars replicated from the AAO master. Copyright 2007, Springer-Verlag.

The other self-assembly technique that can be used to fabricate roll-mountable sheet moulds is based on di-block copolymer deposition and self-organization on relevant substrates.[19,118] Similar to nanoporous AAO, it is well known that the self-assembly of di-block copolymers can access extremely dense and complex nanostructures beyond the reach of top-down fabrication techniques with similar throughput potential. Various techniques have been developed to control the orientation of the nanoscale morphology in the thin film to make it possible for di-block copolymer self-assembly to be used as a template or mask layer for various applications including plasmonics and nanostructured electrodes.[119] Similar to nanoporous AAO, this approach is capable of large areal coverage of high density nanostructures, but with limited feature types. Hui Joon Park *et al.* developed an indirect method of fabricating nanoimprint moulds on arbitrary substrates by dry etching poly(styrene)-*block*-poly(methyl methacrylate) (PS-*b*-PMMA) di-block copolymer to form a soft polystyrene mask upon which they performed a chromium deposition at an angle (i.e. shadow evaporation) to form a hard mask.[118] With a Cr hard mask, Park was able to etch high density 20 nm diameter holes into an SiO_2 layer grown on a silicon substrate at an aspect ratio of ~7.5. This feature aspect ratio is far greater than what can typically be achieved by using the self-assembled polystyrene mask to directly etch into oxide. Soojin Park *et al.* successfully demonstrated di-block

copolymer self-assembly of poly(styrene-*b*lock-ethylene oxide) (PS-*b*-PEO) on flexible polymer substrates cast or imprinted against a sapphire master pattern.[19] Figure 2.9 shows their unique fabrication result. They were able to hierarchically pattern PS-*b*-PEO cylindrical nanodomains across replicated sawtooth grooves from the sapphire master, thus obtaining a hierarchical nanostructure on an inexpensive, flexible substrate. By combining the above described approaches, it should be possible to obtain hierarchically structured, high aspect ratio flexible sheet moulds for roller imprinting purposes.

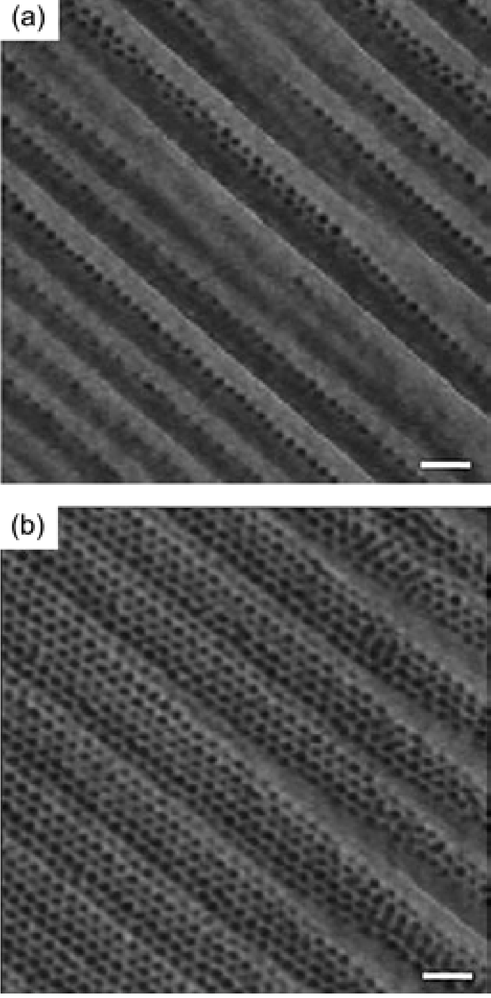

Figure 2.9 Scanning force microscopy (SFM) images of PS-*b*-PEO self-assembled films at different film thickness on patterned poly(butylene terephthalate) substrates replicated from faceted sapphire (pitch: ~130 nm, amplitude: ~15 nm).[19] The PS-*b*-PEO microdomains derived from film thicknesses of a) 23 nm and b) 29 nm are shown. A hierarchically structured surface was obtained which, with additional processing steps, can be used to fabricate sheet moulds for UV roll-to-roll nanoimprinting. Reprinted with permission. Copyright 2010, WILEY-VCH Verlag.

2.3.2 Seamless Roller Mould Fabrication Techniques

The key drawback of wrapping sheet moulds onto a roller is the seam that is left which will place discontinuities in an otherwise continuous resin mould film. For many applications involving discrete devices, such as displays, pattern discontinuity is acceptable. It is fairly straightforward to select the imprint roller diameter and the seam width such that the resin mould surface area is matched to the size requirement for the final device. UV roll-to-roll nanoimprinted resin moulds could then be cut out and used separately in device manufacture, or used as-fabricated in reel form. For some applications, such as anti-reflective films and coatings however, it may be difficult or impossible to make the roller mould surface area larger than what is required for the end use. It may also be difficult to accept the loss of patterned area implied by the seam for cost reasons, particularly if the substrate web material is expensive to produce. For such applications it is important to achieve seamless roller imprinting to maximize the patterned surface area of the resin mould.

Attempts have been made to adapt top-down lithography techniques for flat surfaces and direct them toward the fabrication of roller moulds. It is noteworthy that to date, only beam writing and self-assembly techniques have been reported to achieve consistent, high fidelity nanoscale or near-nanoscale patterns on curved surfaces and cylinders.[6,8,19,22,106-109] For mask exposure techniques such as photolithography, it is difficult to achieve uniform exposure onto a photoresist coated roller. The curvature of the roll cylinder generally requires multiple exposure shots if the light is emitted from a flat rectangular window, and this can generate overlap between exposure fields if streets between fields are undesirable. The angle of incident photons on curved surfaces can also change from one exposure site to the next, and control over reflected light is considerably more

difficult. This can make it difficult to etch nanoscale features onto a roller with adequate fidelity and acceptable CD tolerances. However these known issues have not deterred recent efforts to demonstrate lithography via mask exposure, development and etching of roll cylinders, albeit only for micron scale structures.[15,17] Huang *et al*., for example, combined stepped rotating lithography and electroless nickel plating onto a photoresist coated roller using a a rotation stage with a flat photomask and a UV-LED light source as shown in Figure 2.10.[15] Plated nickel features on the roller could then be used directly in a UV roll-to-roll nanoimprinting process without the added complexity of etching steps. With this setup the smallest reported features were line and space structures with line width of 23 μm, 1.1 μm height and 57.5 micron pitch.

Figure 2.10 Stepped rotating photolithography apparatus shown with rotation stage, roller and photomask plate for the production of seamless roller moulds applicable for use in UV roll-to-roll nanoimprinting.[15] The rotation stage is used to place each region to be exposed directly under the photomask. Each region on the photomask is exposed onto the resist coated roller in a serial process with a UV-LED light source. Reprinted with permission. Copyright 2009, Elsevier B.V.

Jiang *et al.* also used a UV photolithography approach to pattern copper rollers with a dry film resist around the roller and a flexible photomask wrapped around the roller prior to UV exposure on a rotating stage.[17] A ferric chloride wet etch was employed to obtain

200 μm wide grooves in the copper roller. This approach is simpler than that of Huang *et al*. but the dry film resist will leave a seam which will appear on the roller if this technique is used to fabricate densely spaced patterns.

Several beam writing techniques have also been adapted to fabrication of mould features directly onto rollers through a similar approach of mounting the roller onto a precision rotation stage and designing the beam writing apparatus around it. The smallest features fabricated to date were achieved by Saito and Tanaguchi by electron beam lithography against a ZEP520A positive e-beam resist dip coated aluminum roller.[106] E-beam writing followed by development of 520,000 exposed resist dots was carried out as shown in Figure 2.11 to obtain the roller mould. Dot length varied depending on controlled exposure dose, within a fixed range from 190 – 420 nm after development and vacuum deposition of chromium. This led to an approximately linear relationship between exposure dose in μC cm^{-2} and dot length on the roller shown in Figure 2.12 (exposure times are shown in image captions). As the chopped electron beam exposed the resist coated roller while it was rotating at 0.5 m min^{-1}, the higher exposure doses (longer exposure time with constant beam intensity) yielded longer dots. The highest resolution results also highlighted issues with the movement precision of the rotation stage, which is a very important area for further development with all beam writing techniques. Elimination of rotational wobble and velocity changes during beam exposure will be crucial to reducing feature pitch tolerances.

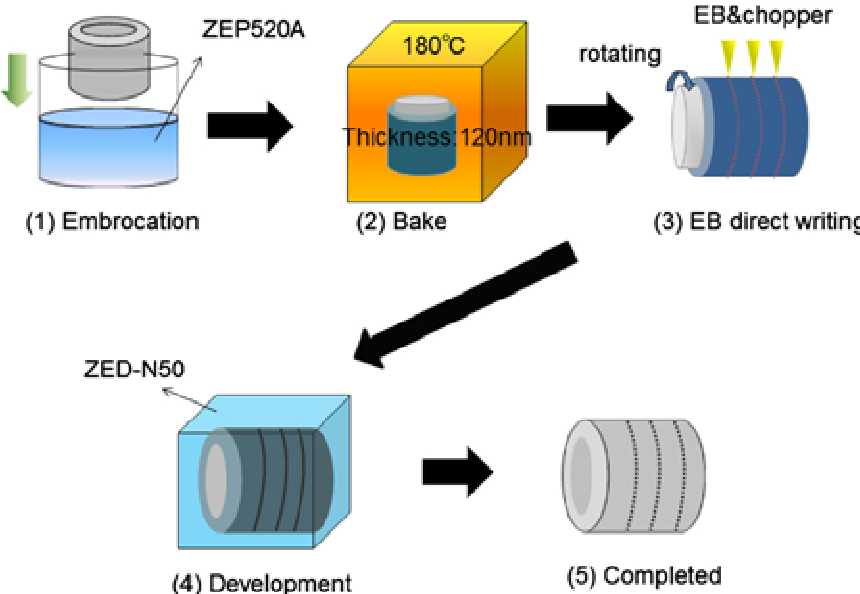

Figure 2.11 Process schematic showing fabrication of a seamless roller mould by dip coating, e-beam writing and resist development.[106] A Cr layer was then deposited by vacuum evaporation using a rotation stage, followed by a lift-off process to reveal high density Cr dots. The use of evaporated metal nanostructures to comprise the roller mould is an increasingly popular way to avoid vacuum etching of the roller itself. Reprinted with permission. Copyright 2014, Elsevier B.V.

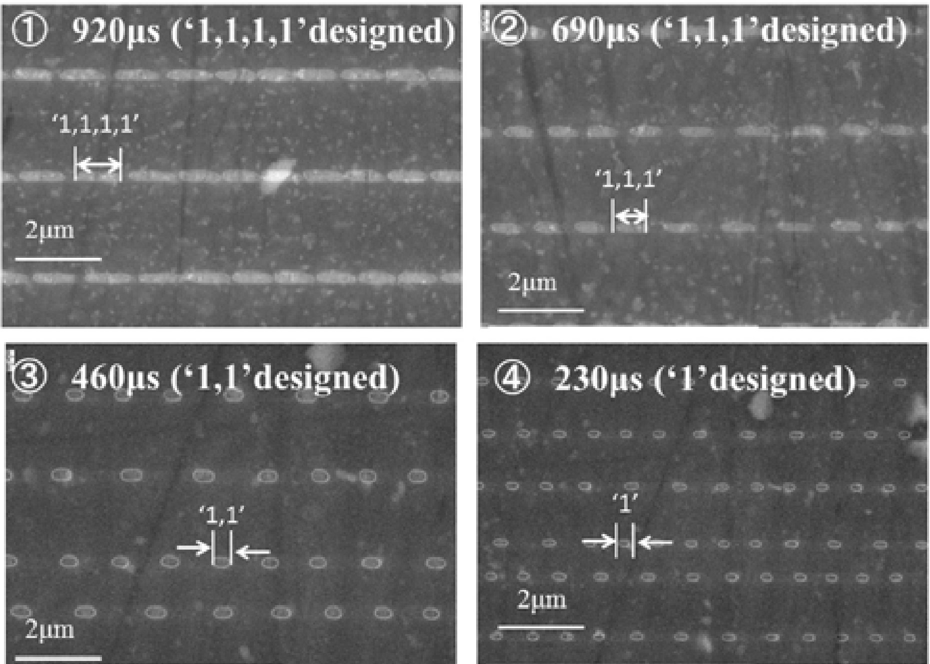

Figure 2.12 SEM overhead views of various Cr nanodot patterns fabricated on an aluminum roller.[106] The image captioning indicates the beam exposure duration before chopping. Longer exposure time while the cylinder is rotating results in smearing of the dots as shown in (1) and (2). The minimum dot diameter obtained in (4) was 190 nm.

Other beam writing techniques adapted for roller mould fabrication include laser lithography of resist coated rollers at 680 μm resolution, as reported by Uh *et al*.[10] Wang *et al.* studied laser ablation of steel foils and magnetron sputtered iron films on fused silica imprint rollers using a Ti:sapphire laser system.[13] Wang was principally concerned with the profile of ablated features, which tend to take on the Gaussian profile of the incident beam, displaying trenches with curved surfaces. In addition, the sidewall draft angle of the ablated features can vary considerably depending on the incident angle of the beam relative to the roller surface. In order to fabricate trenches with vertical sidewalls and flatter bottom profiles, Wang utilized a two-step inclination ablation process. Specifically, the laser beam was passed over the same region twice but from the opposite angle on the second pass in order to fabricate each sidewall individually and create a level trench floor. Figure 2.13 shows AFM scans showing each step of a two-step ablation of a ~1 micron wide trench in an iron film. Note the improved cross-section profile of the trench bottom after the second pass, which appears as a convolution of two ablated Gaussians forming the corners of the trench. While laser-based approaches generally cannot be used to machine nanoscale features because of limitations imposed by the beam wavelength, two-step inclination ablation can be used to fabricate a variety of different microstructures of different shapes and sidewall taper.

To date there has been very little reported in the academic literature on seamless roller mould fabrication using self-assembly approaches. However there has been some activity in the patent literature. Yang *et al.* in their patent describes a method of growing anodic alumina oxide nanopores onto cylindrical surfaces using a scanning graphite cathode.[109] They claim that by limiting the size of the cathode in relation to the cylindrical roller anode, that the electric field can be kept sufficiently uniform for uniform pore growth. In addition, dip-coated or dry film photoresist patterning can be

used to define the field size so that the pores do not taper off, forming a defective region at the field edges. In addition, different fields can contain different pore sizes and pitch by varying the voltage, temperature or anodization time. However, a single field requires several hours of anodization time for sufficient pore growth, therefore fabrication of a large roller mould by stepped growth of porous AAO is expected to be time consuming.

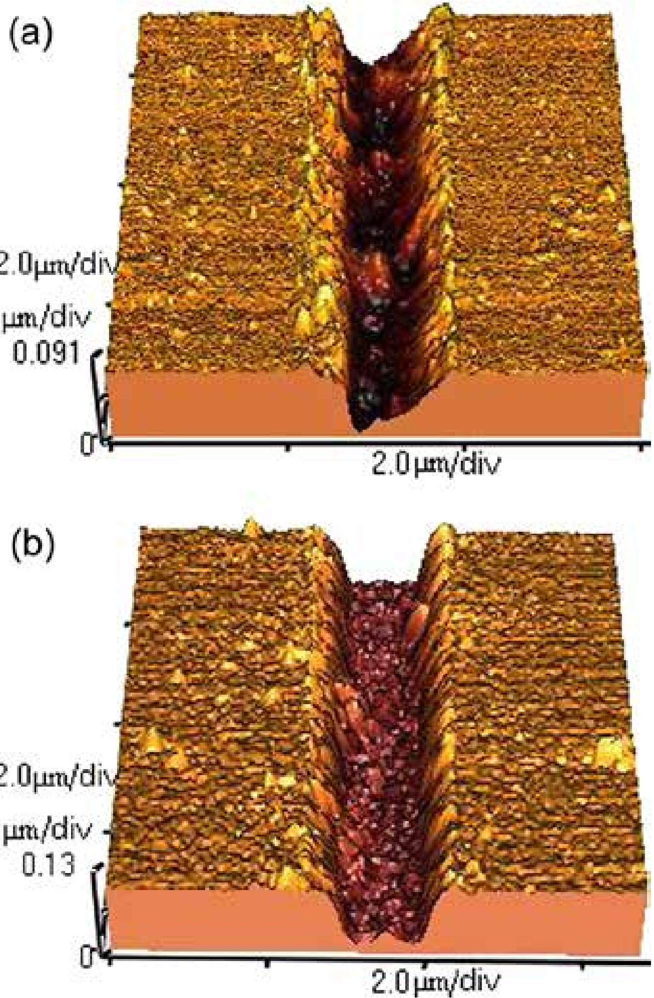

Figure 2.13 AFM scans of a ~1 µm wide trench formed by two-step inclination laser ablation of an iron film sputtered onto a fused silica cylinder.[13] The laser scan speed was 0.16 mm s^{-1} at 10.7 nJ and the inclination angle was 75º. a) First inclination ablation showing sidewalls with differing draft angles. b) Final trench profile after the second inclination ablation. The sidewalls now have approximately the same draft angle. Reprinted with permission. Copyright 2008, Springer Science+Business Media B.V.

2.3.3 Soft Material Approaches to Seamless Roller Mould Fabrication

It has been shown that various conventional top-down beam-writing and exposure techniques can be adapted to the seamless fabrication of features directly onto a metallic roller by use of a precision rotation stage. Stage wobble and slight variations in rotational velocity, resulting in large feature pitch tolerances is one of the key challenges with respect to these seamless roller mould fabrication approaches, particularly for beam writing. One way to get around this technical barrier is a method proposed by Chang *et al.* and Yang *et al.* for the fabrication of micro-lens arrays.[46,47] They first fabricated a rigid mould in silicon with an array of micro-holes which they replicated in polycarbonate using gas-assisted hot embossing. Under proper gas pressure, the polycarbonate is partially filled into the holes, forming a convex micro-lens array due to surface tension. The patterned polycarbonate sheet is then employed in a casting step to form the patterned roller as shown in Figure 2.14. Starting with a featureless silicone or aluminum alloy cylinder with an inset depression around its circumference, the polycarbonate film is wrapped onto the cylinder to form a roller with a hollow shell cavity. Viscous PDMS pre-polymer is then poured into the hollow shell cavity of the roller. After curing of the pre-polymer, the polycarbonate film is peeled off from the PDMS material leaving a soft PDMS roller with a micro-lens cavity array. The microlens array cavities they fabricated had a diameter of ~150 µm, a pitch of ~200 µm and a depth of ~30 µm. This micro-lens cavity roller mould can be immediately used to fabricate resin mould equivalents in UV curable resin. This approach to seamless mould fabrication is quite innovative because the master mould features are fabricated with high precision onto a rigid flat mould, replicated onto a flexible polymer sheet mould and then replicated again to form a roller mould. This gets around dimensional tolerance issues associated with writing features directly onto the roller at the possible expense of fidelity

loss due to the larger number of replication steps needed to obtain the roller mould. In addition, the sheet mould is peeled off and is not left wrapped onto the roller, so there is no visible seam. However, the patterns on the roller are still replicated from a wrapped sheet mould, as such the area where the two ends of the sheet mould are joined will have no pattern. For features with large spacing between them, this approach can produce a truly seamless roller with proper alignment of the sheet mould ends, because the joining region with no pattern can simply occupy the space between features. However the seam gap will be noticible for densely spaced features.

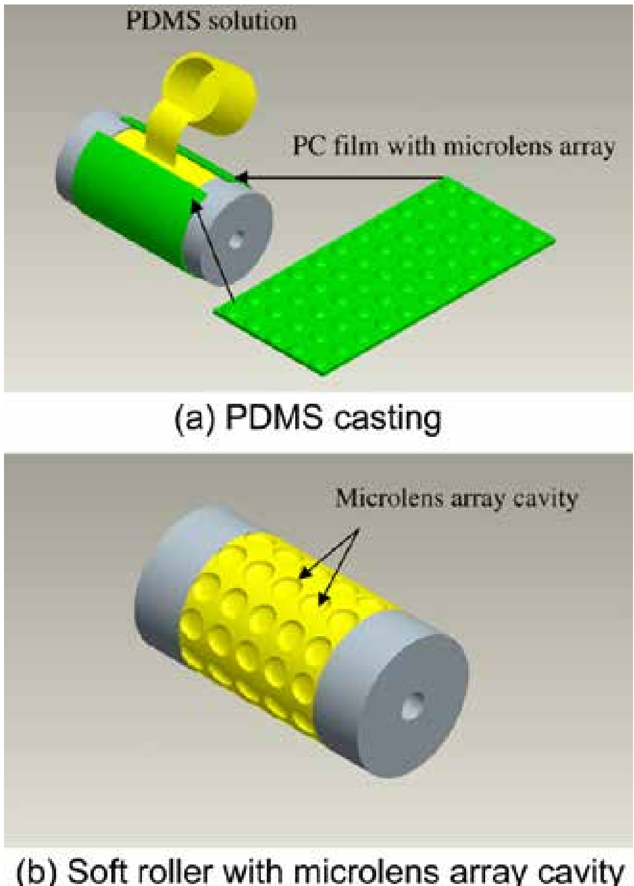

Figure 2.14 Procedure for fabricating a soft PDMS roller with an array of microlens cavities using a polymer sheet mould replicated from a rigid master.[46] a) The polycarbonate sheet mould containing an array of microlens structures is wrapped around a silicone or aluminum alloy cylinder with an inset depression around its circumference. PDMS pre-polymer is poured into the hollow shell cavity as shown. b) After curing of the PDMS, the polycarbonate film is peeled off leaving a soft PDMS roller with a micro-lens cavity array that can be employed in a UV roll-to-roll nanoimprinting process. Reprinted with permission. Copyright 2007, Elsevier B.V.

Another approach toward fabrication of a soft seamless roller mould was proposed by Hwang *et al.* where again a master mould with an array of sub-micron dots was fabricated in silicon, replicated in a polyvinyl alcohol (PVA) sheet which was then wrapped around a glass roller coated with UV curable methacryloxypropyl terminated poly-dimethylsiloxane (mPDMS).[120] UV light was exposed through the poly-vinyl alcohol sheet mould to cure the mPDMS on the roller, after which the PVA sheet mould was dissolved off in water, leaving the replicated mPDMS features on the roller. This approach is very similar to the PDMS casting approach discussed earlier, however dissolution of the PVA sheet mould precludes the need to peel it off, thus eliminating certain classes of defects which arise upon peel separation.

2.4 Concluding Remarks

Currently there are is a large variety of UV roll-to-roll nanoimprinting equipment, as well as roller and roll-mountable sheet mould fabrication techniques being developed that are compatible with resin mould production. As far as equipment is concerned, the main consideration is with how the resin is coated, spread and cured against the substrate backing web. To that end a variety of coating techniques are being developed in order to expand available options to manufacturers, including gravure,[33-35] slot die,[121] and inkjet printing methods.[32] Gravure and slot die coating are generally used to apply a coating over the entire web surface, and their low degree of control over resin consumption rate is offset by the wide range of resin viscosities they are compatible with. Thicker (~10 micron and above), higher viscosity coatings are often applied with these methods. For lower viscosity resins (< 50 mPa·s), inkjet printing is gaining a foothold in the field due to its high level of control over dispense volumes and drop positioning.[32] A drop map can be constructed and dispensed to match (with proper alignment) resin availability with

variations in cavity volume and density across the mould surface. This can allow for very tight control over the residual layer thickness uniformity. Moreover, inkjet printing modules are able to dipsense precisely where needed and can leave the feed substrate blank elsewhere, which can assist with conserving expensive resins for low coverage density applications. In terms of spreading and curing, use of doctor blades, spreading rollers, and mercury-arc UV lamp curing is prolific with little variation in approach.

There are additionally a large variety of techniques being developed to fabricate roller and roll-mounted moulds that are otherwise compatible with resin mould production via UV roll-to-roll nanoimprinting. They fall into two broad categories: replicated sheet moulds that can wrapped around an imprint roller, and seamless roller mould fabrication via direct writing of features onto the imprint roller. With sheet moulds the key advantage is immediate access to nanoscale features. However good adhesion between the sheet and the imprint roller, whether it be by mechanical tensioning or use of adhesives is important to avoid slippage that can damage mould features. It can also be difficult to properly align the features on the sheet mould with the rotation axis of the roller without specialized wrapping equipment.[65] Misalignments will slant imprinted fields relative to the substrate web unless the web is steered to compensate.

Of course, slippage and mounting issues are all surmountable technical challenges. Burgeoning efforts to fabricate features, particularly sub-micron and nanoscale features, directly onto the roller are principally driven by the attractiveness of seamless UV roll-to-roll nanoimprinting. For densely spaced features only beam writing, mask exposure, and self-assembly techniques have thus far been reported to achieve a truly seamless product with sub-micron structures. The major challenge for beam writing approaches is the difficulty in controlling feature pitch when exposing a rotating cylinder, which is difficult

as production scale metallic rollers tend to have considerable inertia and require large forces to move and these forces are difficult to manipulate with nanoscale precision.

Self-assembly techniques, although limited in terms of the types and positioning of features that can be formed on a given surface, are one way to fabricate seamless roller moulds for resin mould manufacturing directed toward applications suited to these features. Self-assembly also has the advantage of being relatively inexpensive to implement in terms of equipment and processing. The major challenges faced in this area are the well known difficulties in achieving long-range ordering of self-assembled features as well as a lack of direct control over defects generated during the assembly process. For block copolymer self-assembly, the development of a reliable large-scale dip-coating method that can produce a uniform coating with low defect-density and long-range order is essential. With nanoporous AAO, there is also a need to improve the fabrication speed, as presently the throughput is too slow for large area aluminum roller anodes when using small cathodes.[109] The precision engineering of a large tubular cathode that could be placed around the aluminum roller with a matching curvature could be one way to address the known throughput limitations.

Chapter 3. Fabrication of UV Roll-to-Roll Nanoimprinted Resin Moulds

In previous chapters we provided an overview of UV roll-to-roll nanoimprinting, equipment and roller mould fabrication techniques compatible with the production of resin moulds. In this chapter we will describe our approach, materials selection and considerations specific to resin mould fabrication against cylindrical surfaces.

UV roll-to-roll nanoimprinting of resin moulds remains a relatively unexplored field of engineering but holds great promise to dramatically reduce the cost of nanolithography for myriad applications. While studies on the performance and applications of soft, flexible resin moulds have been published in the literature using batch mode UV nanoimprinting (UV NIL) as the chosen fabrication technique,[24,26,71] similar reports utilizing UV roll-to-roll nanoimprinting are lacking. However, UV roll-to-roll nanoimprinting is both fundamentally different from batch mode UV NIL and capable of drastically higher throughput. This study highlights these differences, particularly in terms of potential throughput, differences in the nature of the imprint stack and the working surfaces involved. This study also makes use of extremely low cost disposable resin moulds in subsequent batch mode thermal nanoimprint lithography (thermal NIL).[1,24,72] Thermal NIL is one of the early contact lithography techniques discovered in the late 1990's and is well understood for rigid mould and substrate materials.[1] Often the master mould itself or a 2nd generation negative relief replica of the master are used to emboss a thin film of resist on a flat substrate (See Figure 1.1).[57] However, no thermal NIL studies have been done using flexible resin moulds that are 3rd generation "copies-of-a-copy" of the master and where the resulting embossed film is even a 4th generation replica.

At this level of abstraction from the master mould, the method or methods used to replicate each successive generation becomes important. Replication defects and critical dimension (CD) losses are transmitted cumulatively from generation to generation. Surface roughness, or (at low frequencies) surface waviness will also be imparted additively from generation to generation. Importantly, polymerization shrinkage from multiple replication generations employing UV or thermal curing resins is also additive in terms of feature height losses, corner rounding and sidewall tapering.[26,37]

In order to understand the benefit of using thermal NIL for manufacturing applications with resin moulds, it is important to note that production of resin moulds by UV curing methods necessarily entails at least one replication generation from the master mould that will input polymerization shrinkage into the final pattern in the device or resulting product patterned with the resin mould. Readers may refer to Figure 1.11 in Chapter 1 for the generalized process flow from the master mould, to resin mould fabrication via UV roll-to-roll nanoimprinting, to the final device or end product. In the present work, there are two intermediary replication generations between the master mould and the thermal NIL step to obtain the final pattern. A flexible sheet mould (2nd generation) was copied from a flat master, wrapped onto the imprint roller in our UV roll-to-roll nanoimprinting system, and used to fabricate resin moulds on a flexible web line (3rd generation). Here, while it is possible to carry out both replication generations via resin polymerization methods, doing so will result in what we refer to as cumulative polymerization shrinkage from all such steps.[72] On the other hand, thermal NIL utilizes solid thermoplastic imprint media that are not subject to polymerization shrinkage, but instead suffer a much smaller compression shrinkage that can be attributed to free volume losses. For example, the compression shrinkage coefficient for polymethyl methacrylate

(PMMA) is ~5.51 x 10^{-11} per Pa.[122] Under ordinary batch mode thermal NIL process pressures, the compression shrinkage was calculated at only ~0.07%.[123] This is two orders of magnitude less than typical volumetric curing shrinkages of ~8-15% for UV acrylic resins,[124] ~6% for cationic epoxysilsesquioxanes,[82] and ~1-4% for cycloaliphatic epoxides and hybrid formulations.[124] Thus thermal NIL is well suited for use with resin moulds in the manufacture of patterned devices where best possible fidelity to the master is required without sacrificing the benefits of low cost nanolithography with resin moulds. Such potential applications include nanofluidic devices, nanostructured electrodes for solar cells, nanostructured surfaces for biomedical devices, high density data storage media, and electronics.

Another point worth mentioning regarding the synergy between inexpensive, disposable resin moulds and thermal NIL relates to mould damage imparted by the latter. Thermal NIL is often criticized for damaging conventional rigid mould materials due to imprinting of particles and residues under the large applied pressures commonly employed.[125,126] Moreover, if the mould and substrate comprising the imprint stack are rigid materials with strongly differing thermal expansion coefficients, stresses can build up during thermal cycling that are capable of putting defects into the imprinted pattern or even cracking brittle mould materials such as silicon.[33,127] Thermal NIL with a resin mould is a solution to these challenges for various reasons. First, of course, the low cost and excellent availability of resin moulds produced by UV roll-to-roll nanoimprinting allows for easy replacement in case of damage. Second, the conformal nature of resin moulds will prevent the defective area imparted by an imprinted particle from being much larger than the particle itself. Finally, because resin moulds are comprised of polymeric materials, they can also overcome mould damage and systemic defects related to thermal

expansion mismatch during temperature cycling.[127,128] Resin moulds do not fail in brittle fashion and will have thermal expansion coefficients that are generally of closer similarity to thermoplastic NIL resists than rigid, inorganic mould materials.

Finally, resin moulds can also be peel separated with ease after a thermal NIL step. Doing so generally does not damage imprinted features with reasonable aspect ratios, whereas rigid moulds must be vertically separated, requiring a large applied separation force. In this study, fabricated resin moulds obtained an aspect ratio ranging from ~0.3 – 1 at resolutions down to sub-50 nm.

There are two basic production formats utilizing resin moulds in a batch thermal NIL process. As mentioned briefly in Chapter 1, one form factor involves use of the fabricated resin mould reel directly, where the resin mould is passed through the thermal NIL tool as a continuous feed from an unwind reel to a rewind reel, similar to what has been reported for UV NIL.[100] This resin mould form factor can be produced separately or in-line with the thermal NIL tool that utilizes the resin mould reel. Either model has the benefit of easy replacement of the resin mould by simple winding of the resin mould reel, however the thermal NIL tool would have to be custom-built to handle a continuous feed. In the present work, resin moulds are segmented out from the substrate web reel for use individually, which is an alternative form factor that requires more manual handling but is widely compatible with most thermal NIL equipment.

3.1 Materials & Methodology

Table 3.1 provides a listing of the materials and equipment used by our group to demonstrate high resolution UV roll-to-roll nanoimprinting of resin moulds with mixed nanoscale structures. The master mould selected was a 2.5" (84 mm diameter), 300 µm thick discrete-track recording (DTR) hard disk with 100 nm pitch concentric data tracks.[5,129] Since the master was a rigid disk and not in a rectangular format necessary to be mountable onto a cylindrical imprint roller, a process of metal-on-metal electroforming was employed using a commercial plating system (Microform 200, Technotrans) to produce a flexible nickel replica mould with desired thickness and extended dimensions.[9] Nickel electroforming was selected to replicate the master first for its convenience because the master was already conductive, but also because CD losses with conductive masters are negligible on the electroformed copy. Moreover, the technology is very well understood and can obtain defect-free results.[15,42,65] As was discussed previously, these considerations are important for 3rd and 4th generation replications of the master.

A custom-built mounting jig was used to enable fabrication of a 300 µm thick negative relief copy of the master template via nickel electroforming across an extended area of up to 200 mm diameter. Electrodeposition was performed using a nickel sulfamate bath solution without organic additives at pH 3.5, 50 °C bath temperature, and forward DC current density of 11.4 A/dm^2, equivalent to a growth rate of 2.35 µm/min. After manual delamination, the replica is cleaned with acetone, DI water and dried with an N_2 gas jet. Subsequently, the negative replica was used in a 2nd metal-on-metal electroforming step under similar bath conditions to produce the final nickel mould piece. Final laser-cut nickel shims were obtained with rectangular dimensions of 160 x 75 mm (120 cm^2) and

100 - 200 µm thickness. Figure 3.1 shows the entire production scheme from the nickel-on-nickel electroforming stage to final results.

Table 3.1 Materials & equipment used to demonstrate high resolution resin mould fabrication via UV roll-to-roll nanoimprinting.

	Parameter
Mould	2nd generation nickel shim (nickel-on-nickel electroforming)
Resin	YNIL-R2-2 (Young Chang Chemical)
Web	Lexan 8010 Polycarbonate (100 m length, 200 mm width, 125 µm thickness)
Mode of Dispense	Inkjet Print Head (65 mm width)
Droplet Volume	30 pL
Inkjet Dispense Frequency	10 kHz
Spreading Roller Pressure	400 kPa
UV Source	Mercury-Arc Lamp (405 nm h-line peak)
UV Source Intensity	80 W cm^{-1} peak output

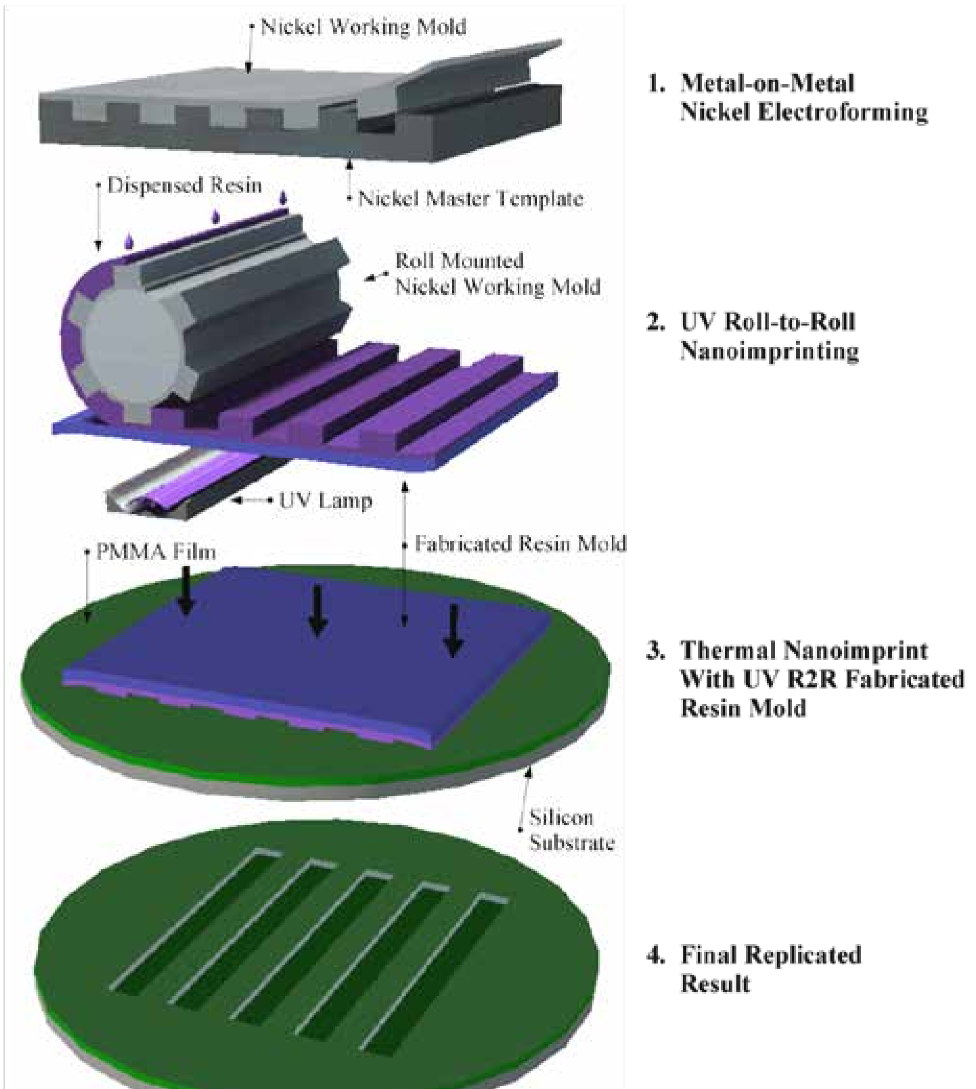

Figure 3.1 Process schematic detailing the major steps in producing high resolution resin moulds via UV roll-to-roll nanoimprinting, followed by demonstration via batch mode thermal NIL. The master mould is copied via nickel electroforming to produce a robust and flexible roll-mountable nickel shim. UV roll-to-roll nanoimprinting is used to copy the nickel roll-mounted mould into a flexible resin mould, which in turn is used in batch mode thermal NIL to produce high fidelity nanostructures in PMMA on silicon.

These nickel replica moulds were mounted in a custom-built SRS 300 UV roll-to-roll nanoimprinting system (Solves Innovative Technology) as shown in Figure 3.2a. A stainless steel slot mounting imprint roller is utilized where discrete sheet moulds of a predetermined size can be mechanically fixed by screws to a mount piece (Figure 3.2b).

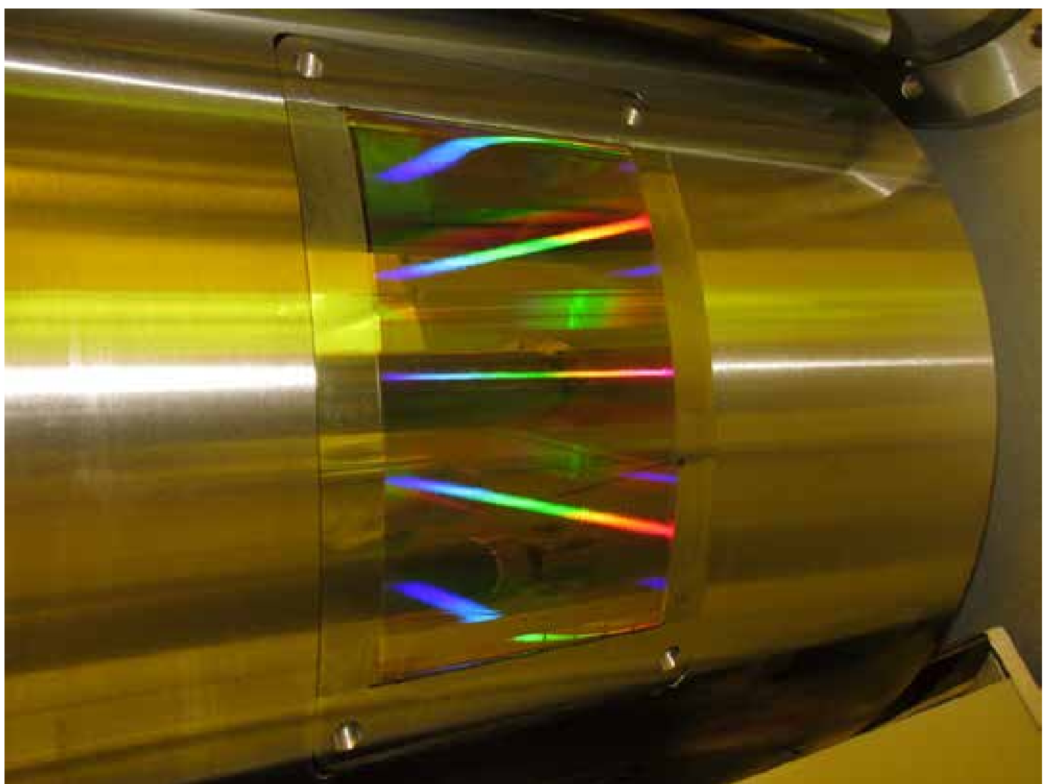

Figure 3.2a) Photograph of SRS 300 UV roll-to-roll nanoimprinting system. b) Photograph of a nickel sheet mould mounted via mechanical fixation onto a slot mount piece fitted into the imprint roller installed with the SRS 300. The imprint roller itself has a diameter of 340 mm and width of 300 mm and total surface area much greater than the total mould area. This is to allow for future expansion in mould size.

The slot mounting imprint roller is capable of mounting sheet moulds sequentially or in parallel, in addition to wrapping around the whole of the imprint roller for research and development purposes as well as applications where seams or dead space are not an engineering constraint.[42,49,65] For our purposes, the desired form factor of the resin mould was of a discrete size, so use of sheet roll-mounted moulds was an intuitive choice. Moreover, sheet mould mounting is typically more practical and cost effective for research and development purposes than employment of seamless roller moulds. It is also worthwhile to note that switching from sheet moulds to a seamless roller mould for manufacturing purposes should not produce any significant technical differences in terms of processing or capability, so long as the mould material, surface properties and mould contour are the same. For representative results to be obtained at the center region of the imprint result, the sheet mould simply needs to be large enough such that edge-related defects do not affect this region.

UV curable resin was dispensed with a 65 mm wide Dimatix Sapphire QS-256 / 30 AAA inkjet dispense head consisting of a line of 256 piezo-controlled nozzles with 30 pL minimum drop size. YNIL-R2-2 resin from Young Chang Chemical, a 10 mPa·s viscosity resin optimized for inkjet dispense was used for these experiments. This transparent UV acrylic resin absorbs strongly at 405 nm H-line. As mentioned briefly in Chapter 1, an acrylic resin was selected because free radical polymerization, which acrylic resins are based on, exhibits the fastest polymerization rates among UV nanoimprint resins. In addition, the curing shrinkage inherent to acrylic resins has the ancillary benefit of promoting clean mould release.

During fabrication, the resin is dispensed as a discontinuous array of drops: 256 lines with a pitch of 250 μm and drop density within the lines dependent on the operating frequency of the dispense head (up to 33 kHz). The resin is dispensed onto the mould, as opposed to the more conventional approach of dispensing onto the web.[30,31] This allows the dispense head to be aligned and fixed over the mould and fire precisely when the mould passes underneath, eliminating the need to align a drop field on the web with the mould during operation. Because the volume of each dispensed drop is very small at 30 pL, the weight of each drop is insufficient to overcome its surface tension while the imprint roller turns, such that the drops will not shift position before the drop field reaches the spreading rollers. The spreading rollers bring the mould carrying the drop field into contact with the substrate web under a pressure of 400 kPa, causing the drop field to merge into a continuous film that fills in the mould cavities. The spreading rollers are composed of a soft polyurethane rubber that provides conformal contact and improves coating uniformity while squeezing out ambient gas. The substrate web selected for this study was Lexan 8010 polycarbonate in the form of 100 m long, 200 mm wide reels of 125 μm thick film. This material forms an excellent bond with all UV acrylic resins our group has tested, such that deposition of an adhesion promoter coating on the film surface is unnecessary. Avoidance of web-deposited adhesion promoters is ideal for manufacturability because it keeps feedstock costs low. Polycarbonate is also widely available in reel form, fully transparent to the visible light spectrum and at least partially transparent to UV-A (315 – 400 nm) and thus suitable for UV exposure through it. Finally, polycarbonate has relatively high glass transition and melting temperatures ($T_{g,}$ 147 °C, T_m 155° C) suitable for batch mode thermal NIL of lower T_g materials such as PMMA (T_g 105 °C) at process temperatures below 155° C. As for the nickel shim mould, it was found unnecessary to lower its surface energy via application of a self-

assembled monolayer (SAM) anti-stick coating, so long as the feature aspect ratio was approximately below 3. The nickel will ultimately obtain an adsorbed coating of resin molecules that serve to lower its surface energy and promote release in peel mode. Note that avoidance of SAM anti-stick coatings for both roll-to-roll and batch mode UV NIL is important because the former degrades in the presence of photo-initiated radicals in the resin and cannot withstand more than a few tens of imprint cycles.[63,64]

Once the resin is spread between the mould and the substrate web, it is cured through the web by a broad spectrum UV mercury-arc lamp (80 W/cm power rating). Separation of the mould from the cured resin imprint is assisted by a deflection roller and an applied web tension of 15 kg on the web feed. Use of high web tension and relatively thick web materials helps to minimize the peeling angle of the cured resin imprint field from the nickel shim roller-mounted mould, reducing the shear stresses on the imprinted features, and thus reducing the likelihood of feature deformation and breakage on separation. Fabrication, peel separation and rewinding of UV roll-to-roll nanoimprinted resin moulds occurred at 10 m min^{-1}.

3.2 High Resolution Resin Mould Fabrication Results

Unlike with polymer moulds fabricated via batch mode processing, exploratory studies at sub-50 nm resolution and with mixed micro- and nanoscale structures utilizing UV roll-to-roll nanoimprinted resin moulds have been sparse. Figure 3.3a shows the nickel DTR hard disk nickel mould after ~10 imprint cycles and a photoresist strip bath to clean off particles and residues. Specifically the figure shows an inverse servo pattern containing a variety of sub-micron and nanoscale mixed features, the top half being the gray code and

bottom half an array of 100 nm diameter holes, known as a burst area. Figure 3.3b shows the replicated YNIL-R2-2 resin mould with good replication fidelity.

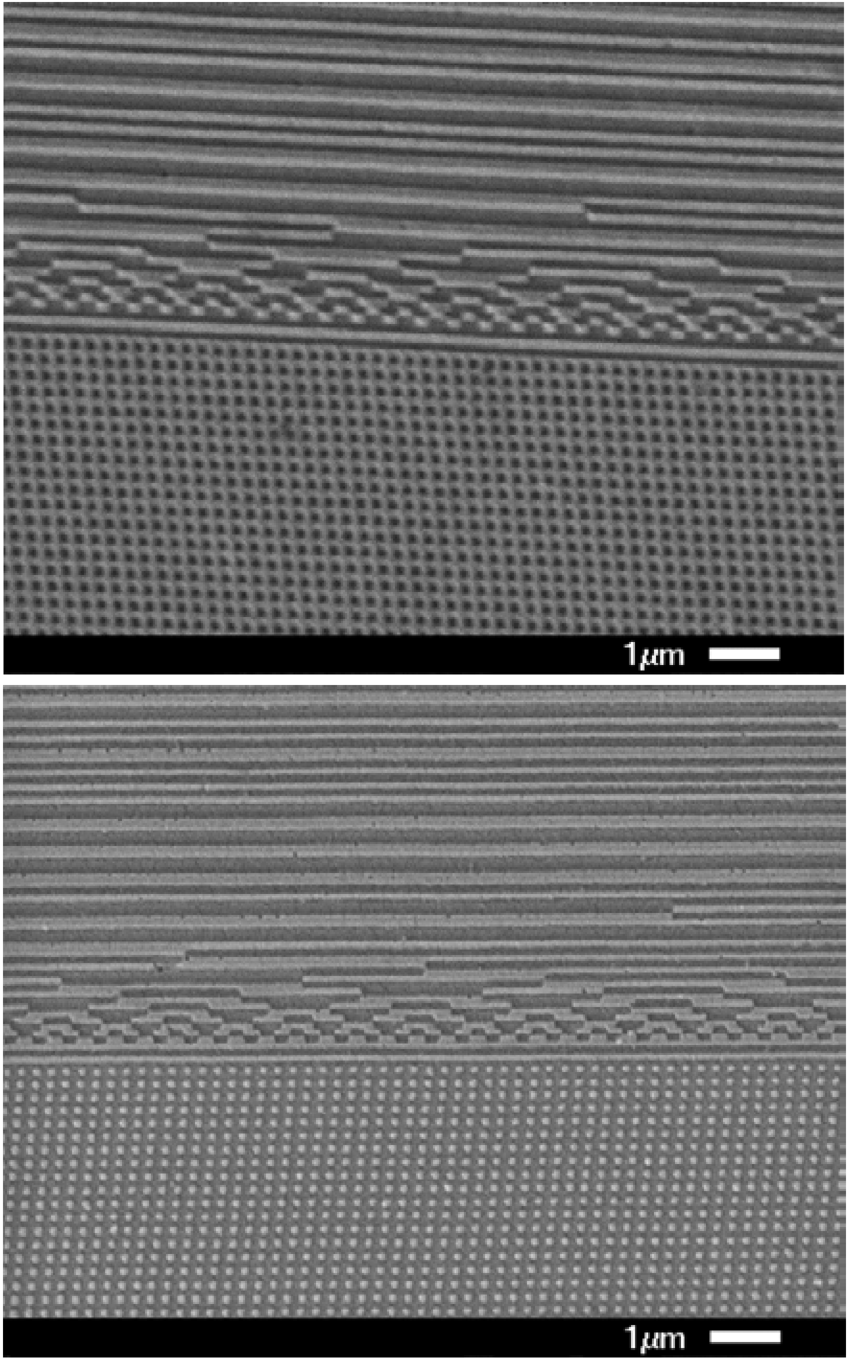

Figure 3.3a) SEM overhead view of an inverse hard disk servo pattern on the nickel working mould, the top half showing the gray code consisting of mixed patterns and bottom half the burst area consisting of an array of 100 nm diameter holes. b) UV roll-to-roll nanoimprinted resin mould copy of the nickel hard disk working mould showing high fidelity reverse tone replication.

There is some slight edge roughening in the line patterns due to some mould defect accumulation and gas trapping, but there are no missing features or large defects. Gas trapping is one of the most frequently observed defect types in UV roll-to-roll nanoimprinting, due to the fact that deposited resin coatings must displace ambient gas confined in all the mould cavities to obtain a defect-free result, which is not trivial. Moreover, ideal solutions such as vacuum or reduced atmosphere chambers are difficult to implement in a system with a continuous web feed. While nothing has been reported specifically for UV roll-to-roll nanoimprinting, various solutions to gas trapping have been developed for batch mode UV nanoimprint that could be adapted to a roll-to-roll format.[59-62,130] One approach involves the use of helium as an exotic gas environment within which the web / resin / mould / imprint roller stack is formed prior to UV exposure. Filling the entire chassis containing the roll-to-roll line with helium, for example, is one way of implementing this environment. Although helium has a lower equilibrium solubility in hydrocarbon liquids as compared to oxygen and nitrogen, the diffusivity (or dissolution rate) of helium is approximately three times greater.[131] This latter parameter is of great importance at high throughput because there will be very little time in the interim between a trapping event and UV exposure, perhaps seconds to a fraction of a second. With three-fold greater diffusivity, trapped helium bubbles will dissolve in the liquid resin far more quickly, allowing a greater range of trapped bubble volumes to fully dissolve in the resin. Pentafluoropropane has also been proposed as an alternative to helium.[59-61] More indirect methods to reduce or eliminate air trapping include building a free path of escape for any large, insoluble volumes of trapped gas into the roll mould design.

Figure 3.4a is an SEM cross-section view of the UV roll-to-roll fabricated resin mould shown overhead in Figure 3.4, demonstrating faithful replication of the nickel mould.

The patterned surface curves upward from the cross-section, exhibiting the flexible nature of the sample. Figure 3.4b is a cross-section of the preamble and data track transition, showing 50 nm linewidth, 100 nm pitch, 40 nm height imprinted lines and spaces. Roughly the aspect ratio for all features ranges from ~0.3 - 1, which is easily low enough for clean peel separation without an anti-stick coating on the mould or an adhesion promoter coating for the substrate web. In cross-section the residual layer is shown to be ~500 nm thick, with a tolerance of about ±100 nm across the entire sample. The residual layer thickness is generally dependent on how the liquid resin is spread against the substrate web prior to UV exposure. High viscosity resins typically obtain greater residual layer thicknesses, given sufficient dispense volume. Residual layer thickness is also modulated by the applied pressure on the spreading roller(s) prior to UV exposure,[34] and the wettability of the resin against the substrate web.[112] Given YNIL-R2-2 has a positive spreading coefficient to polycarbonate and a low viscosity of only 10 cP, a further reduction in residual layer thickness would require a larger applied pressure on the spreading rollers in excess of 400 kPa. Note that for resin mould replication it is not an imperative to minimize or exert control over the residual layer thickness, beyond the fact that doing so would tend to reduce the overall resin coating thickness and thereby increase transparency to UV light.

Since a thin coating is readily obtained with YNIL-R2-2 given its low viscosity, the dispense volume was kept sufficient to planarize the substrate web and provide additional media with which to squeeze out trapped gas under the pressure rollers. However, an important parameter for resin mould fabrication is the surface planarity of the resin mould when it is laid flat, as any long range surface waviness or permanent distortion will be transmitted into subsequent imprinted layers. This can have a detrimental impact on residual layer uniformity, which is often important for subsequent lithography steps in

product manufacture.[57,132] Surface planarity of resin moulds in UV roll-to-roll nanoimprinting, assuming complete filling and uniform spreading, depends heavily on the uniformity of curvature of the mould face. In the case of mounted sheet moulds, the curvature uniformity of the imprint roller backing the sheet mould is also important. This issue will be discussed in further detail later.

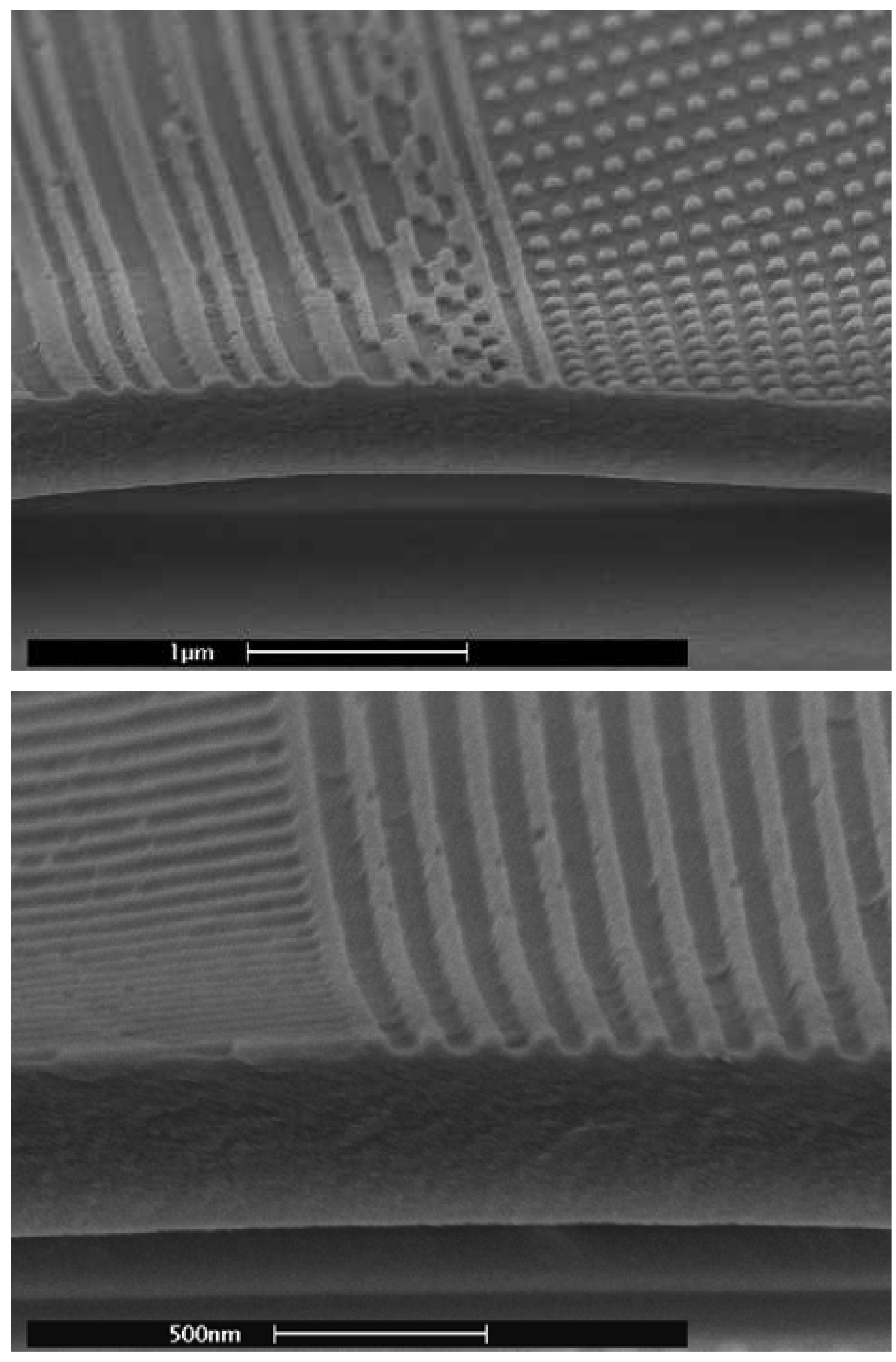

Figure 3.4a) SEM cross-section of UV roll-to-roll nanoimprinted resin mould hard disk servo pattern. Pattern height is ~50 nm. b) SEM cross-section of UV roll-to-roll nanoimprinted preamble and data track transition. Imprinted lines are of 50 nm diameter and 100 nm pitch. The ~500 nm cured resin residual layer is clearly shown, having partially debonded from the 125 μm thick polycarbonate web during sectioning.

3.3 Usage of Resin Moulds in Batch Mode Thermal NIL

To demonstrate a generic batch mode thermal imprint we chose to pattern a 200 nm thick spincast film of polymethyl methacrylate (PMMA) on a 4” silicon wafer substrate, which are commonly used materials in thermal NIL and are appropriate for many high resolution applications of interest, including nanofluidic devices and lithography for electronics. UV roll-to-roll nanoimprinted resin moulds containing 50 nm linewidth, 100 nm pitch, 50 nm height grating arrays were cut from the polycarbonate substrate web feed as 5 cm x 5 cm squares, sandwiched with the PMMA coated 4” silicon wafer and loaded into an Obducat 6” thermal nanoimprinting system capable of handling any substrate size up to 6” area (see Figure 3.1 process scheme). Table 3.2 provides a summary listing of processing parameters. Batch mode thermal nanoimprinting was accomplished at 40 bars of pneumatic pressure at 150º C (PMMA T_g 105º C) with a dwell time of 5 minutes. Adhesion of the cured resin mould to the PMMA film was negligible post-imprint, such that separation and exposure of the patterned PMMA film was accomplished by easy lifting and removal of the mould.

Figure 3.5a shows an overhead view of the 50 nm linewidth, 100 nm pitch line and space pattern fabricated by UV roll-to-roll nanoimprinting shown in cross-section earlier. Figure 3.5b shows the batch mode result in PMMA with excellent pattern fidelity for low aspect ratio, high resolution nanostructures. At higher aspect ratios, or otherwise larger works of adhesion where the intrinsic release performance of the resin mould surface cannot be exclusively relied upon, there are a number of solutions to reduce its surface energy and lower the work of adhesion. This is covered in Chapter 1.

Table 3.2 Process parameters for batch mode thermal NIL using segmented UV roll-to-roll nanoimprinted resin moulds

	Parameter
Mould	YNIL-R2-2 / Polycarbonate Bilayer Resin Mould (5cm x 5cm square cut-out)
Resist	200 nm thick PMMA film (Mn 25,000)
Substrate	4" DSP silicon wafer
Temperature	150° C
Pressure	40 bars
Dwell Time	5 minutes

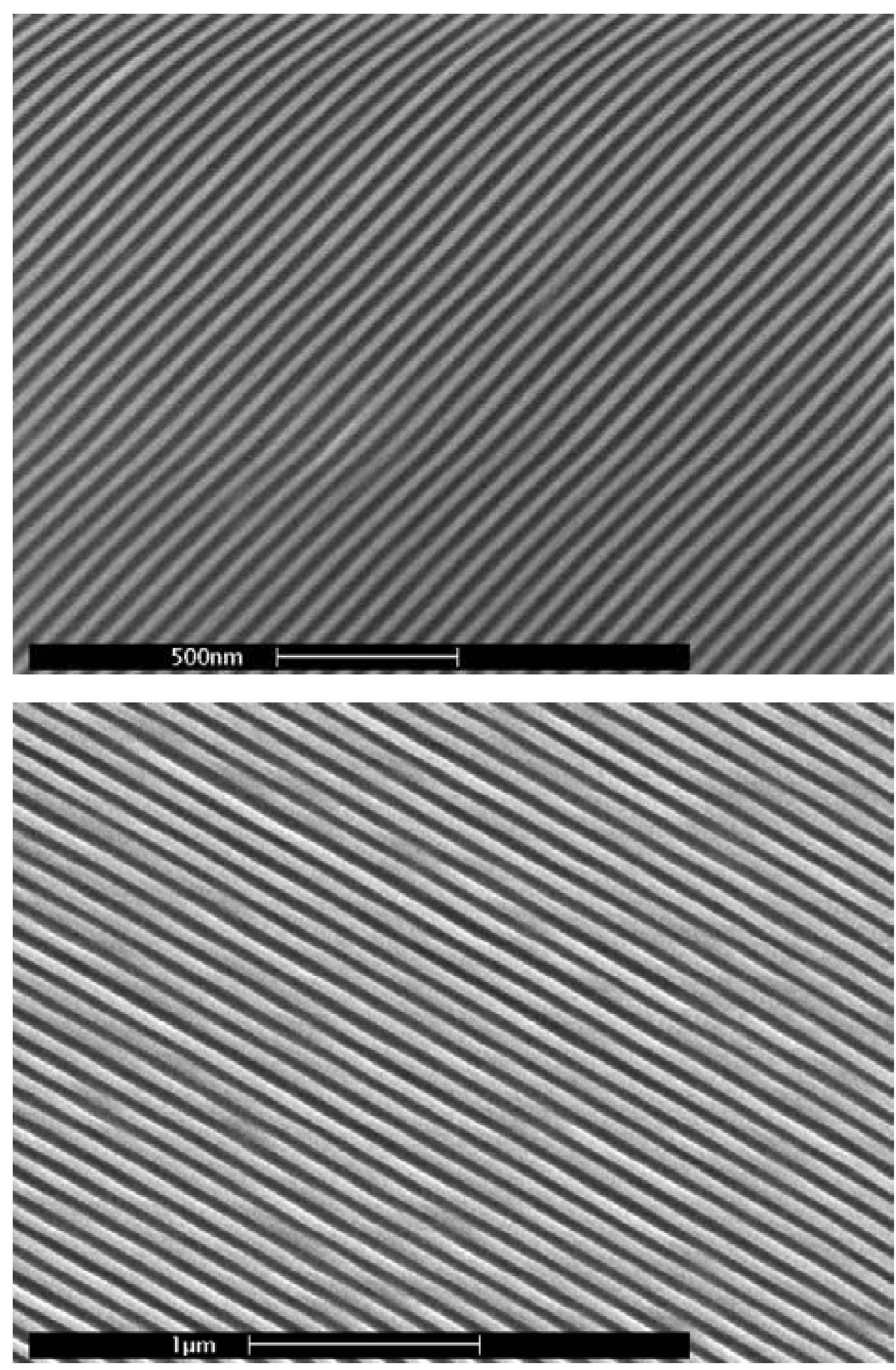

Figure 3.5a) SEM overhead view of UV roll-to-roll nanoimprinted 50 nm linewidth line and space resin mould. b) SEM overhead view of high fidelity replication of the same 50 nm linewidth line and space pattern in PMMA produced by using the UV roll-to-roll nanoimprinted resin mould to pattern a 200 nm thick PMMA film on a 4" silicon wafer.

3.4 Comparison of Imprint Fidelity Across Multiple Replication Cycles

Atomic force microscopy (AFM) using a Bruker Icon Dimension system in tapping mode was employed to probe feature height and surface contour, particularly across mixed, irregular features where variations in feature height are thought to be greatest. AFM section analysis was carried out across the gray code region of a nickel DTR hard disk mould, the UV roll-to-roll fabricated, reverse tone resin mould produced from the nickel hard disk mould, and the final copy in PMMA produced from the resin mould, as shown in Figure 3.6a-c. Height profiles showing the section line are provided in Figure 3.6d-f. Pattern height was measured within a range of 50 – 60 nm on the nickel mould (Figure 6a, d), with variation attributed predominantly to etching effects such as microloading and reactive ion etch (RIE) lag of the master template during fabrication. The resin mould section has a measured 53 – 58 nm pattern height variation (Figure 3.6b, e), though some spaces between features were too narrow to be fully probed by the AFM tip. These feature troughs appear as spike lows in the section graph. For the thermal NIL imprint in PMMA (Figure 3.6c, f) the range of measured feature heights was 48 – 62 nm, or a 14 nm spread compared to 10 nm for the nickel mould, an increase of 40%. The PMMA feature height range for these measurements actually encompasses the equivalent range for the nickel mould, thus any reduction in feature height due to curing shrinkage by the resin mould proved to be difficult to discern from the fluctuations in feature height. This is generally the conclusion from section analysis and examination of multiple locations on both samples.

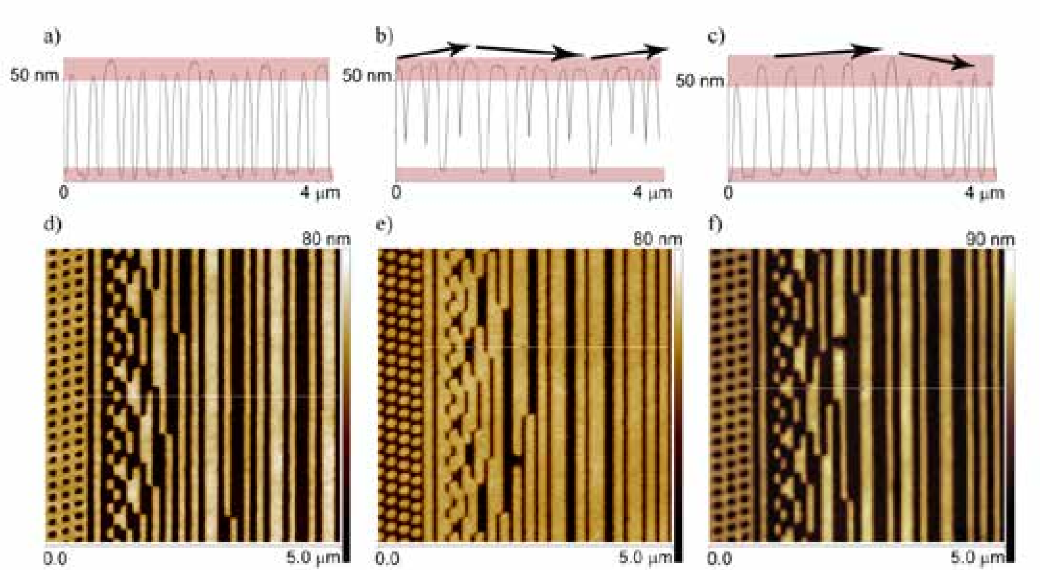

Figure 3.6a-c) AFM section analysis of hard disk gray code region and d-f) AFM height profiles showing the section line where data was captured. Highlighted regions on the section graphs provide a visual guide for the measured height variation of neighboring feature peaks and troughs. a, d) nickel hard disk mould, b, e) UV roll-to-roll nanoimprinted reverse tone resin mould produced from the aforementioned nickel hard disk mould, and c, f) Batch mode thermal NIL imprint produced from the aforementioned resin mould. Arrows indicate the presence of low frequency surface waviness. Note that all scans are raw data, no leveling or computational flattening was carried out.

The additional fluctuations in feature height are attributable to longer range waviness across the surface of the sections in Figure 3.6b and c (denoted by arrows shown). This non-uniformity has peak-to-peak amplitude of about 4 nm on the resin mould (Figure 3.6b), about 8 nm on the PMMA thermal imprint (Figure 3.6c), but is not present as a full or half-wave cycle on the nickel mould section (Figure 3.6a). These long-range waviness effects were also found to be reproducible at other locations across the nickel hard disk mould, resin mould, and PMMA imprint samples.

Because the surface non-uniformity only appears on the resin mould and the PMMA thermal imprint produced from the resin mould, and because it is of too high frequency to be attributable to mould bow, it has been partially attributed to the backing surface

behind the nickel working mould. Here, the stainless steel backing comprises a mount piece with a curved surface that matches the surface contour of our imprint roller (see Figure 3.2b). However this stainless steel backing surface has imperfect cylindrical contour and a brushed grinding finish on the 1 – 10 μm regime corresponding to the surface waviness detected by AFM scans. In other words the backing surface exhibits short- and long-range surface waviness which appears to transmit through the nickel sheet mould into the cured resin surface due to the pressure applied by the spreading rollers and the mechanical tensioning of the nickel mould onto the mount piece. This is shown schematically in Figure 3.7. That non-uniformities from a backing surface, whether it be from the mould backside or the supporting plate, will lead to corresponding pressure non-uniformities is well known to batch mode nanoimprinting.[133] These pressure non-uniformities are caused by elements of the imprint stack conforming, at least partially, to the non-uniform backing surfaces under pressure such that some regions of the imprinted area are raised slightly relative to neighboring regions. In the case of UV roll-to-roll nanoimprinting, the applied pressure is considerably reduced, however this is offset by the fact that every element of the imprint stack besides the backing cylinder is flexible and conformable to applied pressure.

Surface waviness that is thus transmitted to the resin mould is further transmitted into the PMMA thermal imprint (Figure 3.6 c, f), the latter returning the inverse servo pattern provided on the nickel mould. The thermal imprint process itself can also introduce surface waviness into the PMMA film as our equipment was designed for use with rigid mould materials. In our thermal NIL process, pressure is transmitted pneumatically through a non-flat polymer sheet that remains in the glassy state at the embossing temperature, which also has surface waviness that the resin mould is able to conform to (unlike with rigid materials).

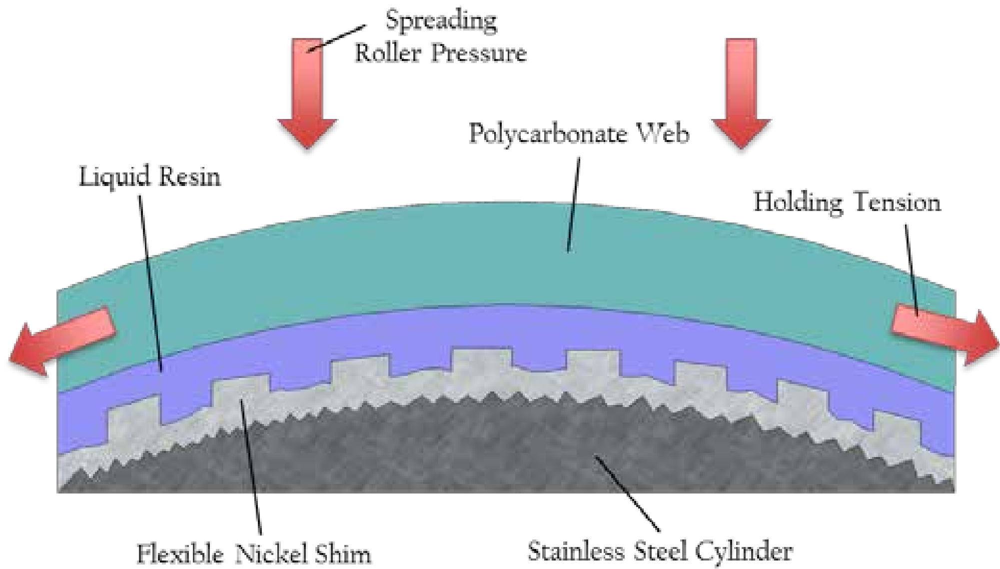

Figure 3.7 Schematic showing a cross-section of the imprint stack under pressure across the UV roll-to-roll nanoimprinting system imprint roller. The brushed grinding finish of the stainless steel cylinder is partially transmitted through the nickel shim mould. The dispensed liquid resin conforms to this surface and is solidified with this contour upon UV curing, obtaining the resin mould surface waviness found in AFM section measurements.

In any case, the resin mould surface contour alone is informative as to the uniformity of curvature of the imprint roller in the UV roll-to-roll nanoimprinting process. For many high resolution applications, and particularly for multi-layer device stacks, it is important that roll-to-roll nanoimprinted resin moulds obtain near-perfect surface planarization and uniformity to minimize film thickness non-uniformities in subsequent device layer lithographic steps. If for example, a UV roll-to-roll nanoimprinted resin mould with pattern height variations was used in a thermal batch mode nanoimprinting process where the residual layer thickness uniformity was important to production of the final device (semiconductors, displays, MEMs, NEMS, labs-on-a-chip, etc.), then excessive pattern height variation could introduce considerable difficulties in the follow-on etching steps. In this situation the final imprint is used as a mask to etch the substrate underneath, and all of the usual considerations of etching uniformity would apply. Surface waviness

transmitted to the mask can lead it to become fully etched away in some areas before others, for example.

Eliminating surface waviness on the resin mould would require that the mould face, and any backing surface in the case of mounted sheet moulds, possess extremely uniform curvature. In practice this is a significant engineering challenge as machining or forming a perfect cylinder with sub-nanometer uniformity and no surface waviness is non-trivial. Particularly since chemical-mechanical polishing techniques that are widely used to planarize flat surfaces are inaccessible to curved surfaces.

Because a fast-curing acrylic resin was used to fabricate the resin mould, effort was made to quantify the extent of shrinkage-related feature height loss using our adopted process scheme (Figure 3.1) by attempting to isolate the shrinkage from the surface fluctuations discussed above. Feature height calculations were made from AFM section profiles for all three replication generations. In order to remove RIE lag and microloading effects, only the widest 250 nm lines and 250 nm diameter troughs in the servo region where the local feature densities were similar were considered. The widest protruding lines and troughs were selected because they were fully probed by the AFM tip. In order to prevent high frequency surface waviness from skewing the results, areas where such a high amplitude surface wave was clearly present were excluded from the calculation and only nearest-neighbor line height/trough levels were calculated to minimize the effect of slope. Results are presented in Table 3.3. Volumetric shrinkages were calculated from measured linear shrinkage values using the formula

$$V_S = \frac{100}{\left(1 - \frac{L_S}{100}\right)^3} - 100 \tag{3.1}$$

where L_s is the linear shrinkage (%) and V_s is the volumetric shrinkage (%). Derived average volumetric shrinkages were helpful in confirming that the process shrinkage from any single (or all) replication cycles was within a range that is typical for acrylate resins (~3 – 15%).[36,37] Note that with the exclusions provided above, the standard deviation of measured feature height loss remains large. Thus these results are only used to indicate that the average process shrinkage is within an expected range and that thermal NIL compression shrinkage, as discussed earlier, is not a dominant factor.

Table 3.3 Line height shrinkage calculations from AFM profile measurements for the nickel roll-mounted mould – resin mould replication step and for the full three stage cycle, i.e. nickel roll-mounted mould – resin mould – PMMA thermal imprint (height losses from nickel electroforming steps are assumed negligible and are not considered).

	Average Height Loss (nm)	**Average Linear Shrinkage (%)**	**Volumetric Shrinkage (Derived, %)**	**Standard Deviation**
Nickel roll-mounted mould – resin mould	~2 nm	3.7	11.9	±1.5 nm (±2.5% Linear)
Nickel roll-mounted mould – resin mould – PMMA thermal imprint	~1 nm	1.5	4.6	±1.3 nm (±2.3% Linear)

AFM height profiles of the 50 nm linewidth, 100 nm pitch data track region were also acquired and are presented in Figure 3.8. Figure 3.8a, for example, shows in detail the presence of crevices and some line roughening due to the feature diameter approaching the standard grain size of electrodeposited nickel.[25] Figure 3.8b & c shows that replication of the nickel mould pattern tended to smooth off high frequency mould roughness, though lower frequency narrowing or widening of mould lines does appear to get transmitted all the way to the PMMA thermal imprint. While mould crevice replication does not appear in Figure 3.8b or c, tiny resin extrusions on the sidewalls of

lines on the resin mould can be discerned in SEM cross-section (Figure 3.4b). These extrusions could be the result of resin filling in the nickel mould crevices. Further reduction in average grain size and some modifications to the electrodeposition conditions should help reduce these roughening effects.

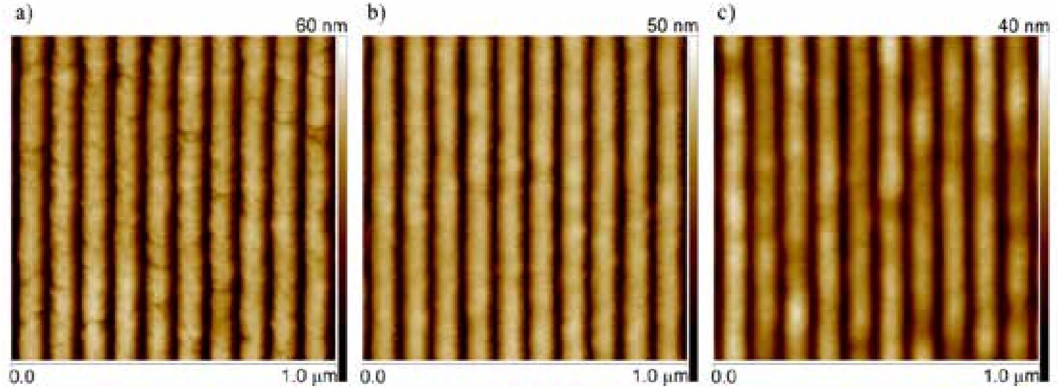

Figure 3.8a-c) AFM height profiles showing the detailed line topology of the 50 nm linewidth, 100 nm pitch data track region of a) the nickel hard disk mould, b) the UV roll-to-roll nanoimprinted resin mould (reverse tone), and c) the batch mode thermal NIL imprint produced with the aforementioned resin mould.

3.5 Concluding Remarks

New technologies to enable high resolution lithography at very low cost are needed for economical mass production in targeted application areas such as nanofluidics, biomedicine, data storage media, and electronics. In this Chapter, UV roll-to-roll nanoimprinting is demonstrated as a mass production method for producing high resolution resin moulds with nanoscale as well as mixed micro- and nanoscale features. Up to 10 m min^{-1} throughput was achieved with patterned area of up to 120 cm^2. Resin moulds fabricated by roll-to-roll processing can be fabricated inexpensively enough to be used only once, or several times until defects are accumulated, and then it can be disposed of or recycled. This creates tremendous efficiency gains by eliminating mould

cleaning steps and it provides a solution to inherent mould degradation and defect accumulation associated with re-use. In addition, the adopted process scheme where only one UV curing replication step is performed, followed by thermal NIL, minimizes cumulative volumetric curing shrinkage and loss of feature height across multiple replication steps.

With the inherent advantages of UV roll-to-roll nanoimprinting for nanoscale mould replication, there are certain challenges that, if addressed and solved, will spur wider adoption of the technology. One important challenge is in optimizing the surface planarity of replicated resin moulds. The fact that fabrication of resin moulds occurs against a curved surface is one of the key differences between UV roll-to-roll nanoimprinting and that of batch mode UV nanoimprinting highlighted in this study. Surface waviness appears across the surface of our replicated resin moulds and is also observed with greater amplitude on our thermally embossed PMMA film surfaces. Particularly in the former case, this phenomenon was attributed to corresponding waviness on the backing surface of the imprint roller in our UV roll-to-roll nanoimprinting apparatus. Non-planar resin mould and backing surfaces in the thermal NIL step also appear to contribute to greater surface waviness in embossed PMMA films. These results should be of interest to researchers in the field. In particular, machining or forming rollers and curved surfaces with extremely uniform curvature and sub-nanometer surface waviness is a significant engineering challenge. Current technologies, such as chemical-mechanical polishing, are only effective at planarizing flat surfaces. New technologies, or adaptations to existing technology are needed to achieve similar uniformity on imprint rollers in order to prevent transmission of this waviness to the surface of replicated resin moulds. Obtaining an ideally planar resin mould surface is important for high precision lithography in semiconductor and data storage media

applications, or fabrication of any multi-layer device stack where multiple etching steps are involved and nanoscale precision is required. Assuming curvature uniformity issues on cylindrical roller moulds can be solved, adaptations to thermal NIL equipment and processing to achieve uniformly flat negative relief replicas of resin moulds in thermoplastic resist materials should be straightforward.

This study has also examined the effects of multiple iterative or descended copies from a nickel master out to the 4th generation, and through multiple material carrier types (nickel, UV cured acrylic resin, PMMA). It was found that the combined feature shrinkage of a single UV curing replication cycle followed by thermal NIL was small enough to not have a substantial effect on replication fidelity and uniformity in terms of measured feature height.

There is still considerable room for further investigation of resin moulds with higher aspect ratio features above 3 where most nanoimprinting techniques (roll-to-roll as well as batch mode) encounter difficulties obtaining clean separation and thereby high yield. In particular at these high aspect ratios and with high density features, nickel roller-mounted moulds have increasing difficulty in separating cleanly due to their relatively high surface energy, particularly fresh nickel surfaces that have not had their surface energy reduced by adsorbed organics from the resin. This is where intrinsically low surface energy polymeric roll and roller-mounted moulds such as silicones play a role. This will be the subject of Chapter 4.

Chapter 4. Surface Delivery and Covalent Bonding of Release Agents to Resin Mould Surfaces

4.1 A Brief Theoretical Treatment on Work of Adhesion and Demoulding Failure in Nanoimprint Lithography

As demands on mould feature density and aspect ratio continue to increase, it becomes important to examine means to modify resin mould surfaces to reduce their surface energy and thus improve release performance in subsequent lithography steps. As mentioned in Chapter 3, when feature aspect ratios exceed approximately a value of 3, nanoimprinting and contact lithography techniques that rely on filling of mould cavities becomes more difficult in terms of obtaining acceptable yield post-separation. There is of course, a surface area dependence on whether an imprinted feature will fail. If the work energy per unit area of pulling apart the resin mould from the imprint resist in air to eliminate the interface and create two new surfaces is

$$W_V = \gamma_{1V} + \gamma_{2V} - \gamma_{12} \tag{4.1}$$

then demoulding failure will occur when the total resin mould / resist surface formation energy exceeds the cohesive surface formation energy of the imprint resist itself

$$A_{12}(\gamma_{1V} + \gamma_{2V} - \gamma_{12}) > 2A_1\gamma_{1V} \tag{4.2}$$

where A_{12} is the resin mould / resist interfacial area, A_1 is the cross-sectional area of the imprinted resist feature, W_a is the work of adhesion with subscript V denoting an air (vapour) environment, γ_{1V} is the formation surface energy of the resin mould, γ_{2V} is the formation surface energy of the resist, and γ_{12} is the resin mould / resist interfacial energy in mJ m^{-2}. Note that in this Chapter the term "resist" is used to denote any imprint media, whether it be a thermoplastic material, a photoresist, a UV curable resin or other patternable material. Reversible failure of moulded features is modeled in Figure 4.1a. Thus, as the ratio A_{12}/A_1 becomes large, Equation 4.2 becomes more likely to be true

and the imprinted feature fails cohesively. This ratio is most sensitive to increasing aspect ratio. For high density (high surface area) nanoimprint lithography with a resin mould where A_{12}/A_1 is relatively small, failure can still occur through the bulk of the resist or resist residual layer (in the case of thin resist films). A similar energy criterion would then apply where failure occurs when the total resin mould / resist surface formation energy exceeds the cohesive surface formation energy of the resist across a given cross-sectional area of the bulk resist or resist residual layer (in the case of thin resist films). This is illustrated in Figure 4.1b. Also, in the case of thin resist films, failure can instead occur at the interface with the substrate (Figure 4.1c).

Note that the total work of adhesion for an interface is a combination of chemical bonds across the interface, molecular entanglements as would occur in diffusion or adsorption mechanisms, and intermolecular interactions such as dispersive, polar and hydrogen bonding forces. Surface roughening will also directly increase the interfacial work of adhesion, and technically the mould surface structures are a type of roughening, though for lithography purposes all other forms of surface roughness are purposefully avoided to minimize further contributions to the work of adhesion from mechanical interlocking.

The efficiency by which an applied load is converted to the energy required to separate the interface depends on the plastic and elastic properties of the materials involved, the loading geometry, the size and geometry of material flaws, as well as the presence of any internal stresses. Surface energy models do not describe the strain energy stored in resist materials due to deformation and collapse (another form of material failure), and are applicable only to the reversible formation of new surfaces. However, this treatment is sufficient to convey the importance of keeping $\gamma_{1V,}$ the resin mould surface energy in air,

as low as possible for use in subsequent lithography steps since the other surface energy and interfacial area contributions to the work of adhesion are often difficult to influence due to engineering or process constraints. For a thorough treatment of polymer failure mechanisms, readers are directed to various texts available elsewhere.[134,135]

Incidentally, solid material phases have experimentally inaccessible surface energies. Thus, γ_{1V}, γ_{2V} and γ_{12} cannot be evaluated directly. The work of adhesion can be inferred from the Young-Dupré equation

$$W_{LS} = \gamma_{VL} + \gamma_{VS} - \gamma_{LS} = \gamma_{VL}(1 + \cos\theta) \quad (4.3)$$

where W_{LS} is the liquid-solid work of adhesion, γ_{VL} is the vapour-liquid surface energy (or surface tension), γ_{VS} is the vapour-solid surface energy, γ_{LS} is the liquid-solid surface energy and θ is the liquid-solid-vapour system contact angle. Note that Equation 4.3 is defined only for liquid-solid systems and solid-solid systems will have differing values.[136] However, qualitatively when θ values are small for liquids in contact with a given solid in air, for example, solid-solid works of adhesion also tend to be large so long as similar mechanisms that lower the interfacial energy with the solid are operating in both cases. In any case, the significance of the Young-Dupré relation is that it relates the work of adhesion to more readily measurable values and shows that the contact angle is a thermodynamic quantity, which can be related to the work of adhesion and interfacial free energy terms. In general, the work of adhesion will be high when θ values are small and vice-versa. This forms the theoretical basis for using contact angle measurements to qualitatively differentiate between a larger or smaller work of adhesion in lieu of precise solid-solid surface formation energy measurements.

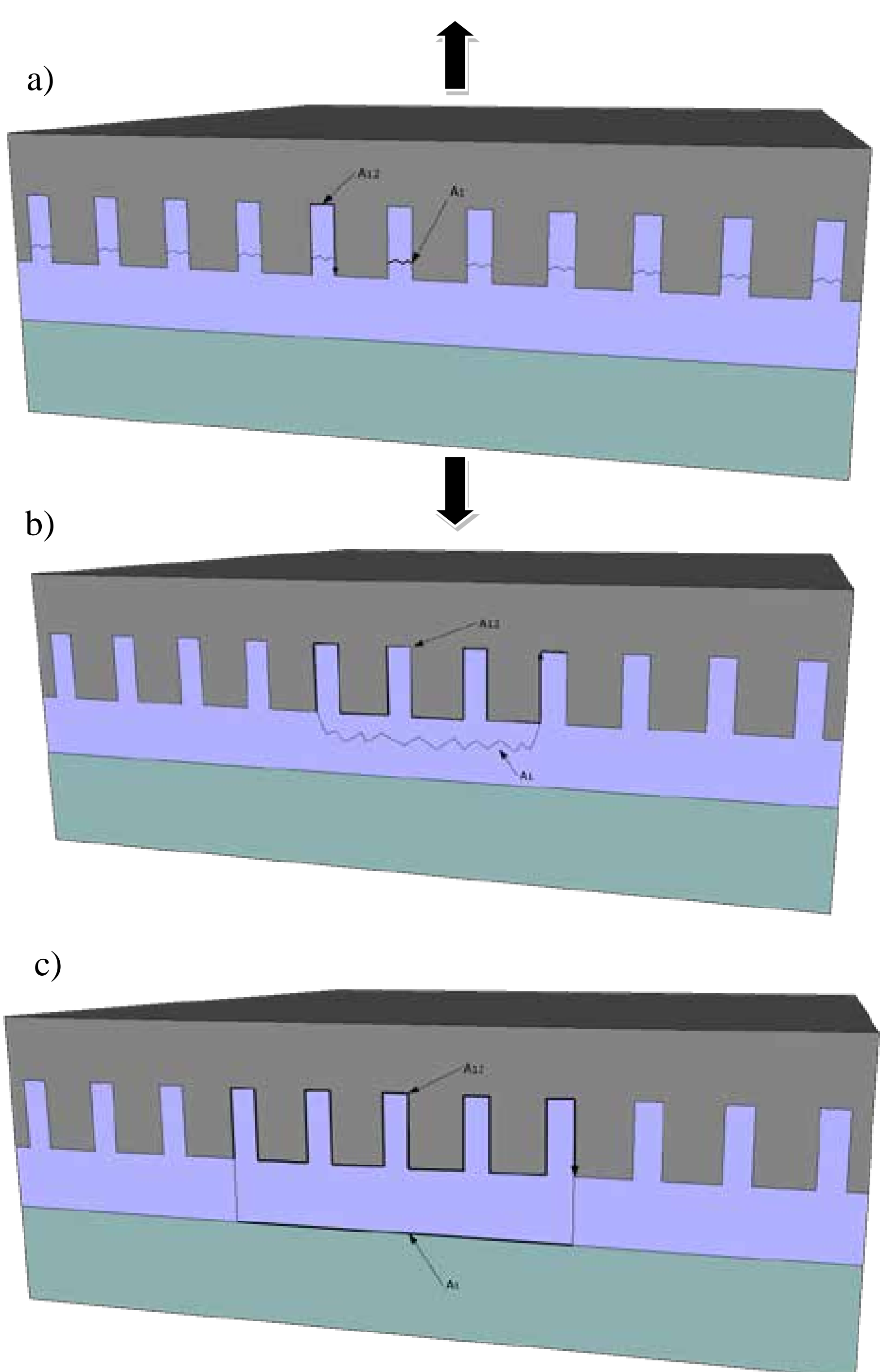

Figure 4.1 Reversible material failure under an applied separation force (note arrows) in a nanoimprint stack with a resin mould (grey), resist (blue) and substrate (green). Failure occurs when the work of adhesion, $A_{12}(\gamma_{1V} + \gamma_{2V} - \gamma_{12})$ between the mould and the resist exceeds the formation surface energy of the resist (cohesive failure), or the separation surface energy of the resist/substrate interface $2A_1\gamma_{1V}$ (interfacial failure). a) Failure through high aspect ratio features in the resist. b) Failure through the bulk of the resist. c) Failure across the resist/substrate interface.

4.2 Comparison of Surface Modification Methods to Improve Release Performance

When a nanoimprint lithography step (whether it be batch mode or roll-to-roll) fails due to the work of adhesion being too large, defect generation on separation of the mould occurs. Defects include pull-outs, bent and collapsed structures, as well as caking of resist onto the mould. For resin moulds containing high aspect ratio structures, a large work of adhesion in a subsequent lithography step will also have the effect of increasing the peel separation angle, which can also lead to bent and collapsed structures, particularly for discrete, high aspect ratio features. Work of adhesion- and separation-related defects present an engineering challenge, particularly for high density and high aspect ratio nanoimprinting and it is of interest to study and obtain new methods to lower the work of adhesion through surface energy modification. Most reports in the literature dealing with surface modification of mould materials to improve release fall into three categories:

1) Where the bulk mould material is selected specifically for its release properties and possesses intrinsically low surface energy.[66,69,77-82,105]
2) Where the bulk mould material is selected for reasons other than release performance (mechanical robustness, stiffness or conformality, hardness, transparency, thermal expansion properties, resistance to fracture, ease of fabrication, etc.), and a release agent is incorporated into the bulk material at a given concentration with the expectation that a similar concentration of this agent will be expressed on the surface of the mould.[29,72] This applies mostly to polymerizable resins which go through a liquid/solid phase transition and was described earlier in Chapter 1.

3) Where the bulk mould material is selected for reasons other than release performance and the surface of this material is directly modified via an anti-stick coating or self-assembled monolayer (SAM) to improve release performance.[24,73-76,137,138]

Intrinsically low surface energy mould materials generally comprise of fluorocarbon materials (~16 – 25 mJ m^{-2} depending on chemical makeup) and silicones (~22 – 25 mJ m^{-2}).[139,140] Such mould materials were discussed briefly in Chapter 1 and readers are invited to look there for further discussion. In short however, intrinsically low surface energy thermoplastic materials such as ETFE and Teflon cannot be fabricated at high throughput because of the high viscosity of these materials and the difficulty in achieving a sufficiently low cavity fill time to be competitive with UV roll-to-roll nanoimprinting of resin moulds. The high pressures required to replicate the master mould with these materials also places the master at risk of damage from cracking, or imprinting of particles and residues. Intrinsically low surface energy thermoset materials such as PFPE and fluorinated silsesquinoxanes are costly, and do not have the curing speed of acrylate resins.[85]

Mixing of release agents (generally fluorocarbon and siloxane small molecules and oligomers) into the bulk of polymer mould materials was covered in some detail in Chapter 1. In brief, this approach has difficulty in obtaining high surface concentrations of release agent within a short period of time that are anchored to the mould surface. All three characteristics are desired for UV roll-to-roll nanoimprinting of resin moulds for use in subsequent lithographic processes.

Use of SAM coating techniques that are directly applied to mould surfaces is strongly advantaged in that the bulk mould material can be selected for desirable properties other than release performance, and the SAM coating is only applied to modify the surface for improved release. Anti-stick SAM coatings can easily achieve similar low surface energies as the equivalent bulk material.[76,137,138] This is generally a more efficient means to obtain desirable release properties over bulk fluoropolymers, silicones, or other intrinsically low surface energy bulk materials that often have a set of undesirable bulk properties as a counter-balance to their desirable surface properties. The difficulty with current technologies to apply SAM anti-stick coatings is with the mode and speed of deposition and the robustness of the coating on polymeric materials. Anti-stick coatings can be applied via vapour deposition, liquid immersion or various vacuum sputtering approaches, but they all are incompatible with roll-to-roll processing (liquid immersion, vacuum), or have deposition times that are too long to feasibly integrate into a roll-to-roll line (vapour). Moreover, these deposition modes would constitute additional processing steps in the line that would greatly complicate fabrication. The lifetime, or robustness of the anti-stick coating depends on the deposition chemistry (if any) and mould surface dynamics. For silane anti-stick SAM chemistries, polymer mould surfaces typically have to be hydroxylated with an oxygen plasma treatment step or sputter deposition of an oxide coating. Sputtering requires vacuum and is thus incompatible with roll-to-roll processing. Incorporation of an atmospheric oxygen plasma treatment step in a roll-to-roll line is possible, however only small areas (~8 – 12mm diameter) can be treated per nozzle and the plasma will have difficulty infiltrating to the bottom of higher aspect ratio polymer mould nano-cavities under high throughput conditions.

Ideally, a roll-to-roll compatible method to deposit release agents directly onto resin moulds should have the same polymerization chemistry as the resin coating, such that it can participate in the phase change polymerization from liquid to solid while remaining concentrated at the mould surface. This Chapter introduces a new surface modification method that seeks to accomplish precisely this while maintaining compatibility with high-throughput roll-to-roll fabrication of resin moulds.

4.3 The Unique Properties of PDMS and h-PDMS

A key aspect of the surface chemistry modification method presented in this Chapter is its use of silicone as the roll-mounted mould material for UV roll-to-roll nanoimprinting. This material has several unique properties that continue to draw interest from the research community. First, silicones have excellent ambient gas permeability. For example, the nitrogen permeability of polydimethylsiloxane (PDMS) is on the order of ~400 Barrers (10^{-10} $cm^2 \cdot s^{-1} \cdot cmHg^{-1}$), as compared to thermoplastic fluoropolymers such as PTFE at ~4 Barrers.[141,142] The high nitrogen and oxygen permeability of PDMS greatly assists with dissolution of contacting trapped air bubbles common to UV roll-to-roll nanoimprinting, as other researchers have demonstrated.[85] Poor gas permeability is a key drawback of most fluoropolymers, particularly where the cavities of a given mould are fully enclosed or where there is no free path of escape for trapped air to be squeezed out.[85]

Silicone elastomers are also among the few known mould materials that are capable of nanoscale resolution, but can obtain an elastic modulus that is significantly lower than most polymerized resins that are cured against it.[68,69] This unique property assists with

peel separation by giving silicone roller mould cavities and features a certain degree of forgiveness if the peel angle is large relative to the aspect ratio of the cured resin structures, or if there is vibration or slippage during separation that causes shear stresses to be imposed at this interface.

Silicone elastomers are typically used to replicate a master mould via casting from a liquid pre-polymer mixture and thermal curing in an oven, which does not require elevated pressure and is thus a relatively low risk replication process as far as damage to the master is concerned. Although silicones are subject to curing shrinkage and this is disadvantageous as it would input shrinkage from multiple replication generations in a roll-to-roll resin mould nanoimprinting process, the additional shrinkage is reasonably small at about 1-2% (linear shrinkage) and is an acceptable trade-off for their advantageous properties.[143]

The most commonly used silicone elastomer in the literature, Sylgard 184 PDMS, is widely used as a soft NIL stamp.[66,93,144-149] However it suffers from certain drawbacks related to its poor mechanical stiffness, such as feature collapse and pairing at higher aspect ratios. Moreover, for structures that are spaced too widely apart, PDMS suffers from what is known as roof collapse where the mould bows toward the substrate under applied pressure. PDMS also strongly absorbs non-polar solvents and other non-polar small molecules and oligomers, leading to significant feature distortion from swelling.[150] These difficulties led to the development of a stiffer, more heavily crosslinked silicone known as hard PDMS, or h-PDMS.[68] Whereas Sylgard 184 PDMS generally obtains a Young's Modulus of ~2 MPa,[151] the most heavily crosslinked formulations of h-PDMS can generally achieve up to 9 MPa.[69] The increased stiffness overcomes many of the

aforementioned issues with Sylgard 184 PDMS, and the two materials are typically combined into a bi-layer composite mould where a thin h-PDMS layer carries the mould pattern and is backed by a thick layer of Sylgard 184 PDMS to ensure conformal contact across the substrate.[69] h-PDMS/PDMS composite moulds have been used to achieve resolutions of ~40 nm.[152] However, the increased modulus of h-PDMS comes at the cost of embrittlement, and it is well known in the literature that the h-PDMS layer cracks easily during peel separation with the master mould or with cured resin imprints making adaption to a roll-mountable form factor difficult.[80] This adaption to a roll-mountable size and form factor was accomplished in the present work by modifications to the h-PDMS formulation chemistry and bi-layer mould fabrication process. Thus we were able to integrate a large area roll-to-roll compatible h-PDMS/PDMS bi-layer sheet mould into the resin mould fabrication scheme as shown in Figure 4.2, and utilize it to produce resin moulds via UV roll-to-roll nanoimprinting. More details on this result and fabrication method to produce roll-mountable h-PDMS/PDMS bi-layer moulds will be provided in the materials & methodology section.

This brings us to one of the most unique and relatively unexploited properties of silicones, and the focus of this Chapter. After curing, silicone elastomers such as PDMS and h-PDMS variants will always contain ~0-5% by weight of un-crosslinked, low molecular weight dimethylsiloxane oligomers as a byproduct.[150,153] This occurs because the thermal curing of PDMS and h-PDMS is imperfect and does not go to completion. Thus, there will always be a constituent of loose dimethylsiloxane oligomers distributed throughout the cured PDMS (or h-PDMS) solid. This is particularly the case at ordinary curing temperatures of ~60 °C, which is relatively low and increases the probability of non-participation in the polymerization reaction. These oligomers can be transferred to a

variety of surfaces, including resin surfaces cured against it.[153] This is shown via x-ray photoelectron spectroscopy (XPS) survey emission spectra shown in Figure 4.3 for a cured resin film surface that was cured against an h-PDMS/PDMS bi-layer sheet. For this reference result, the resin formulation was chosen to be silicon-free so that the silicon in the transferred dimethylsiloxane oligomers would appear as a minor Si2p peak centered at 102.1 eV, which is typical for the siloxane bonding configuration.[154,155]

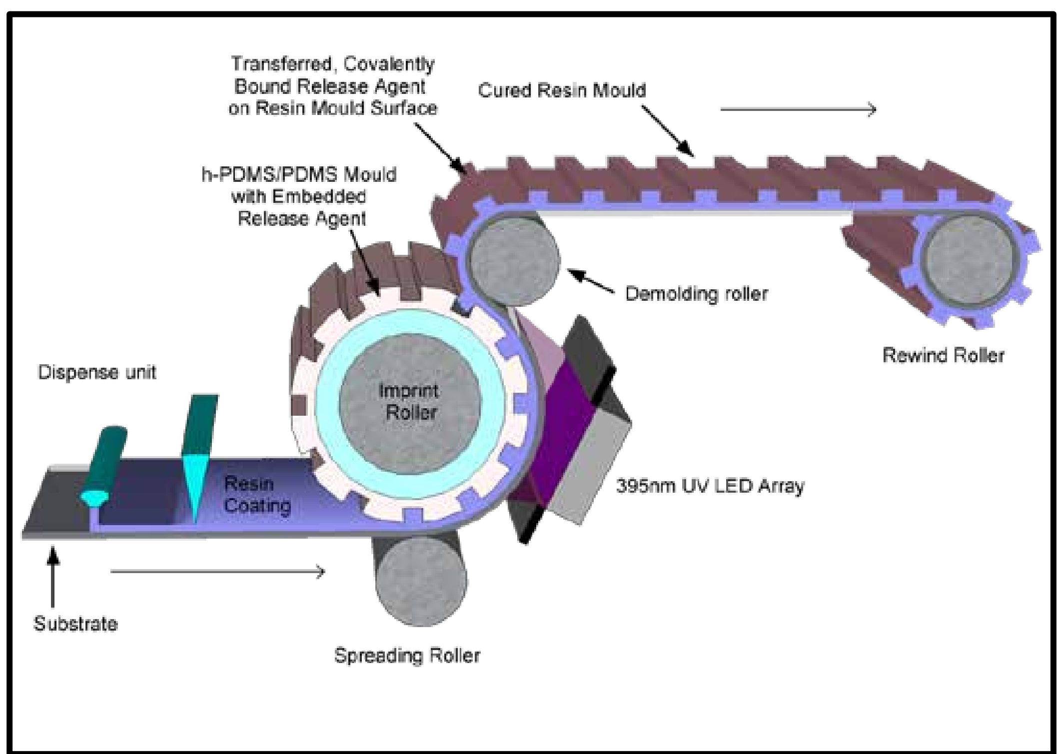

Figure 4.2 Process schematic for fabrication of resin moulds via UV roll-to-roll nanoimprinting with incorporation of a custom h-PDMS/PDMS roll-mounted mould with embedded monomethacryloxypropyl-terminated polydimethylsiloxane (mPDMS) reactive release agent. Transfer of mPDMS to resin mould surfaces is accomplished *in situ* during fabrication. The transferred release agent participates in the polymerization reaction to form the resin mould and will thus be covalently bound to the surface of the resin mould. The improved release property of the resin mould attributed to the presence of the transferred release agent will then assist with release in subsequent lithography steps.

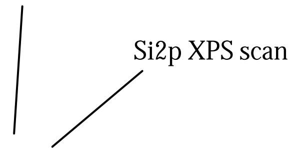

h-PDMS/PDMS composite
test mould prior to cut-out

Survey XPS Scan

Figure 4.3 *(At Left)* Small scale h-PDMS/PDMS test mould fabricated against a silicon master, prior to trimming and mPDMS exposure. (*At Right*) XPS survey scan of a blank resin film cured against an h-PDMS/PDMS sheet showing the transfer of silicon in the form of un-reacted dimethylsiloxane oligomers. (*Inset*) High energy resolution scan of the Si2p peak from transferred dimethylsiloxane oligomer chains.

When silicone materials are first cured into a solid, and assuming uniform mixing of the various pre-polymer components, these un-reacted oligomers are distributed evenly throughout the bulk of the material. Surface migration then occurs from the bulk to the surface of the solid silicone to lower the surface energy. If, for example, these loose dimethylsiloxane chains were removed from an otherwise equilibrium state silicone mould surface by curing and separation of UV curable resins against it, this would establish a concentration gradient with the bulk silicone, driving additional loose chains to the surface to replace what was removed. While there are migration as well as removal rate dependencies that are not yet well understood, this property of silicones does introduce the possibility of a renewable, transferrable release agent. Moreover, the required surface concentration of dimethylsiloxane oligomers to significantly improve release is quite small as will be presented in more detail later.

4.4 Delivery of Reactive Release Agent via a Soluble h-PDMS/PDMS Composite Roll-Mountable Polymer Mould

The notion of transferring release agents from the mould to a roll-to-roll nanoimprinted resin mould surface is both novel and intriguing, however it is not sufficient to simply transfer inert dimethylsiloxane oligomers. These transferred molecules would not be covalently bound to the polymerized network comprising the resin mould, and would remain mobile at the surface. Because of their uncontrolled mobility, inert dimethylsiloxane oligomers may not be effective in promoting release between a given resin mould and the resist used in a subsequent lithography step because there is no mechanism to localize them at the resin mould / resist interface. Moreover, those dimethylsiloxane oligomers that do, by chance, remain at this interface would be subject to removal from the resin mould and transfer to the resist surface, which is undesirable. In the present work, reactive dimethylsiloxane oligomers were artificially introduced to h-PDMS/PDMS bi-layer roll-mounted moulds for the purpose of transfer to resin moulds *in situ* with their fabrication via UV roll-to-roll nanoimprinting.

Low molecular weight, methacrylated dimethylsiloxane oligomers are soluble in solid silicone moulds (see Appendix A for theoretical arguments and calculations to this effect), and behave similarly to their native inert equivalents, allowing replacement or augmentation by simple exposure of the silicone mould to liquid state monomers. Figure 4.2 also shows how the transfer process works during UV roll-to-roll nanoimprinting of resin moulds utilizing a h-PDMS/PDMS bi-layer mould as mentioned previously. This scheme shows how methacrylated dimethylsiloxane release agent dissolved in the h-PDMS/PDMS mould is transferred to resin mould surfaces during UV roll-to-roll nanoimprinting.

Unlike with other release agent coating techniques, this approach allows the transferred release agent to participate in the polymerization reaction that forms the resin mould. The release agent will thus become part of the polymerized network and be covalently bound to the surface of the resin mould, having the effect of a permanent modification to the surface chemistry. Moreover, because transfer occurs *in situ* with fabrication, no additional in-line process steps are required. The additional processing to expose the reactive release agent to the roller- or roll-mounted mould occurs off-line and is straightforward. By this method it is demonstrated herein that it is possible to locally deliver anchorable release agents to resin mould surfaces for the purposes of reducing their surface energy in a manner compatible with roll-to-roll processing, and thereby improve the release properties of resin moulds in subsequent lithographic processes.

4.5 Materials & Methodology

In terms of materials, there are four important inputs: the master mould, the roll-mounted mould, the reactive release agent, and the resin mould formulation. The master mould is copied to the roll-mounted mould which is then exposed to the reactive release agent for transfer to the cured resin mould surface as shown in the workflow schematic provided in Figure 4.4.

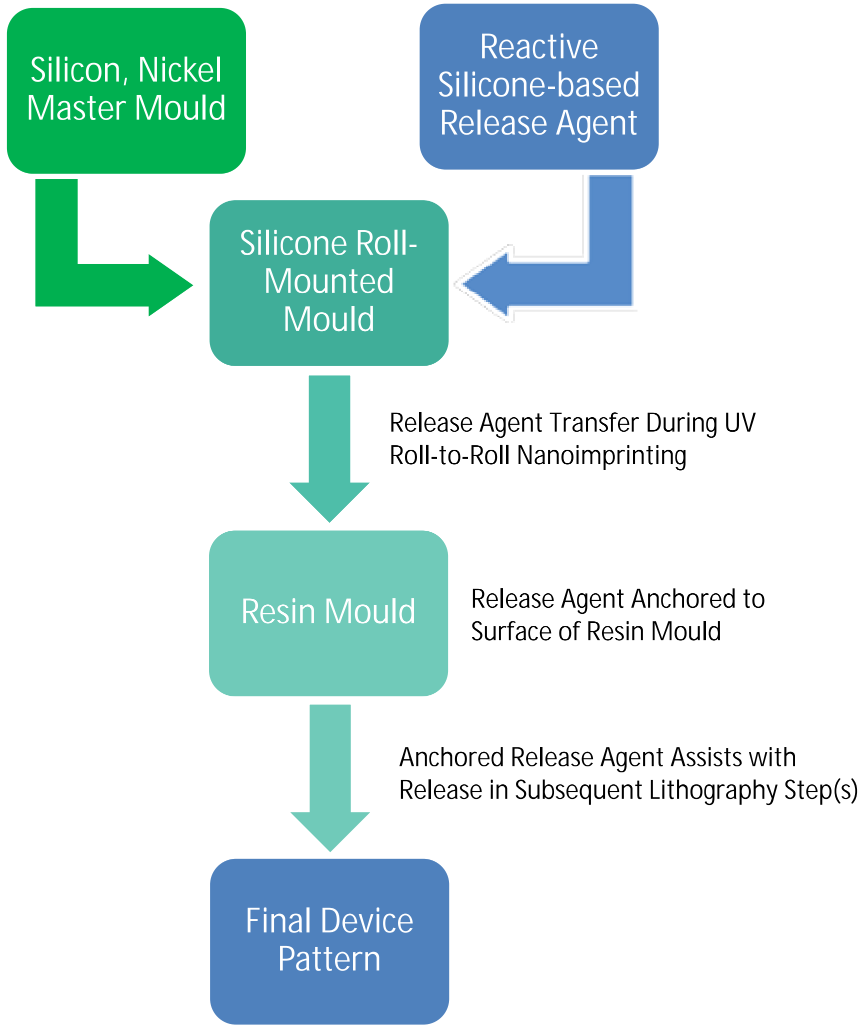

Figure 4.4 Workflow schematic showing the fabrication of a silicone roll-mounted mould from a master, followed by absorption of a liquid, reactive silicone-based release agent. The surface tension of the release agent must be lower than that of the silicone mould surface to promote migration to said surface. Resin moulds are fabricated by UV roll-to-roll nanoimprinting against the silicone mould with embedded release agent, allowing transfer of the release agent to the resin mould surface. Because the release agent is reactive (methacrylated), it participates in the resin mould polymerization reaction and is covalently bound at the surface of the resin mould. The anchored release agent assists with release in subsequent lithography step(s) utilizing the resin mould.

4.5.1 Master Mould Preparation and Replication into h-PDMS/ PDMS bi-layer Silicone Roll-mounted Moulds

Masters comprised of 250 nm linewidth aspect ratio (AR) 1 grating, 500 nm diameter AR 1 pillar, 500 nm linewidth AR 4 grating and 500 nm diameter AR 4 pillar master moulds obtained in silicon (fabricated via photolithography) or in nickel (negative replica copied from patterned photoresist via nickel electroforming). The precise dimensions for each mould are given in Table 4.1. Regardless of the master mould material used, the surface was exposed to an oxygen plasma descum for two minutes in order to clean and populate the surface with hydroxyl groups. The master moulds were then exposed to a 1H,1H,2H,2H-perfluorodecyltrichlorosilane (FDTS) vapour under vacuum for 2 hours in order to form a monolayer anti-stick coating on their surfaces. Following which the moulds were thoroughly cleaned by DI water to remove loose FDTS chains, dried by nitrogen gas gun and baked at 180 °C for 2 hours.

Table 4.1 Dimensions & feature geometries of master moulds used for h-PDMS/PDMS roll-mounted mould replication.

	Dimensions	**Feature Diameter (Linewidth) (nm)**	**Feature Height (nm)**	**Feature Pitch (nm)**
250 nm linewidth, AR 1 grating mould	20 mm x 10 mm	280	280	500
500 nm diameter, AR 1 hole mould (pillar imprint)	160 mm x 75 mm	500	500	1000
500 nm linewidth, AR 4 grating mould	20 mm x 20 mm	500	2000	1000
500 nm diameter, AR 4 hole mould (pillar imprint)	20 mm x 20 mm	500	2000	1000

Replication of the master moulds into an h-PDMS / PDMS bi-layer silicone roll-mounted mould was chosen for the intrinsically low surface energy of silicones,[139,140] the high resolution and high aspect ratio capability of h-PDMS,[69] transparency to UV light, and perhaps most importantly, miscibility with silicone-based reactive release agents but with a limited swelling response thanks to the highly cross-linked nature of the h-PDMS layer. Sylgard 184 PDMS is well known to swell considerably upon exposure to miscible solvents.[150] This has the effect of severely distorting features in conventional PDMS moulds. However, by replicating the negative relief structures of the master mould into h-PDMS, the swelling response to silicone-based release agent absorption can be mitigated. Unfortunately, h-PDMS is also quite brittle as a consequence of its higher cross-link density and fails via cracking using the well-known formulation provided by Schmid & Odom,[68,69] even with a soft PDMS backing layer.[69] It was found that this literature formulation was only useful for small scale moulds given their cracking density. Thus, in order to drastically improve handling and scalability for purposes of producing large area roll-to-roll compatible bi-layer moulds, an adjustment to the h-PDMS formulation weightings was necessary.

h-PDMS was prepared from VDT-731 (Gelest) vinyl PDMS prepolymer, HMS-301 (Gelest) hydrosilane prepolymer, platinum divinyltetramethyldisiloxane catalyst (SIP6831.2LC, Gelest) and 2,4,6,8-tetramethyltetravinylcyclotetrasiloxane modulator (87927, Sigma-Aldrich). Table 4.2 shows the current and literature weight proportions for the h-PDMS formulation for comparison. The amount of VDT-731 (the viscous prepolymer component) was increased by ~8.8% to 3.7 g in order to improve flexibility and crack resistance at the expense of the stiffness, or modulus of h-PDMS. The modulator component was increased from “one drop” (~0.01 – 0.02 g) to 0.05 g (~1%

wt.) for the same purpose, as well as to increase the pot life of the mixture to ~2 hours at room temperature. 3.7 g of VDT-731, 50 μL of platinum catalyst, and 0.05 g of modulator were thoroughly mixed and degassed under vacuum for 1-2 minutes. 1 g of HMS-301 was then added to the mixture, followed by spincoating at 6000 RPM for 30 seconds onto the master mould, forming an ~13.5 μm thick h-PDMS film. The h-PDMS films were allowed to gel at room temperature for two hours. The films were not baked at elevated temperature (as in the literature) as doing so led to dewetting of the FDTS coated master mould surface. Sylgard 184 (Dow Corning) was then poured on top of the gelled h-PDMS films (~3 mm thick layer) and cured for at least one hour at 60 °C. This method relies on adhering the Sylgard 184 PDMS to h-PDMS via infiltration into the partially cured h-PDMS, which is among the strongest known PDMS bonding methods.[156] After curing, the h-PDMS/PDMS composite moulds were carefully trimmed and peel separated from the master. For grating moulds, the peel separation direction was always oriented parallel to the grating lines. Large roll-to-roll compatible h-PDMS/PDMS composite moulds of 160 x 75 x 4 mm size were produced from nickel shim masters, while smaller test moulds and sheets (from 20 x 10 x 3 mm to 30 x 30 x 3 mm in size) were fabricated against silicon masters and diced wafers, respectively.

Table 4.2 h-PDMS formulation from literature with comparison to the present modified formulation for large area roll-mountable h-PDMS/PDMS moulds.

	VDT-731 (g)	**Platinum divinyl-tetramethyl-disiloxane catalyst (uL)**	**2,4,6,8 tetra methyl-tetravinyl cyclotetra-siloxane inhibitor (g)**	**HMS-301 (g)**	**Young's Modulus (MPa)**
Schmid & Odom[68,69]	3.4	18	One drop (~0.01 – 0.02)	1	Up to 9 MPa (usually 7-8)
Modified Formulation	3.7 (77.4% wt.)	50 (~1% wt.)	0.05 (1% wt.)	1 (20.6% wt.)	~6 Mpa STDev ±0.4

4.5.2 Exposure and Absorption of Silicone-based Reactive Release Agent by h-PDMS/PDMS bi-layer Silicone Roll-mounted Moulds

Asymmetric monomethacryloxypropyl-terminated polydimethylsiloxane (mPDMS, MW 600-800, 6-9 mPa·s, Gelest MCR-M07) was selected as the methacrylated release agent after predictive solubility calculations were carried out to determine which release agents would be miscible in solid silicones (see Appendix A). An oligomeric reactive siloxane was chosen for several reasons, most importantly to promote solubility with the h-PDMS/PDMS bi-layer mould. Polymer / solvent miscibility is governed by thermodynamics, in particular the increase in the entropy of mixing typically becomes progressively smaller as the molecular weight of the components of the blend increase.[157] Monomer units in polymer chains are covalently bound in linear fashion, thus the number of possible configurations per unit volume that chains in the mixture can be arranged in becomes smaller as chain length increases. Thus the increase in configurational entropy is generally small for polymer blends and approaches zero for very high molecular weight polymers.[157] Flory-Huggins interaction parameter calculations also found that a short-chain oligomer is a better choice for promoting solubility from the standpoint of thermodynamics (see Appendix A). Short chain oligomers can furthermore diffuse more easily to the surfaces of solids, given a concentration gradient or thermodynamic driving force to lower the mould surface energy, which is useful for promoting transfer. Finally, short-chain dimethylsiloxane oligomers have the lowest surface tension due to higher methylated content from terminal groups.[158]

Pure mPDMS release agent can be applied immediately to as-fabricated h-PDMS/PDMS moulds without any special pre-treatment. Note however, that full immersion of the h-PDMS/PDMS composite moulds was avoided, as the PDMS backside surface of the

composite mould would absorb mPDMS and swell significantly more than the h-PDMS layer, causing the h-PDMS patterned face to bend in a concave manner, making contact and spreading of the resin against the h-PDMS surface difficult. Instead, as shown in Figure 4.5, mPDMS was pooled exclusively on the h-PDMS mould face such that the surface was completely covered for 15 minutes. This was ample exposure time to ensure the mPDMS soaked entirely through the 13.5 μm h-PDMS layer and swell a portion of the PDMS backing layer such that the physical bending response of the composite mould would indicate that the h-PDMS layer was saturated with mPDMS. In general, the PDMS backing layer begins to swell within ~5 minutes of exposure to mPDMS pooled on the h-PDMS mould face.

After mPDMS exposure, excess release agent is poured off into a container for re-use and the remainder is removed with high pressure nitrogen gas. This will usually leave a thin residual coating of mPDMS on the composite mould surface, as mPDMS is non-volatile (only about ~3% of low molecular weight components will evaporate at room temperature). Moulds with features capable of diffracting visible light will typically no longer diffract light after mPDMS exposure due to the presence of this residual coating having a refractive index that is similar to the h-PDMS structures. This coating is removed by carrying out an initial imprint process and disposing of the first imprint field, which removes the excess by participation in the polymerization of the resin.

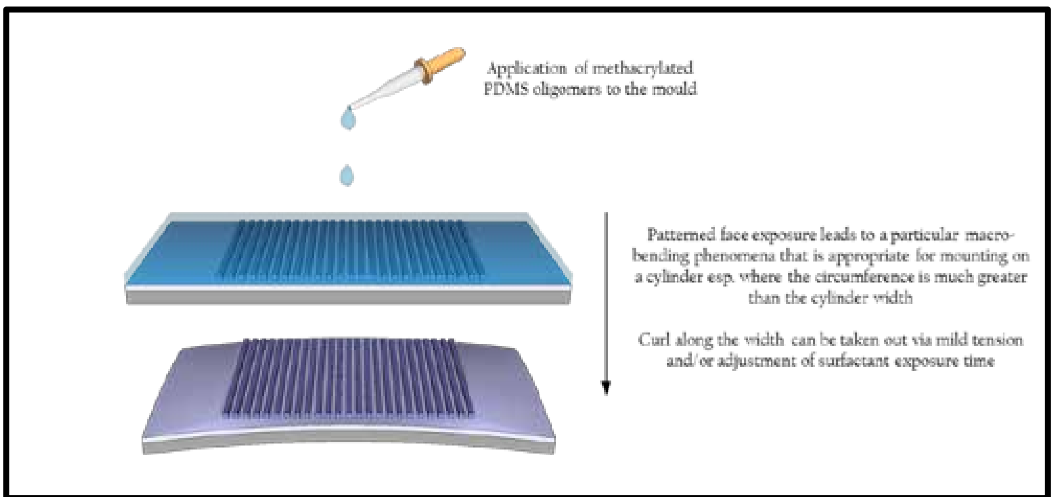

Figure 4.5 mPDMS deposition scheme onto h-PDMS/PDMS composite moulds via pooling on the patterned h-PDMS face. Swelling of the PDMS backing layer immediately adjacent to the h-PDMS film occurs within about ~5 minutes of mPDMS exposure, causing a swelling mismatch and convex bending of the composite mould as shown.

4.5.3 Transfer of mPDMS from h-PDMS/PDMS bi-layer Silicone Roll-mounted Moulds to Fabricated Resin Moulds During UV Roll-to-Roll Nanoimprinting

Following the mPDMS release agent exposure step, fabricated h-PDMS/PDMS moulds were wrap mounted in our lab-scale UV roll-to-roll nanoimprinting system (SRS 400, Solves Innovative Technology) as shown in Figure 4.6. This tool is capable of mechanically affixing standard mould sizes of 160 x 75 mm as well as smaller, irregular sized moulds via tape affixation or fabrication of a customized slot mount. Resin deposition is carried out via inkjet dispense following a pre-programmed drop map. With inkjet printing, resin dispense takes the form of discrete micro-droplets dispensed with an inkjet print head across an arbitrary rectangular area, within certain outer boundaries. This is controlled by a programmed drop map using computer software that controls the inkjet dispense apparatus. This drop map can be adjusted in terms of both area and

positioning along the imprint drum width in order to facilitate use of arbitrary mould sizes and mounting positions. The density of dispensed drops can also be varied by adjusting the operating frequency of the inkjet print head or by changing the throughput of the roll-to-roll system. Increasing the drop density also constitutes an increase in the total volume dispensed over a given area, all else being equal. The print head itself contains a line of 256 piezo-controlled dispense nozzles. The operating frequency can be adjusted from 10 kHz – 30 kHz. After passing through the spreading roller, which applies a 400 kPa line pressure transient, the drop map becomes a continuous resin coating sandwiched between the roll-mounted mould and the substrate web.

125 μm thick, 300 mm wide and 100 m long polycarbonate reels with double-sided protective covering layers were used as the substrate web material for similar reasons as given in Chapter 3. Spreading of the resin drop field onto the polycarbonate web is obtained via soft rubber spreading rollers, followed by high intensity 395 nm UV LED exposure (peak irradiance of 8 W cm^{-2} at the array emitting window) at 1 meter min^{-1} to ensure complete curing. This will cure the resin coating against the h-PDMS/PDMS mould with embedded mPDMS, allowing transfer of surface mPDMS to the newly fabricated resin mould. Finally, the resin mould is peel separated from the h-PDMS/PDMS mould as the polycarbonate web line is drawn away from the imprint drum. More detailed discussion on the performance characteristics of the SRS 400 and general information on resin mould fabrication can be found in Chapter 3 and elsewhere.[32]

Figure 4.6 Large area 160 x 75 x 4 mm, 500 nm diameter AR 1 hole h-PDMS/PDMS composite mould mounted on the SRS 400 UV roll-to-roll nanoimprinting system, post-mPDMS exposure, after the 1st imprint to remove residual mPDMS. At left, zoomed in side view. At right, zoomed out front view.

4.5.4 Test Bed Resin Formulation for UV Roll-to-Roll Nanoimprint Fabrication of Resin Moulds and Blank Resin Films

In terms of resin selection for fabrication of resin moulds, a test bed resin comprised of 1,6 hexanediol diacrylate monomer, neopentyl glycol diacrylate crosslinker, and diphenyl(2,4,6 trimethylbenzoyl) phosphine oxide photoinitiator was formulated (see Table 4.3). These components were selected as they are silicon-free for the purpose of later detection of transferred mPDMS via XPS characterization. They are also widely used in the literature and in commercially available resin formulations, and are inexpensive. The obtained formulation has a low viscosity of ~9 mPa·s for compatibility with inkjet dispense, which is the mode of resin deposition used by our UV roll-to-roll nanoimprinting system. Linear shrinkage of ~5% is typical for this formulation against reference moulds with sub-micron structures (cf. typical linear shrinkage range for acrylates of ~1-6%).[36,37]

Table 4.3 Test bed resin formulation for fabrication of resin moulds via UV roll-to-roll nanoimprinting. Formulation is silicon-free for the purpose of characterizing mPDMS release agent transfer from h-PDMS/PDMS roll-mounted moulds.

	1,6-hexanediol diacrylate (monomer)	**neopentyl glycol diacrylate (cross-linker)**	**Diphenyl(2,4,6 trimethylbenzoyl) phosphine oxide (photoinitiator)**	**Mono-methacryloxy-propyl terminated Polydimethylsiloxane – asymmetric (MPDMS)**
Molecular Weight	226.27	212.24	348.37	600 – 800
Boiling Point °C	295	268	520	>205
Density g/cm^3	1.01	1.031	1.17	0.96
Wt. %	59	39	2	<<1 (at surface, w/ trace amounts in cured bulk)
Structure				

4.5.5 Characterization Methods for Fabricated Resin Moulds and Blank Resin Films with Transferred mPDMS

UV roll-to-roll nanoimprinted resin mould samples produced as above were characterized via field emission scanning electron microscope (FESEM, JEOL JSM-6700F). For cross-section imaging, resin mould samples were immersed in liquid nitrogen and then broken to cleanly expose the cross-section profile. Samples were coated with platinum prior to analysis.

Characterization results were collected from 30 x 30 x 0.125 mm blank (featureless), cured resin films using the Table 4.3 resin formulation on polycarbonate substrates. mPDMS was transferred to these samples from 30 x 30 x 3 mm h-PDMS/PDMS sheets at

1 m min^{-1} throughput. These resin film samples were characterized via advancing water contact angle measurements and X-ray photoelectron spectroscopy (XPS) surface analysis. In order to assist with separating the presence of mPDMS from the native un-crosslinked dimethylsiloxane oligomers transferred to these resin films from the h-PDMS/PDMS sheet, the latter sheets were partially extracted with solvents. Here it must be noted that highly soluble solvents such as diisopropylamine, triethylamine and hexanes cannot be used to extract un-crosslinked oligomers from h-PDMS/PDMS composite sheets (or moulds) due to swelling mismatch. Because these solvents cause such dramatic swelling of PDMS, with swelling ratios in the range of ~1.3 – 2.13,[150] the mismatch stress with h-PDMS becomes so great that the h-PDMS fails due to cracking. The crack density is typically great enough that reliable surface measurements of resin films cured against h-PDMS/PDMS sheets extracted in this manner are not feasible (esp. dynamic contact angle measurements). Extraction of monolithic h-PDMS sheets was also attempted, however uniform de-swelling of h-PDMS by immersion in progressively less soluble solvents as recommended by Lee *et al.* proved to be extremely challenging.[150] Because the change in swelling ratio from one solvent to the next is often significant (for example, diisopropylamine – toluene $\Delta \sim 0.82$), and because the new solvent must diffuse non-uniformly from the bath at the surface of the h-PDMS sheet into the bulk, a large swelling mismatch develops upon exchange of solvents that leads to material failure. Thus, lower solubility solvents were used to partially extract the h-PDMS/PDMS sheets such that while the native un-crosslinked oligomers were not completely removed from the h-PDMS surface, their concentration was greatly reduced relative to the amount of mPDMS release agent introduced to the h-PDMS/PDMS sheets (see Results & Discussion for further details). h-PDMS/PDMS sheets were thus immersed in sequential baths of 2-propanol, acetone and ethyl alcohol for 24 hrs each

following the order of descending swelling ratio. Other solvents were attempted, however those that were known to have a PDMS swelling ratio $\gtrsim$1.1 failed due to cracking. All baths were left at room temperature and agitated with a stir bar. The bath sequence was repeated twice, such that the extraction process lasted for 6 days. Following the final bath immersion, the h-PDMS/PDMS sheets were dried under vacuum overnight and were then exposed to mPDMS release agent as laid out previously.

XPS characterization of cured resin films was carried out with a VG ESCALAB 220i-XL ultra-high vacuum system. Data was collected in the form of survey scans and high energy resolution scans of carbon 1s, oxygen 1s and silicon 2p peaks. The presence and amplitude of the silicon 2p peak was used to indicate the presence and relative concentration of transferred siloxane chains from the h-PDMS/PDMS mould. The resin composition was deliberately chosen to be silicon-free for this purpose. The instrument was equipped with a monochromatic Al Kα (1486.6 eV) source and a concentric hemispherical energy analyzer. The analysis chamber pressure was ~10^{-10} Torr. Survey and high energy resolution scans were collected with pass energy of 150 eV and 10 eV, respectively.

Blank, cured resin films fabricated using the Table 4.3 resin formulation with transferred mPDMS were also characterized as to their wetting performance via advancing water contact angle measurements. This was also done to provide a complementary measurement to XPS and thereby gain additional insight into the relative release performance of these surfaces. Contact angle measurements were acquired with a Rame-Hart Contact Angle Goniometer (NRL 100) using the tilted plate method to acquire the advancing water contact angle.[159] The advancing water contact angle used herein is

defined as the leading angle measured at the point of incipient forward motion of the entire sessile drop. The tilting plate method overcomes certain difficulties arising from measurement of the static contact angle. For example, the evaporation of the static sessile drop in non-saturated atmospheres combined with variable delays between drop formation and data capture often leads to significant experimental error. Additionally, the tilted plate method does not require a deposition needle to contact the sessile drop, which is also a source of significant experimental error.[159] A known drawback of the method is the dependence of the advancing contact angle measurement on how the sessile drop is formed on the sample surface, which plays a critical role in determining the shape of the drop contact line.[159] Our instrument deposits the sessile drop from a dispense tip located just above the sample surface, such that the dispense tip is very close to the sessile drop but does not actually contact it during or after drop formation. Drop placement was carried out while the holding plate was level and care was taken to ensure that the drop contact line was approximately circular and reproducible prior to commencement of the experiment. The volume of the drop was always 40 μL. Profile images of drops were taken using a CCD camera at 640 x 480 pixels while backlit with a diffused halogen lamp. The camera was attached to the stage apparatus which could be inclined by a manual turning crank. The stage was inclined slowly to minimize vibration at about 1° s^{-1} until within about 3-4° of incipient forward motion (acquired from prior measurements). Then the stage was inclined in increments of approximately 1°, followed by immediate image capture and contact angle measurement. During contact angle measurement, the computer software will project an outline of the previously captured position of the sessile drop on the live video monitor. When downhill motion of the trailing edge of the sessile drop was observed, this data point was saved (generally the leading edge of the drop will move first, followed by both the leading and trailing edges).

Measurements continue in 1° increments until the drop moves discernibly but the advancing and receding contact angles do not change appreciably from the prior measurement (≤ 0.3° change, respectively). This indicates that the entire drop moved, as opposed to slippage of only a portion of the contact line. The data point captured upon observation of this motion of the entire sessile drop is termed the advancing water contact angle. For each sample, five different locations on the surface were measured and two samples were fabricated for each set of conditions for a total of N = 10 measurements for each data point.

4.6 Characterization of Modulus for Modified h-PDMS Formulation

Tensile mechanical testing was carried out on h-PDMS strips that were punched from flat, featureless h-PDMS sheets produced using our modified h-PDMS formulation provided in Table 4.2 for the purpose of determining the modulus and the ultimate tensile stress (UTS). An Instron 5569 Universal Testing System with pneumatic side-action grips was used as shown in Figure 4.7 to apply a progressive tensile load to 20 x 5 x 0.53 mm thick strips for the purposes of determining the modulus. The tensile load was measured with a 10 N load cell. The strain was measured using a non-contact video extensometer at an extension rate of 1 min^{-1}, giving a strain rate of 0.05 min^{-1}. The mean tensile modulus of this formulation was found to be ~6 MPa measured across 7 specimens (see Figure 4.8). Alternatively, where the axial strain at failure is taken as a figure of merit denoting a sample with more uniform mixing and lower defectivity, then the modulus of the sample with the largest axial strain at failure given as ~6.5 MPa can also be taken as a reasonable measure. This compares to 1.8 MPa for Sylgard 184 PDMS

and ~9 MPa for h-PDMS as provided in the literature.[68,143] Thus, our revised h-PDMS formulation retains an approximate majority of the stiffness of the original formulation and a reasonable resolution limit of roughly 100 nm can be assigned.

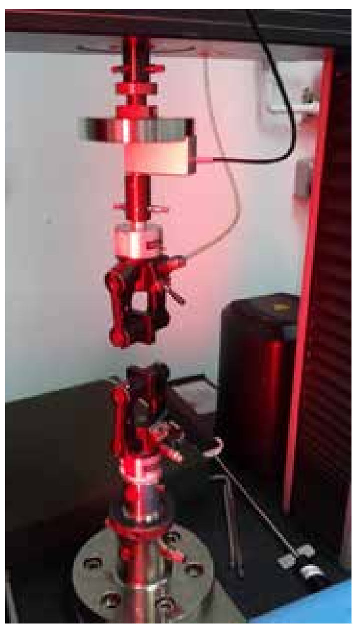

Figure 4.7 Instron 5569 Universal Testing System with pneumatic side-action grips and a mounted 20 x 5 x 0.53 mm h-PDMS strip. The overhead grip is attached to a 10N load cell. The strain was measured using a non-contact video extensometer at an extension rate of 1 mm min^{-1} (strain rate of 0.05 min^{-1}).

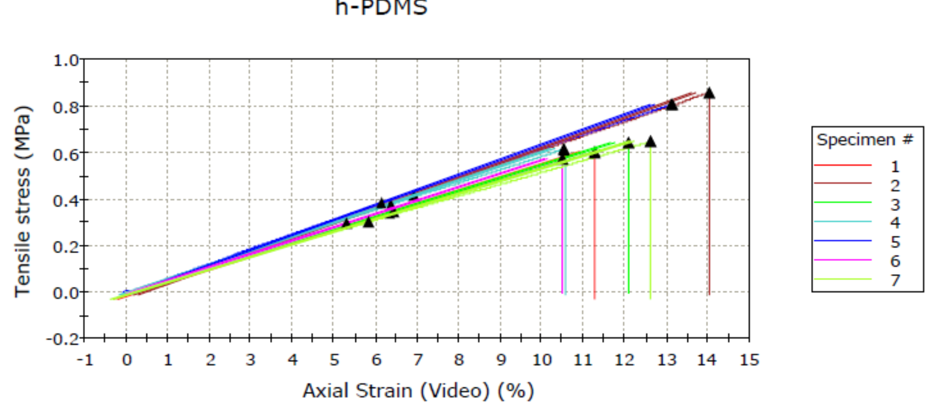

	Modulus (Young's - Cursor) (GPa)	Maximum Tensile stress (MPa)	Tensile stress at Yield (Offset 0.1 %) (MPa)	Tensile strain at Yield (Offset 0.1 %) (%)
1	0.00560	0.60168	0.33980	6.35210
2	0.00648	0.85737	0.41688	6.93128
3	0.00557	0.64301	0.34753	6.47062
4	0.00602	0.61376	0.37663	6.39834
5	0.00645	0.80574	0.38235	6.15444
6	0.00572	0.57162	0.29341	5.31745
7	0.00539	0.64531	0.29996	5.81173
Mean	0.00589	0.67693	0.35094	6.20514
Standard Deviation	0.00044	0.10958	0.04480	0.51672

Figure 4.8 Stress-strain plot for the modified h-PDMS formulation, measured across 7 20 x 5 x 0.53 mm h-PDMS strips. Mean Young's Modulus was measured to be ~6 MPa, while the sample with the largest axial strain obtained a Modulus of ~6.5 MPa.

4.7 mPDMS-exposed h-PDMS/PDMS Bi-layer Roll-Mounted Mould Results

As briefly mentioned earlier, an h-PDMS pattern-carrying layer was crucial in mitigating the swelling response of the h-PDMS/PDMS bi-layer roll-mounted mould. This is not to say that h-PDMS does not swell in response to mPDMS absorption, however h-PDMS was instrumental in keeping the degree of swelling small and therefore fully reversible. Other silicones such as Sylgard 184 PDMS are known to swell to such a large extent when absorbing good solvents that irreversible deformations can occur.[150] The swelling response of h-PDMS to good solvents is much smaller than conventional Sylgard 184 PDMS due to its crosslink density. For h-PDMS, the molar mass between crosslinks in the polymerized network, M_c of VDT-731 is 987 g mol^{-1}, while the molecular weight of

a basic unit of dimethylsiloxane is 74, so the number of repeat units between crosslinks x is only ~13 – 14.[68] In contrast, M_c for Sylgard 184 is roughly double, at 1957 g mol^{-1} giving an x of ~26 – 27.[149] The reduced number of repeat units between crosslinks (or conversely, the heavier crosslink density) increases the thermodynamic barrier to mPDMS dissolution as given by Kovac's modified Flory-Rehner model equation at equilibrium for heavily cross-linked polymers ($x < 100$)[160]

$$\frac{\partial}{\partial n_s}\left(\frac{\Delta G_{mix}}{k} + \frac{\Delta G_{elastic}}{k}\right) = 0 = ln(1-\upsilon_2) + \upsilon_2 + \chi\upsilon_2{}^2 + \frac{\rho_2 V_1}{M_c}\upsilon_2{}^{\frac{1}{3}} + \frac{\rho_2 V_1}{2xM_c}\upsilon_2{}^{\frac{1}{3}} \qquad (4.4)$$

where ΔG_{mix} is the free energy change upon mixing of a polymer and solvent, $\Delta G_{elastic}$ is the free energy change due to swelling of the polymer network, υ_2 is the volume fraction of the polymer in the swollen gel, $\frac{1}{\upsilon_2}$ is the swelling ratio, χ is the Flory-Huggins interaction parameter, ρ_2 is the polymer density, M_c is the average chain molecular weight between crosslinks, $\frac{\rho_2}{M_c}$ is the crosslink density in the polymer, and V_1 is the molar volume of the solvent. The first three terms on the right hand side of Eqn. 10 take into consideration the free energy change due to mixing, while the final two terms account for the negative entropy change due to swelling. It can be seen that the swelling terms will become large as M_c and/or x become small (cross-link density becomes very high). If a relatively high molar volume solvent such as mPDMS is also used (625 – 833 cm^3 mol^{-1}), then the swelling ratio required to balance the equation will be small. The relative concentration of cross-linker (HMS-301 for h-PDMS) in the formulation also plays a role in determining whether cross-links are actually formed at all available sites, however, as a first approximation the above values indicate that the degree of swelling of the structure-carrying h-PDMS film is greatly reduced relative to a PDMS equivalent.

Figure 4.9 shows the macro effect of the mPDMS release agent exposure step to the h-PDMS/PDMS mould contour for small test moulds of 20 x 10 x 3 mm size. The inset shows the pristine h-PDMS/PDMS mould prior to mPDMS exposure. It can be seen that the diffractive effect of the 250 nm grating mould structures is maintained but that the diffraction is no longer uniform because of the mould curvature. For strictly rectangular mould geometries, where one areal dimension is much shorter than the other, the swelling mismatch between the h-PDMS and PDMS layers causes the mould to take on a cylindrical contour where mPDMS exposure occurs through the h-PDMS patterned face. This bending contour allows for easy mounting to a roll-to-roll mould cylinder or imprint drum as shown previously in Figure 4.6. This geometry-dependent bending effect is well suited to an imprint drum with a large circumference / width ratio. For h-PDMS/PDMS moulds that are relatively wide, the bending effect along this dimension can be taken out with mounting tension, or by reducing the mPDMS exposure time. The objective of an optimally long mPDMS exposure time is simply to ensure the availability of a large volume of absorbed release agent near the h-PDMS/PDMS mould surface, to serve as a release agent source while in service. After release agent exposure the mould is in a non-equilibrium state in the sense that excess release agent will continue to diffuse further into the PDMS backing layer over time until a uniform release agent concentration throughout the bulk of the silicone mould is established. Optimal saturation of the h-PDMS layer and immediately adjacent PDMS is helpful for the purposes of shifting the mPDMS concentration gradient front as far into the PDMS backing layer as possible. Ample exposure time of 15 minutes was given in order to maximize release performance over multiple UV roll-to-roll nanoimprinting cycles. Note that longer exposure times (>15 minutes) generally lead to failure of the composite mould via propagation of edge cracks that are initiated upon cutting and trimming the fabricated h-PDMS/PDMS mould

out of its cast, thus care was taken to tune the exposure time below the failure threshold. Further studies are required and are planned to optimize the mPDMS exposure time to minimize the swelling mismatch while still saturating the h-PDMS layer with mPDMS and thus maintaining optimal mPDMS transfer to resin mould surfaces. The results of these studies will hopefully allow a more precisely defined, reduced exposure time of less than 5 minutes, which is where swelling mismatch can be visually observed.

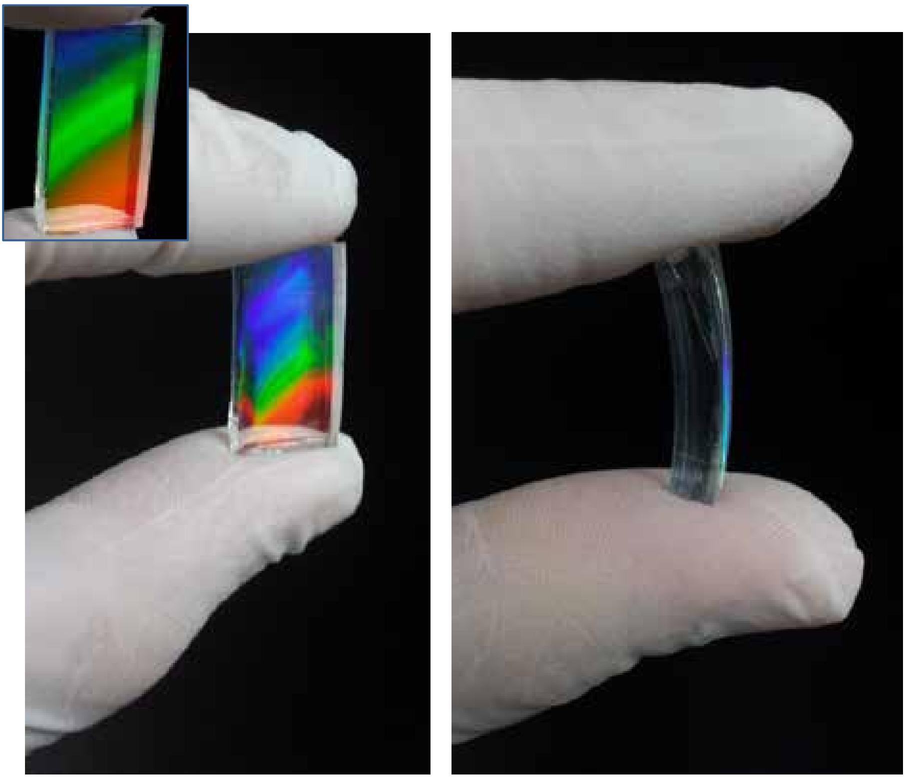

Figure 4.9 Macro-bending effect of mPDMS exposure on 20 mm x 10 mm x 3 mm, 250 nm linewidth AR 1 grating h-PDMS/PDMS test mould. (At left) front view, (Inset) original appearance after trimming, prior to mPDMS exposure, (At right) side view showing the cylindrical contour of the test mould.

4.8 Resin Mould Fabrication Results Utilizing mPDMS-Exposed h-PDMS/PDMS Composite Roll-Mounted Moulds

Following absorption of mPDMS as described above, h-PDMS/PDMS roll-mounted moulds fabricated using our modified formulation were used to deliver the mPDMS release agent to UV roll-to-roll nanoimprinted resin surfaces *in situ* during actual fabrication. In order to avoid self-polymerization of the mPDMS within the h-PDMS/PDMS mould during UV roll-to-roll nanoimprinting, 395 nm peak UV / deep violet LED exposure was used to cure our test bed resin such that the incident light was of sufficiently low energy that it could only activate the resin photoinitiator to drive the polymerization. The emission band for the UV LED arrays in the SRS 400 is quite narrow at 380 – 420 nm, which is well outside the self-initiation threshold for acrylates (<267 nm).[161] In contrast, conventional mercury-arc UV lamps have broadband emission, and typically have a 254 nm emission peak that is only partially absorbed by PDMS.[162] We have found that use of mercury-arc UV lamp irradiation causes the mPDMS release agent to self-polymerize in the h-PDMS/PDMS composite mould without a photoinitiator. Self-polymerization extends the polymerized network deep into the bulk of the h-PDMS/PDMS mould, making clean separation impossible. Thus, only UV-A (320 – 400 nm) or deep violet exposure is recommended for the UV roll-to-roll nanoimprinting step to produce resin moulds with transferred mPDMS. This can be accomplished with properly filtered UV lamp light or with UV LED exposure as described.

Resin mould samples were produced from 250 nm AR1 linewidth grating, 500 nm linewidth AR4 grating and 500 nm diameter AR4 hole mPDMS-exposed h-PDMS/PDMS moulds (see Table 4.1) for the purpose of examining the effect of swelling on replication

fidelity. Control samples were also produced from pristine h-PDMS/PDMS moulds that were not exposed to mPDMS, and finally for the 250 nm AR 1 linewidth case, the master mould itself was cleaved for comparison with cleaved resin mould samples via SEM cross-section. Figure 4.10 shows representative 250 nm linewidth AR 1 grating, Figure 4.11 that of a 500 nm linewidth AR 4 grating and Figure 4.12, 500 nm diameter AR 4 pillar imprint SEM micrographs.

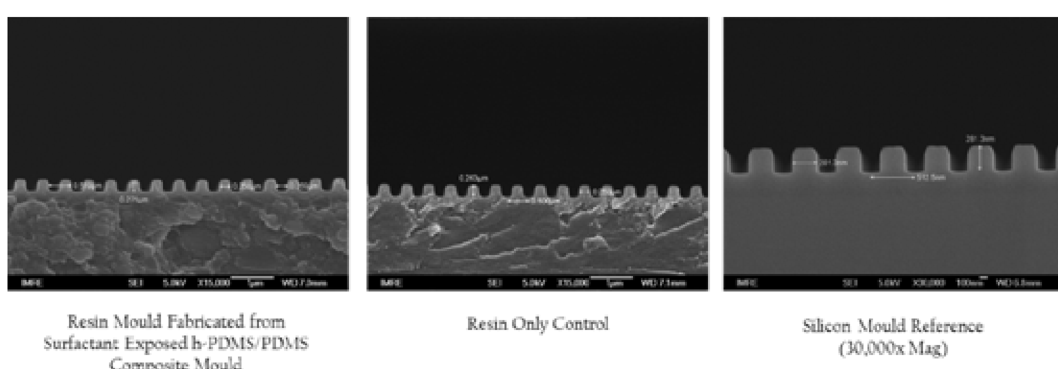

Figure 4.10 *(At Left, Center)* Cross-section SEM micrographs of 250 nm linewidth, AR1 resin mould samples and *(At Right)* mould cross-section. (*At Left)* Resin mould sample fabricated against an mPDMS exposed h-PDMS/PDMS mould. (*At Center)* resin mould sample fabricated against a pristine h-PDMS/PDMS mould (control sample). (*At Right)*, reference cross-section of the silicon master mould for assessment of overall shrinkage.

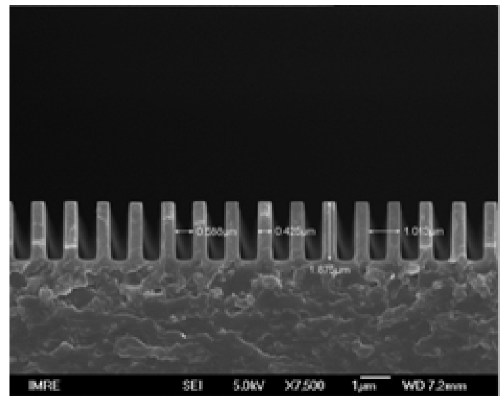

0.5 µm Linewidth, AR4 Resin Mould Fabricated from Surfactant Exposed h-PDMS/PDMS Composite Mould

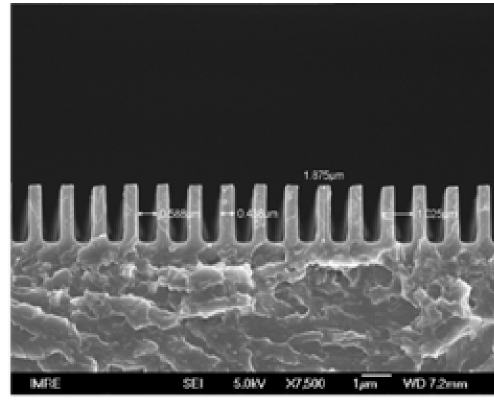

Resin Only Control

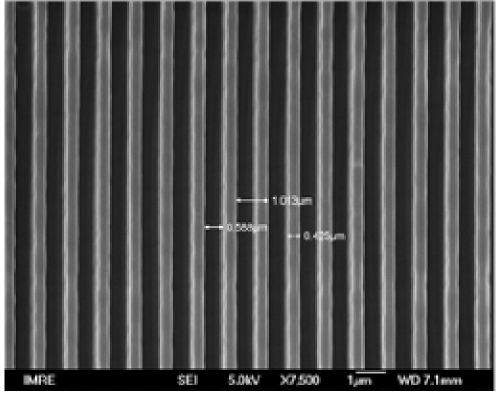

Figure 4.11 Cross-section and overhead SEM micrographs of 500 nm linewidth, AR 4 resin mould samples. *(At Left, Bottom)* Resin mould sample fabricated against an mPDMS exposed h-PDMS/PDMS mould. *(At Right)* Resin mould sample fabricated against a pristine h-PDMS/PDMS mould (control sample).

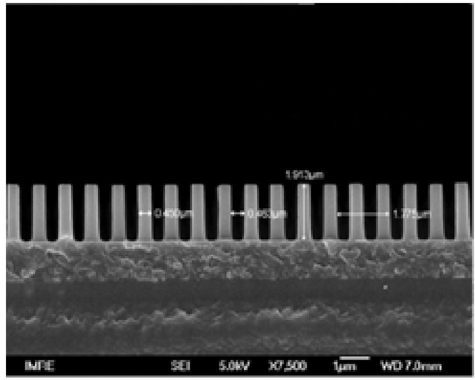

0.5 μm Linewidth, AR4 Resin Mould
Fabricated from Surfactant Exposed h-PDMS/PDMS Composite Mould

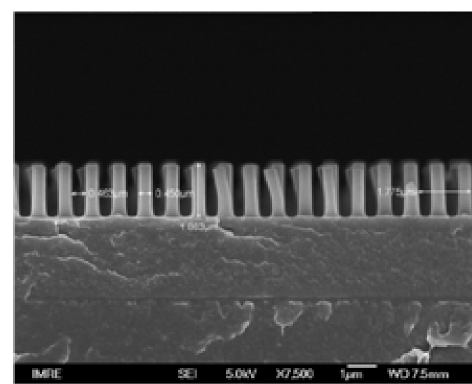

Resin Only Control

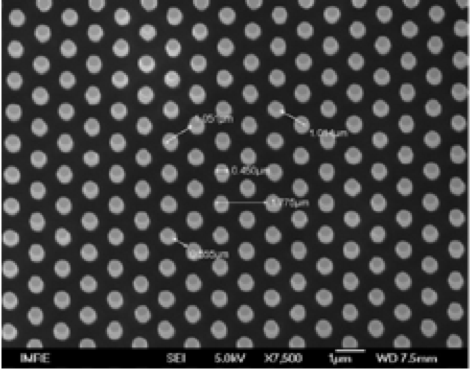

Figure 4.12 Cross-section and overhead SEM micrographs of 500 nm diameter, AR 4 pillar resin mould samples. *(At Left, Bottom)*, resin mould sample fabricated against an mPDMS exposed h-PDMS/PDMS mould. *(At Right)* Resin mould sample fabricated against a pristine h-PDMS/PDMS mould (control sample).

Lateral feature diameter, feature height and pitch were measured for all cases. In comparing the resin mould samples produced from mPDMS exposed h-PDMS/PDMS moulds against the control case, virtually all measurements were identical or within a variance of ±1.5% with the exception of the height measurement for the 500 nm diameter AR 4 pillar imprint sample, where the control sample suffered from partial collapse. This partial collapse proved to be unavoidable due to the adhesion of the h-PDMS/PDMS mould to the high aspect ratio resin structures leading to a large angle of separation. Release performance for the mPDMS exposed h-PDMS/PDMS case was improved,

likely due to the presence of a high concentration of mPDMS release agent at the interface.

In any case, such a small variance between mPDMS-exposed and mPDMS-free control sample measurements cannot be distinguished from measurement or instrument error. Thus differentiating loss of critical dimensions due to mPDMS swelling was not observed. This was quite a remarkable result in that the expected outcome was for there to be a difference in the total shrinkage of the resin mould features between samples produced from an mPDMS-exposed h-PDMS/PDMS mould and control samples that were produced from a pristine h-PDMS/PDMS mould. h-PDMS will swell upon absorbing mPDMS, and the additional swelling will increase the CD losses imposed on the resin mould features in addition to all other sources of shrinkage. However, the same overall pattern shrinkage was observed in both cases.

We speculate that the h-PDMS/PDMS mould actually absorbed low molecular weight components of the resin in both cases. Silicones in general, and PDMS in particular, are well known to absorb low molecular weight, low surface tension hydrocarbon liquids such as organic solvents.[150,163,164] For the pristine h-PDMS/PDMS mould (control case), the patterned h-PDMS layer may have simply absorbed certain components of the resin and swelled in response to this absorption. The mPDMS-exposed h-PDMS/PDMS mould may have been able to achieve a nearly identical degree of swelling by exchanging mPDMS for the liquid resin in contact with it. mPDMS is soluble in the liquid resin, thus it is possible for the mPDMS to diffuse out into the resin while resin components diffuse into the h-PDMS layer, allowing the h-PDMS to obtain a degree of swelling nearly identical to the control case. Given that the majority of the test bed resin components are

small molecules with molecular weights of <250 Daltons (see Table 4.3), and that this swelling change would only need to occur at the patterned surface of the h-PDMS layer, it is conceivable for these swelling changes to occur very quickly. Thus, typical liquid resin exposure times of ~1 minute prior to curing could be sufficient to obtain this result. Clearly, however, the matching resin mould feature dimensions are the product of a complex system behaviour that we don't yet fully understand and further work is needed to better track the swelling behaviour of the h-PDMS patterns during processing.

Aside from the nearly identical feature dimensions, the overall appearance of the imprinted resin mould structures in both cases are also nearly indistinguishable. We note the lack of wrinkling or striations along the sidewalls of the resin mould samples produced from mPDMS-exposed h-PDMS/PDMS moulds. This implies that the h-PDMS swelling response to mPDMS absorption was fully reversible and did not permanently deform the mould features. This is a welcome result from the perspective of maximizing fidelity to the master.

With respect to the 250 nm linewidth AR1 grating results, we can arrive at a linear shrinkage of ~11% in terms of feature width relative to the master mould cross-section SEM shown in Figure 4.10. From Choi we know that there will be a linear polymerization shrinkage of ~2% from replication of the master mould in h-PDMS.[143] Therefore the linear shrinkage attributed to other sources is about ~9%, which is about 4% greater than the reference shrinkage for our acrylate test bed resin. This additional 4% shrinkage is attributed to the swelling response of the h-PDMS layer of the h-PDMS/PDMS roll-mounted mould.

While the overall linear shrinkage is relatively large and requires further optimization, the SEM results do provide confirmation that UV roll-to-roll nanoimprint lithography with mPDMS exposed h-PDMS/PDMS roll-mounted moulds is feasible and that resin moulds can be fabricated at high aspect ratio with this arrangement. Large area fabrication of a 160 x 75 mm sub-micron structured resin mould is thus presented in Figure 4.13 containing 500 nm diameter, AR1 pillars using the 160 x 75 x 4 mm rectangular h-PDMS/PDMS mould shown in Figure 4.6. Aside from an edge exclusion required due to oxygen inhibition, it is straightforward to obtain high quality resin moulds from mPDMS exposed h-PDMS/PDMS composite moulds. Work is ongoing to provide an inert gas atmosphere to eliminate these edge defects.

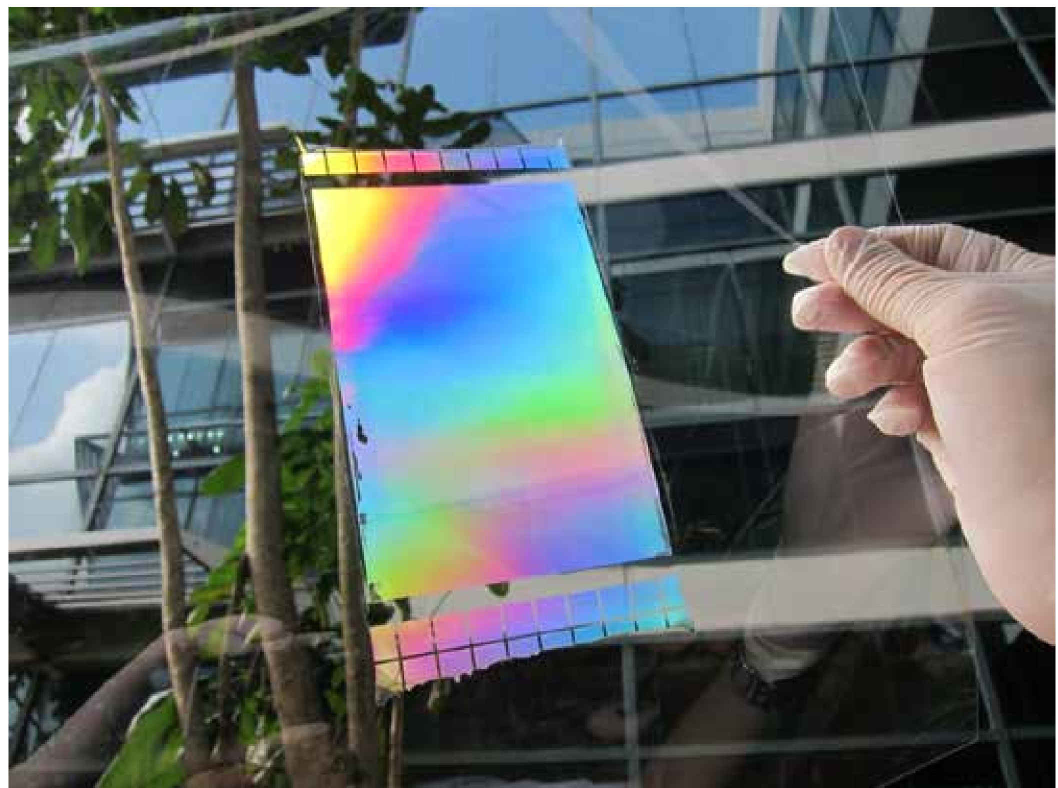

Figure 4.13 Large area 160 x 75 mm, 500 nm diameter AR1 pillar resin mould fabricated via UV roll-to-roll nanoimprinting from an mPDMS exposed h-PDMS/PDMS composite mould. Test metrology fields are shown to either side, which intersect with the resin coating edge. Edge defects originate from oxygen inhibition.

4.9 XPS Characterization of mPDMS Transfer to UV Roll-to-Roll Nanoimprinted Resin Films

To gain insight into the degree of transfer of mPDMS to UV roll-to-roll nanoimprinted resin moulds, the evolution of mPDMS transfer over multiple imprint cycles and its effect on surface wetting behaviour was studied against series of 30 x 30 x 0.125 mm blank (featureless), cured resin samples fabricated against mPDMS exposed, extracted h-PDMS/PDMS sheets. Figure 4.14 shows a series of XPS survey scan results for the 1st, 5th and 10th cured resin films produced sequentially from a single mPDMS-exposed h-PDMS/PDMS sheet, and a reference resin film that was cured against an mPDMS-free

h-PDMS/PDMS sheet. Table 4.4 provides the high energy resolution XPS scan results for the Si2p peak in counts per second (CPS), the Si2p/C1s ratio, and the corresponding advancing water contact angle measurements for selected imprint cycles after mPDMS exposure and the unexposed, extracted reference. First, it is visually apparent in comparing the 1st imprint sample with the reference result that the Si2p peak CPS is more than triple the extracted reference case and after 10 imprint cycles it remains about 1.5 times above reference. Thus it can be concluded with certainty that mPDMS release agent is being transferred to the surface of the polymerized resin films and have likely participated in the polymerization reaction and are thus covalently bound to the surface.

The Si2p/C1s ratio is also a useful normalized measure of the relative mPDMS surface concentration over multiple imprint cycles. It is insensitive to sampling variations in the form of differences in instrument detection efficiency as well as variations in the kinetic energy of core electrons emitted from the sample. We have used the C1s peak as the total carbon signal from the analyzed sample surface, inclusive of the resin film components and the transferred mPDMS. By normalizing the Si2p peak to the total C1s carbon peak, we are able to address the above sampling variations.

At low surface concentrations of mPDMS, changes in the Si2p/C1s ratio will better approximate the actual change in relative surface concentration of mPDMS between samples, as the concurrent change in the volume fraction of carbon from transfer of mPDMS to the resin film surface will be negligible. Thus it can be seen that the 10th imprint sample obtains an Si2p/C1s ratio that is still more than double that of the extracted reference (note that both h-PDMS/PDMS moulds used to fabricate these samples were extracted as described in the Experimental section), which is a good

indication that after 10 imprint cycles, the majority of silicone chains on the resin mould surface are mPDMS.

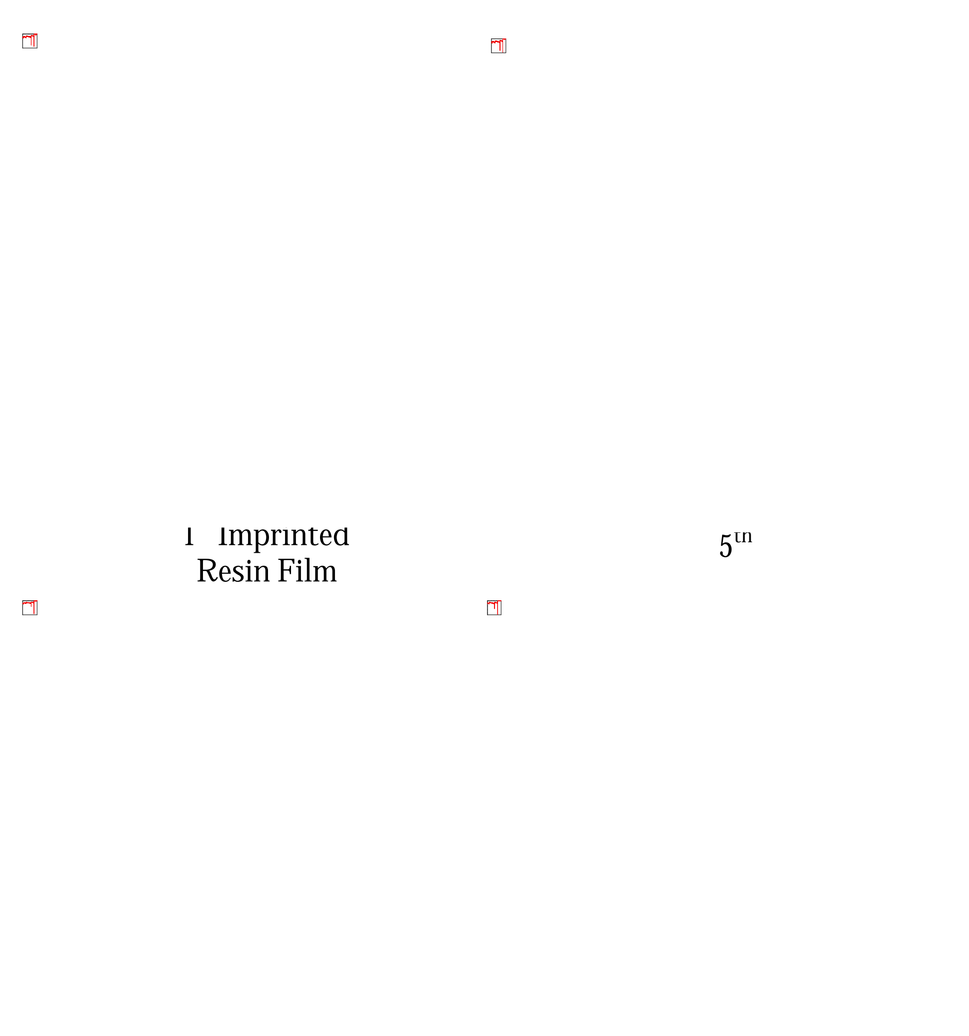

Figure 4.14 Series of XPS survey scans showing the evolution of the O1s, C1s and Si2p peaks on resin films fabricated from an extracted, mPDMS-exposed h-PDMS/PDMS sheet. 1st, 5th, and 10th imprint cycles are shown along with a reference scan of a resin film cured against an unexposed mPDMS-free, extracted h-PDMS/PDMS sheet.

Table 4.4 XPS & advancing water contact angle measurements of mPDMS transfer to fabricated resin moulds vs. no. of imprint cycles.

	1st Imprint	**2nd**	**3rd**	**4th**	**5th**	**10th**	**Ref**
Si2p CPS (Arb. Units)	113	95	80	57	62	46	34
Si/C Ratio	0.28	0.1	0.09	0.06	0.057	0.04	0.018
Advancing H_2O (°)	90	85	86	85	86	87	85

Figure 4.15 and Figure 4.16 are plots of the Si2p peak CPS and the Si2p/C1s ratio with increasing number of imprint cycles, respectively. Figure 4.15 was fitted to a single term exponential decay on a best-fit basis. Exponential decay provided the best fit given the fact that the mPDMS available for transfer at the h-PDMS/PDMS mould surface for a given imprint cycle would depend on the available mPDMS remaining from the prior cycle, which is a classic characteristic of exponential decay. The exponential decay formula is given in differential form as follows

$$\frac{\Delta N}{\Delta x} = -\lambda N \tag{4.5}$$

which has the solution

$$N(x) = N_o e^{-x/\lambda} + y \tag{4.6}$$

where N is the number of mPDMS molecules comprising the Si2p peak, x is the number of imprint cycles, λ is the exponential decay constant, N_o is the initial mPDMS quantity available for transfer prior to the first cycle $x = 0$ (more generally, $N_o + y$), and y is the

residual at x = ∞ where the model does not decay to zero. Adjusted R-square values of 0.94 for this fit to the Si2p peak CPS confirms that the fit is satisfactory.

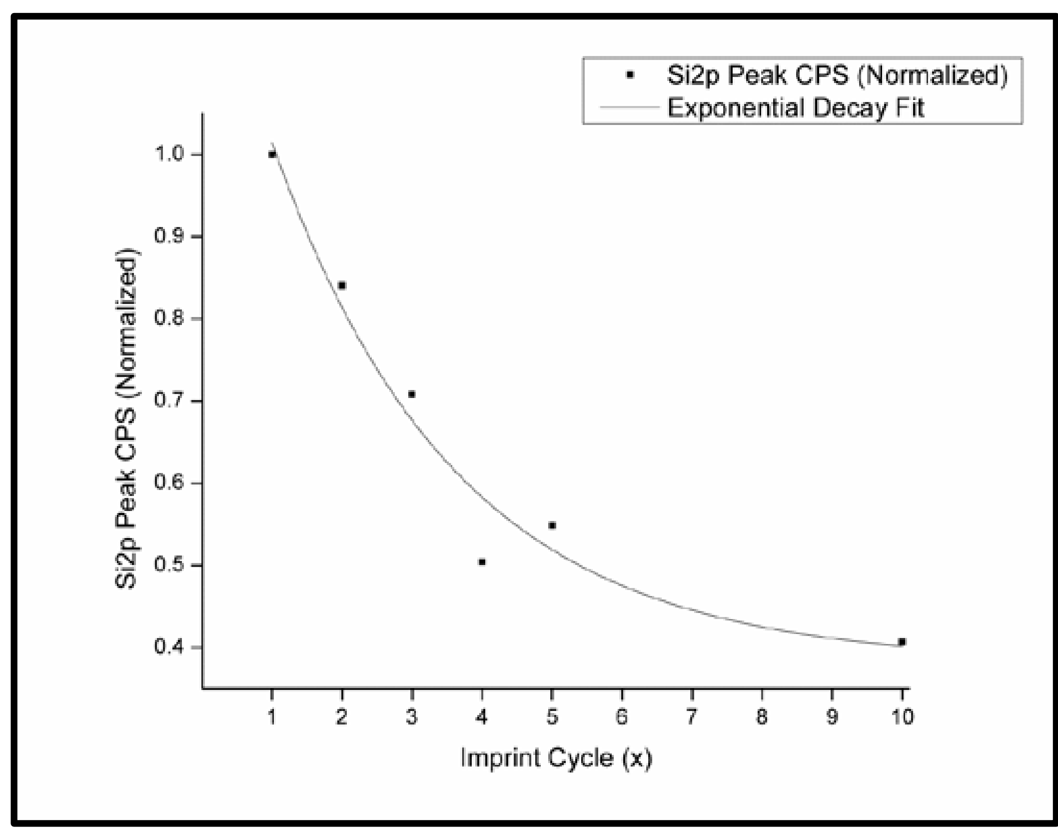

Figure 4.15 Plot of the normalized Si2p peak CPS, as acquired via XPS surface analysis of sequentially fabricated UV roll-to-roll nanoimprinted resin film samples cured against an mPDMS-exposed, h-PDMS/PDMS sheet. The scatter plot was fitted to a single term exponential decay with an adjusted R-Square of 0.94.

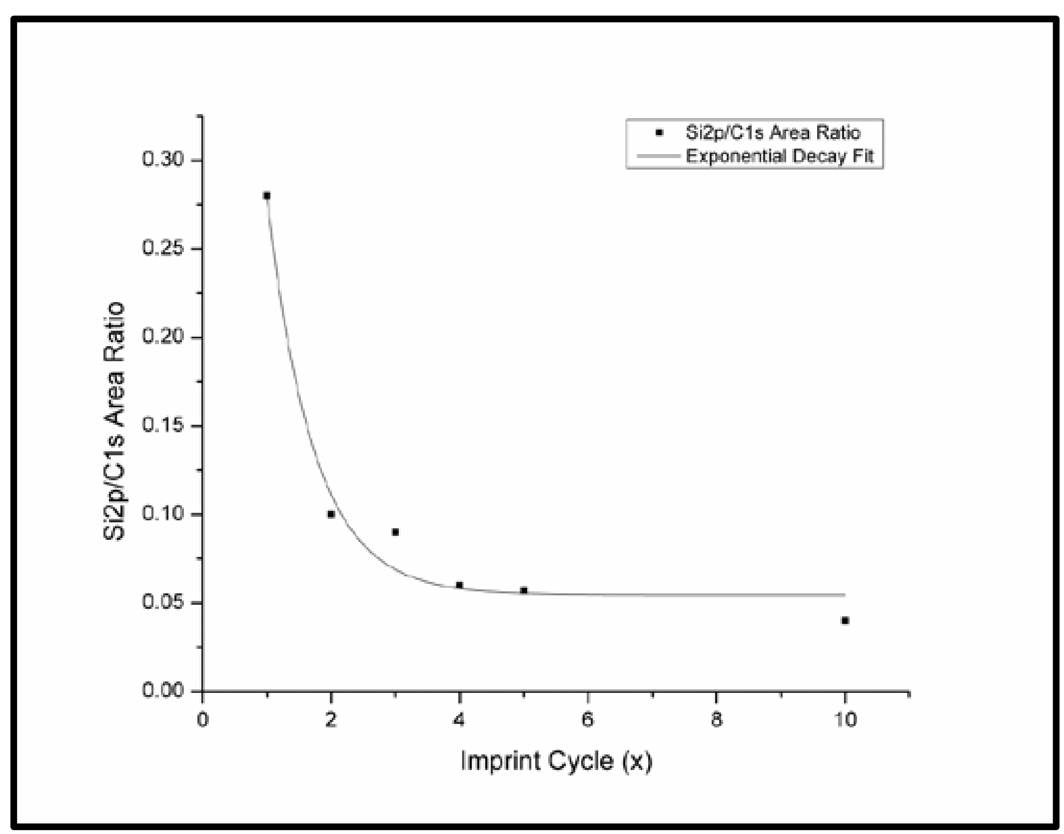

Figure 4.16 Plot of the Si2p/C1s ratio, as acquired via XPS surface analysis of sequentially fabricated UV roll-to-roll nanoimprinted resin film samples cured against an mPDMS-exposed, h-PDMS/PDMS sheet. The scatter plot was fitted to a single term exponential decay that is intended to guide the eye.

The exponential character of the decline in mPDMS transfer to resin films with increasing number of imprint cycles is interesting and worthy of further discussion. It is believed that the exponential decline arises from the nature of mPDMS losses from the swollen h-PDMS/PDMS mould with successive imprint cycles. In terms of contributing factors to mPDMS release agent losses, there are four:

1) Desirable losses due to incorporation of mPDMS chains at the h-PDMS/resin interface into the polymerizing (solidifying) resin of prior samples which are removed by peel separation.

2) Losses due to resin flow while the resin is being squeezed across the mould by contact with the substrate web.

3) Losses due to grafting of mPDMS to h-PDMS chains (with transfer of a photoinitiator radical to one or the other), or entanglement of polymerized mPDMS with h-PDMS chains.

4) Losses due to simple diffusion of mPDMS into the resin from the h-PDMS surface while the h-PDMS is in contact with liquid resin but prior to polymerization. mPDMS that is not polymerized at the h-PDMS/resin interface but instead diffuses into the bulk of the resin coating is effectively lost.

For all of the above, the loss rate of mPDMS with an increase in the number of imprint cycles is dependent on the actual number of pristine mPDMS molecules at the interface at the time of each cycle, which is indicative of exponential decay. Note that time is not used in the above treatment as the mPDMS losses are not continuous with time but are correlated with discrete events. Exponential decay arising from 1) is self-evident. For the second contributor, if the direction and velocity of the resin squeeze flow is relatively fixed for each imprint cycle, then there is likely to be a dependence on the actual number of mPDMS molecules at the interface at the time of each event, due to prior squeeze flow convection cycles removing the more easily accessible mPDMS. The third contributor to loss also has a probability of occurrence that is dependent on the concentration of mPDMS at the h-PDMS surface, as excited radicals must find an mPDMS molecule for grafting or polymerization to occur. Finally, for the fourth contributor, the amount of loss per imprint cycle is dependent on the flux of mPDMS molecules across the h-PDMS/resin interface and the contact time. The former is given by Fick's Law

$$J = -D\frac{\partial \phi}{\partial x} \qquad (4.7)$$

where J is the number of molecules to cross a unit area per unit time, D is the diffusion coefficient in $m^2\ s^{-1}$, and ϕ is the concentration at position x. Assuming the contact time is constant for each imprint cycle, the contact time multiplied by the flux gives the total mPDMS loss per imprint cycle. Since ϕ will decrease at the h-PDMS surface with successive imprint cycles due to mPDMS losses from all contributing factors, the flux (losses) into the resin will also decline. This will also lend exponential character to the mPDMS transfer decay. Thus, as the number of molecules of mPDMS at the interface per unit volume declines over time, the flux into the resin will also decline. In summary, there are multiple sources of mPDMS loss with exponential character which serve to explain the exponential decline in mPDMS transfer to cured resin films.

It is also of interest to note from the exponential decay shown in Figure 4.15, that the best fit obtains a definite positive residual value, y of 0.38, or ~38% of the Si2p peak CPS for the 1st imprint sample. This could be preliminary evidence that the mPDMS surface concentration will level off with increasing number of imprint cycles as a balance is struck between the rate of removal of mPDMS chains and their diffusion rate to the surface from the bulk. Removal of mPDMS chains from the surface will set up a concentration gradient with mPDMS dissolved in the bulk of the h-PDMS/PDMS mould, however the diffusion coefficient and steepness of the concentration gradient required to balance the rates is not yet known and further study is required to further prove and quantify this process. The migration of mPDMS from the bulk of the h-PDMS/PDMS composite mould to the patterned h-PDMS surface is one of the principal reasons for using a soluble silicone mould for uptake of mPDMS, as this would allow for the steady

transfer of mPDMS over a large number of imprint cycles. These results indicate that steady transfer of mPDMS is possible but further tuning of the throughput to balance mPDMS losses with the migration rate to the h-PDMS/PDMS mould surface is required.

4.10 Advancing Water Contact Angle Characterization of mPDMS Transfer to UV Roll-to-Roll Nanoimprinted Resin Films

mPDMS transfer was also monitored via advancing water contact angle measurements against blank, cured 30 x 30 mm resin films (following the Table 4.3 resin formulation scheme) on polycarbonate substrates fabricated against mPDMS exposed, extracted h-PDMS/PDMS sheets. Results are intended to provide a useful measure of changes in the wetting performance and hydrophobicity of the resin film surface with increasing number of imprint cycles and changes in mPDMS transfer. Advancing water contact angle measurements are also a useful complementary measurement to XPS results for the purpose of gaining additional insight into the release performance of resin moulds fabricated under similar conditions.

Figure 4.17 provides a plot of the advancing water contact angle with increasing number of imprint cycles for comparison with XPS results shown in Figure 4.15, Figure 4.16 and Table 4.4. The advancing water contact angle for the first sample (90°, SD ±0.82°, N=10) reflects the removal of excess mPDMS from the surface of the h-PDMS/PDMS mould after the mPDMS exposure step. Thereafter the contact angle stabilizes at about 86° and the scatter of measurements as measured by the standard deviation shrinks until the 4th imprint cycle where the standard deviation starts to increase. By the 10th imprint

cycle the mean contact angle actually increases slightly while the standard deviation reaches a maximum (± 1.76°) for the sample set. The standard deviation of the 10th imprint cycle still overlaps the equivalent ranges for prior cycles, such that the increase in mean contact angle may simply be due to measurement error. However the changes in the measurement scatter with increasing number of imprint cycles is interesting and may be due to a slight increase in the surface roughness from sample to sample. In any case, the advancing water contact angle is remarkably insensitive to the decay in mPDMS transfer to the resin surface with increasing number of imprint cycles.

A stable advancing water contact angle of ~86° compares well against reference resin films cured against blank nickel shims, which yielded contact angles averaging about 66° (SD ±1.2°, N=10). Thus transfer of mPDMS to cured resin films is able to achieve a stable ~20° increase in the advancing water contact angle in comparison to release agent-free reference samples.

Advancing water contact angle measurements were also carried out against cured resin films (again, following the Table 4.3 resin formulation scheme) with varying weight concentrations of mPDMS and 3,3,4,4,5,5,6,6,7,7,8,8,9,9,10,10-heptadeca-fluorodecyl methacrylate (HFMA, Sigma-Aldrich) mixed directly into the resin formulation is provided in Figure 4.18. Contact angle vs. increasing weight percent concentration of release agent in the resin is plotted out for the purpose of comparing mPDMS transfer from h-PDMS/PDMS sheet moulds to the competing approach of mixing reactive release agents into the resin formulation and curing against nickel shims. mPDMS and HFMA were chosen as representative of methacrylated silicone-based and fluorocarbon-based release agents.

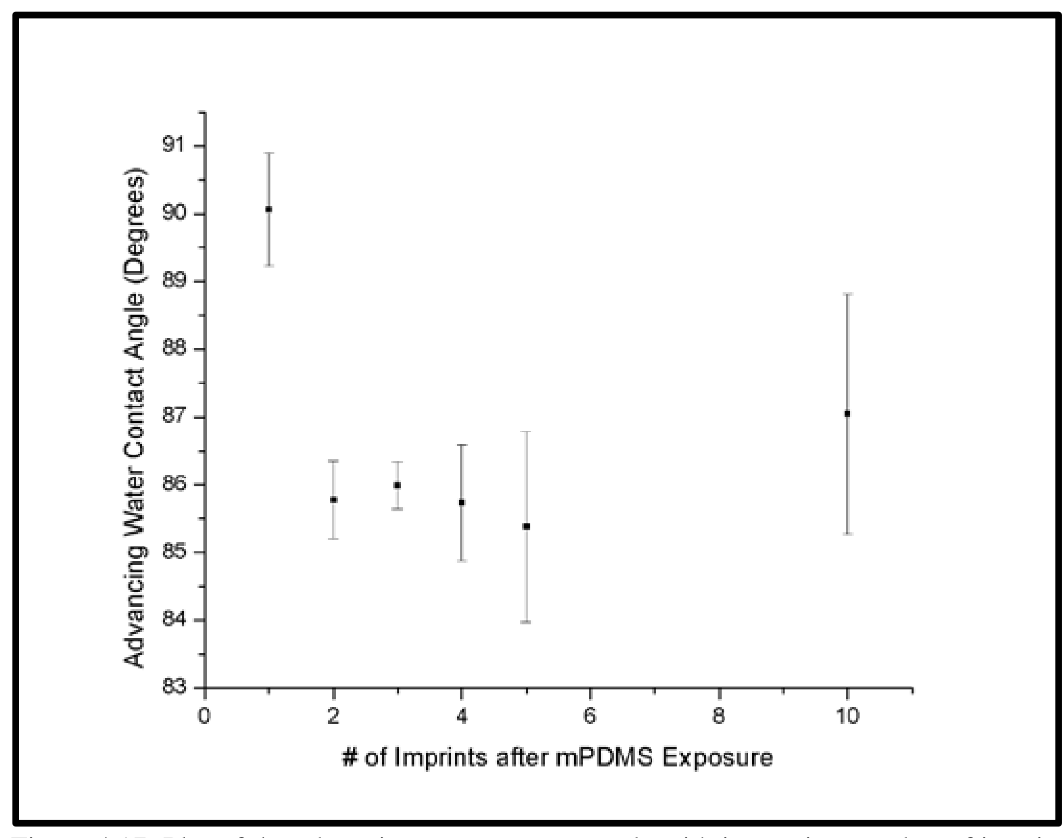

Figure 4.17 Plot of the advancing water contact angle with increasing number of imprint cycles for comparison with XPS results shown in Figures 4.15 & 4.16 (see also Table 4.4). The advancing water contact angle for the first sample (90°, SD ± 0.82°, N=10) reflects the removal of excess mPDMS from the surface of the h-PDMS/PDMS mould after the exposure step. Thereafter the contact angle stabilizes at ~86°.

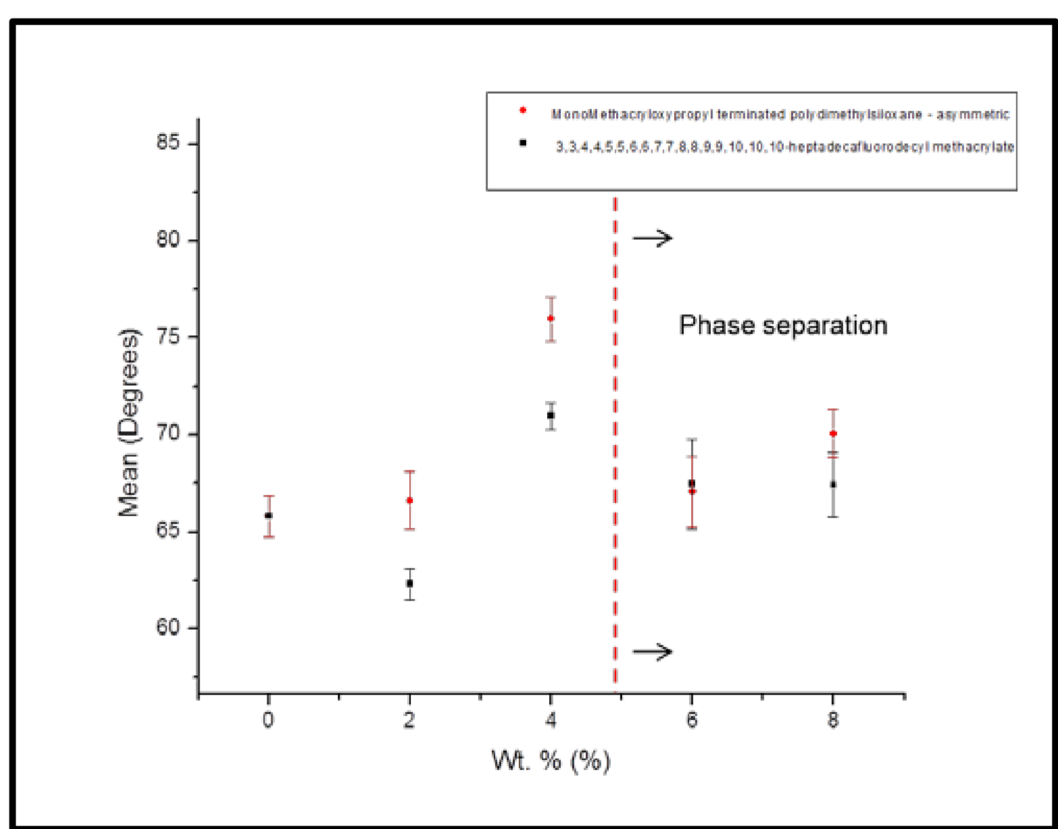

Figure 4.18 Scatter plot of advancing water contact angle vs. release agent concentration in wt. % for mPDMS and HFMA impregnated resin films. mPDMS is shown as dark squares and HFMA is shown as grey diamonds. Both were mixed directly into the test bed resin formulation (Table 4.3) prior to curing against blank nickel shims. Each data point represents 5 measurement sites per sample across 2 samples, for N = 10 measurements. Above 4% wt. concentration, both release agents underwent phase segregation as shown.

Results indicate that incorporation of release agents into the resin formulation at best results in an ~10° increase in mean advancing water contact angle, from ~66° to ~77° (SD ±1.2°, N=10) when using 4% wt. mPDMS. 4% wt. HFMA only resulted in an ~5° (SD ±0.7°, N=10) increase under the same conditions. At concentrations above 4% wt. both mPDMS and HFMA will spontaneously phase segregate resulting in a decline in the advancing water contact angle when measured outside the release agent aggregated region. This illustrates the difficulty in achieving a significant increase in the contact

angle and corresponding decline in surface energy by mixing release agents into the bulk resin formulation, as a high concentration of release agent is required to significantly influence the surface chemistry but issues with solubility and phase segregation prevent higher concentrations from being feasible. mPDMS transfer from h-PDMS/PDMS silicone sheet moulds, by contrast, is able to sustain an ~10° improvement over a 4% wt. mPDMS resin film case with additional room for improvement.

4.11 Concluding Remarks

This work represents an early yet successful inquiry into the use of an absorbant mould to deliver reactive release-enhancing agents via transfer to resin mould surfaces *in situ* during UV roll-to-roll nanoimprint fabrication. These release agents are capable of participating in the polymerization of UV curable resin *locally* at the interface with an h-PDMS/PDMS composite mould. This novel approach enables a permanent surface modification to resin moulds without modifying the bulk properties of the resin or changing the resin formulation itself such that the resin material can be selected for other beneficial properties such as stiffness or conformality, hardness, transparency to UV light, and survivability at elevated service temperatures.

A modified h-PDMS formulation was developed for the purpose of scaling h-PDMS/PDMS composite moulds to large area without failure due to cracking. The heavily cross-linked nature of h-PDMS was helpful in mitigating the swelling response to mPDMS exposure for the purpose of ensuring full reversibility while still absorbing adequate volumes of release agent such that useful high aspect ratio structures could be fabricated with mPDMS anchored to their surfaces. A method was developed to expose

h-PDMS/PDMS composite moulds to mPDMS release agent through the h-PDMS patterned face such that the expansion mismatch caused the mould to bend in a controllable, convex manner. Further studies are underway to minimize the mPDMS exposure time while retaining transfer performance during resin mould production.

It was shown that transfer of mPDMS to blank resin mould samples from h-PDMS/PDMS bi-layer sheet moulds resulted in an advancing water contact angle stabilized at ~20° above the release agent-free reference for at least 10 imprint cycles, which should be indicative of improved release performance. Further improvements are likely as the system thermodynamics and diffusion rates become better understood. Improvements are likely to be found most easily by modifying the UV curable resin to de-swell the h-PDMS based on the finding that contact with a small molecule resin formulation determines the swelling response during UV roll-to-roll nanoimprinting to form the resin mould. Fully de-swelling the h-PDMS patterned surface could expel a significant quantity of release agent across the liquid resin / h-PDMS interface, which can be captured at the surface of fabricated resin moulds if the UV roll-to-roll production line is run at very high throughput or where contact time with the resin is minimized. Fully de-swelling the h-PDMS patterned surface would also greatly reduce feature shrinkage in resin moulds fabricated from it.

Chapter 5. Conclusions & Future Work

5.1 Contributions & Important Findings

Mass manufacture of resin moulds for use in subsequent lithographic processes represents a potentially disruptive technology in the field of nanolithography with multiple near-term commercial applications. As a particular form of bi-layer polymer mould, resin moulds enjoy a unique niche amongst competing materials because of the beneficial properties of each layer in its construction. The cured resin, pattern-carrying layer can be formulated to obtain high stiffness and hardness for pattern stability while the backing layer can be selected for flexibility and conformality to the substrate. A high modulus, high hardness pattern-carrying layer backed by a soft conformal layer has been described by many as an ideal structure for NIL moulds.[70,80,165] The present work emphasizes a key difference between resin moulds and other competing polymer mould materials (esp. composite multi-layer mould materials) in that resin moulds are inherently compatible with UV exposure-based roll-to-roll processing. Resin moulds produced via UV roll-to-roll nanoimprinting thus possess all of the advantages of a bi-layer composite mould in addition to being easy to scale-up to high throughput. This was demonstrated by actual fabrication of UV roll-to-roll nanoimprinted resin moulds at 10 meters min^{-1}, a record high speed in the literature, and utilization in a subsequent batch mode thermal NIL process.[32] Resin moulds produced in this manner can be fabricated inexpensively enough to be used only once, or several times until defects are accumulated, and then can be disposed of or recycled. This overcomes one of the main difficulties with conventional batch mode thermal NIL, that of damage accumulation to the mould due to the high process pressures involved, by providing a facile and inexpensive means of replacing it. Simply replacing the mould is also much more efficient than undergoing complex cleaning steps to reclaim the mould after contamination.

Chapter 3 also provides a useful exploration of resin moulds at nanoscale resolution with mixed micro- and nanoscale features down to 50 nm diameter. Results showed that high resolution mixed nanostructures can be faithfully replicated in PMMA on silicon substrates via thermal NIL using UV roll-to-roll nanoimprinted resin moulds. Moreover curing shrinkage was minimized with only the resin mould fabrication step inputting curing shrinkage into the final pattern. This was an important consideration given that the final pattern was a 4th generation replica of the master. By utilizing nickel electroforming to produce the sheet mould replica of the master, and thermal NIL as the proposed means of obtaining final device patterns, cumulative curing shrinkage can be avoided.

The present study found that this multi-generation replication scheme resulted in overall feature shrinkage small enough to not significantly impact imprint fidelity in terms of measured feature height. Instead, the dominant contributor to non-uniformity vis-à-vis the roll-mounted nickel mould was found to arise from the cylindrical non-uniformity of the imprint roller in our UV roll-to-roll nanoimprinting system. The surface planarity of resin moulds produced via roll-to-roll processing methods is one important challenge highlighted in Chapter 3. Surface waviness appeared in AFM section profiles of replicated resin moulds and was also observed with greater amplitude on PMMA surfaces embossed with resin moulds. Especially with regard to resin mould surfaces, there is a worthwhile engineering challenge in obtaining imprint roll cylinders with near-perfect cylindrical curvature such that resin moulds cured against these surfaces will obtain uniformly flat surfaces from them.

Chapter 4 provides another significant contribution to the field of UV roll-to-roll nanoimprinted resin moulds in the development of new means to permanently modify the

surface chemistry of resin moulds in order to promote release during subsequent lithography steps. This was accomplished without having to modify the bulk properties of the resin coating comprising the resin mould or the resin formulation used to produce the coating, which allows the bulk properties of the resin to be selected or developed for desirable properties other than release performance.

The method takes advantage of, and enhances one of the native characteristics of thermally cross-linked silicone solids: that of surface migration of unreacted low molecular weight dimethylsiloxane oligomers and their transferability to other surfaces. This dissertation provides a means of transferring a reactive variant of these oligomers from bi-layer silicone roll-mounted moulds to resin mould surfaces during *in situ* polymerization and fabrication of the resin mould via UV roll-to-roll nanoimprinting. By dissolving a reactive silicone oligomer release agent into the silicone roll-mounted mould, transferred release agent is able to participate in the polymerization reaction at the surface of the formed resin mould and covalently bond itself to this surface. This renders a permanent surface modification to the resin mould. *In situ* release agent transfer avoids additional in-line processing steps inherent to other surface modification techniques such as silanized SAM anti-stick coatings and delivers release agent molecules directly to the surface of the resin mould.

In developing this technique, information was required on compatible silicone polymer-solvent systems to drive transfer of the dissolved agent to resin moulds. Theoretical calculations of solubility for polymer-solvent systems (see Appendix A), particularly dissolution of linear chain methacrylated silicone oligomers in PDMS, was used to predict two things. First, whether it was possible to dissolve these molecules in PDMS given a sufficiently low total molecular weight for the oligomer, and second, the

approximate threshold chain length where solubility models would predict insolubility based on molar volume considerations. This was instrumental in obtaining some baseline information on what molecules, compositional groups, and what chain molar volumes would dissolve in PDMS.

Additional innovations were required to render the silicone mould compatible both with scale-up to roll-to-roll size and absorption of significant amounts of liquid release agent without cracking or permanent distortion of surface features. h-PDMS was chosen as a heavily cross-linked pattern-carrying layer and was crucial in mitigating the swelling response to absorption of release agent. This allowed for reversible swelling of the h-PDMS features without permanent distortion of imprinted, cured resin features on sample resin moulds in comparison to control samples that were fabricated with an h-PDMS/PDMS sheet mould that was not exposed to any release agent. SEM cross-section imaging showed that cured resin features appeared essentially identical with and without exposure of the h-PDMS/PDMS sheet to release agent, which indicated that the h-PDMS patterned surface adopts a swelling conformation that reflects the characteristic swelling ratio of the contacting liquid resin with great speed. In order to address cracking issues, a modified formulation of h-PDMS was developed for the purpose of allowing bi-layer h-PDMS/PDMS silicone roll-mounted moulds to be scaled to roll-to-roll compatible size and absorb significant quantities of release agent without failure during fabrication or while in service.

In order to prevent the swelling mismatch of the bi-layer silicone mould upon absorption of the release agent from leading to undesirable concave bending with respect to the patterned face of the mould, a release agent exposure method was developed such that the release agent was exposed to the h-PDMS/PDMS roll-mountable mould exclusively

through the h-PDMS face. Once mounted, release agent transfer was accomplished to resin mould samples with sub-micron resolution and aspect ratios up to 4. Dense 250 nm gratings as well as 500 nm pillar structures were fabricated, showing the versatility and compatibility of the approach with both linear and discrete structures.

Release agent transfer was characterized via XPS surface analysis and advancing water contact angle measurements of blank resin films. XPS was used to obtain evidence that transfer of reactive silicone release agent actually took place and to obtain a measure of the transfer decay with successive imprint cycles against the release agent-exposed h-PDMS/PDMS roll-mounted mould. Preliminary evidence was found in measuring the silicone Si2p to carbon C1s ratio that the decline in transfer levels off after about 5 imprint cycles and further transfer lifetime studies are underway to verify the XPS studies.

Finally, advancing water contact angle measurements on blank resin films showed a stable increase of ~20° over reference films produced without transfer of release agent even after 10 imprint cycles. With further improvements in understanding the surface migration rate of the artificially introduced silicone release agent, and better matching of the process throughput with the migration/replacement rate, it is expected that sustainable rates of transfer to resin mould surfaces can be accomplished, ideally over many hundreds of imprint cycles.

To conclude, a significant effort to develop resin mould fabrication technology using UV roll-to-roll nanoimprint processing, obtain control over resin mould surface chemistry, and analyze the effects of the surface chemistry modification is presented herein. Multiple innovations in terms of mould materials, process engineering and creative use of

polymer-solvent dissolution and migration effects were accomplished. Finally, successful integration of new materials and process requirements into the UV roll-to-roll fabrication of resin moulds was achieved.

5.2 Current Challenges & Opportunities for Further Study

This section will deal with known challenges and opportunities for further research with respect to the work presented in Chapter 4. The known challenges and opportunities involved in the production of resin moulds via UV roll-to-roll nanoimprinting were covered previously and in more detail in Chapter 3 (see especially, 3.4 & 3.5).

With respect to surface chemistry modification of resin moulds via reactive release agent transfer from silicone moulds, there are many useful points to discuss. First, performance improvements would be highly desirable. Currently, a sustainable advancing water contact angle of 85° for blank resin mould films, while significantly greater than the advancing water contact angle of resin films without release agent transfer, would be of still greater utility at even lower surface energy (e.g. contact angles in excess of 100°). In assessing the possibility of further reductions in the surface energy it is important to note available data on the advancing water contact angle of solid (pure) materials that are similar in chemical composition to monomethacryloxypropyl-terminated polydimethylsiloxane (mPDMS). For example, pure solid PDMS produced from a variety of reaction chemistries generally takes on an advancing water contact angle in the range of 110 - 120°.[166] Thus currently, an advancing water contact angle of 85° is roughly 74% of what can be achieved with a pure solid silicone surface, laying aside obvious differences in molecular weight and chemical structure. Although a contact angle of this magnitude is not possible to achieve with a transfer process to a resin mould

surface that is not a pure silicone, the above is a useful comparison in that it provides an idea of the limits to what is achievable in theory. In the present work, an advancing contact angle in excess of 90° was achieved on the first imprint when the concentration of transferred mPDMS release agent was significantly higher from surface excess present on the h-PDMS/PDMS mould from the mPDMS pooling exposure step. This result may provide some insight into what is achievable with short-chain oligomeric silicones if a larger amount can be sustainably transferred to resin mould surfaces through additional process engineering, for example. This would constitute an improvement to about 80% of a pure silicone surface. Still higher performance would require some further engineering of the release agent chemical composition.

Further on the topic of swelling and de-swelling, another opportunity for further study lies with a further exploration of the interaction between the h-PDMS pattern carrying layer and the liquid resin during UV roll-to-roll nanoimprint fabrication of resin moulds. One of the important findings of the present work was that, so long as the swelling response to the release agent exposure step is fully reversible, the h-PDMS pattern carrying layer will adopt a swelling conformation that is characteristic to the liquid resin it is in contact with and will do so at high speed (< 1 min). This effect was described as a de-swelling response to contact with the predominantly small molecule hydrocarbon liquid resin, as the swelling response to hydrocarbons was expected to be less than that to mPDMS, which also has low molecular weight but is chemically more similar to solid silicones. However, the swelling response of solid silicones to various hydrophobic liquids is a very complex phenomena and a further experimental inquiry into the swelling ratios of h-PDMS to resin chemistries of interest as well as mPDMS and other release agent candidates would be worthwhile.

One particular experiment of interest in terms of influencing the swelling behaviour of h-PDMS during UV roll-to-roll nanoimprinting of resin moulds would be to introduce a polar and/or hydrogen bonding constituent to the resin formulation. Certain simple solvents are either immiscible or have a very low swelling ratio with PDMS, for example.[150] Introduction of a component to the resin mould resin formulation that is a poor solvent to the h-PDMS layer may cause it to de-swell significantly in response to contact. This has been shown to occur with ordinary poor solvents in NIL-related processing by other workers,[167] and solvent swelling/de-swelling of PDMS generally has been used effectively in contact lithography as well.[168] This approach would have two-fold benefits. First, further de-swelling of the h-PDMS pattern-carrying layer of the h-PDMS/PDMS roll-mounted mould would reduce the overall pattern shrinkage of UV roll-to-roll nanoimprinted resin mould features. Second, de-swelling of the h-PDMS layer may expel a significant amount of release agent across the h-PDMS/resin interface due to volume conservation. The latter event could potentially be exploited by curing the resin in the midst of de-swelling, thus capturing a significant quantity of the expelled release agent at the surface of the resin mould.

In terms of lifetime and the robustness of release agent transfer to UV roll-to-roll nanoimprinted resin moulds, there is further work to be done to prove out whether the beneficial effects of the release agent transfer can last for many hundreds of imprint cycles. It should be noted that the present work is only a preliminary study that describes and demonstrates the new ideas and innovations involved in accomplishing surface chemistry modification of resin mould surfaces *in situ* during UV roll-to-roll nanoimprint fabrication. Lengthy lifetime studies are not within the scope of the present work, however such feasibility studies for the purpose of commercialization would be appropriate. Prior to lengthy lifetime studies, however, it would be most efficient to

optimize the chemical structure of the release agent molecule, as well as optimize the availability and amount of release agent transfer as described above. It would also be of utility, once optimal materials and processing had been developed, to further characterize the migration or renewal rate of release agent to the surface of the roll-mounted silicone mould and match the throughput of the UV roll-to-roll nanoimprinting process to this rate.

More extensive lifetime studies could then follow the abovementioned optimizations. As was highlighted previously in Chapter 4, the fact that the advancing water contact angle held steady after 10 imprint cycles even with declining mPDMS transfer is very encouraging in this regard. If the migration/renewal rate to the h-PDMS surface can be stabilized and matched with the throughput of the UV roll-to-roll nanoimprinting process to fabricate resin moulds, then a sustainable transfer of mPDMS to resin mould surfaces can be achieved over many more imprint cycles with a concomitant permanent, stable reduction in resin mould surface energy.

5.3 Outlook & Concluding Remarks

As the demand for low cost nanolithography continues to expand, and as demand for higher aspect ratio, higher density fabrication of micro- and nano-structures continues to rise, innovative low-cost, high throughput and non-conventional enabling technologies for nanolithography continue to draw great interest from researchers and industry. The present work represents an early movement toward high performance resin moulds for high resolution, high aspect ratio nanolithography that maintains the excellent cost and throughput profile of roll-to-roll processing. There are myriad potential applications that

this technology can avail and the potential to commercialize some form of roll-to-roll processed resin mould as a low-cost nanolithography consumable remains excellent.

Since 2010 when our first effort in UV roll-to-roll nanoimprinting began, we have seen the technology develop in great strides thanks to the existing body of knowledge and experience already available from development of batch mode nanoimprinting techniques. Throughputs of at least 10 meters min^{-1} are now standard and sub-50 nm resolutions have been demonstrated.[32] Now the challenge is to tackle some of the nagging yield issues inherent to UV batch mode and roll-to-roll nanoimprinting alike, namely air trapping against liquid resins and control over the interfacial energy and adhesion of contacting liquids with solids in the imprint stack. Our adoption of a composite silicone mould that can be scaled to roll-to-roll compatible size represents an important step toward addressing these critical yield-determining factors. The excellent gas permeability, release performance, and facile master replication properties of silicone remain a unique combination in the area of mould materials. Gas permeability is particularly valuable to a roll-to-roll process given its continuous nature making it difficult to implement vacuum or exotic gas atmospheres to promote removal or dissolution of trapped bubbles.[2,59,60] The use of h-PDMS in the form of an h-PDMS/PDMS composite mould is also new to roll-to-roll processing as previously its brittleness was such that only small batch mode-type moulds could be produced without risk of cracking failure. We look forward to further innovative uses of novel silicones in UV roll-to-roll nanoimprinting and device applications in the months and years ahead.

Obtaining control over the surface chemistry of resin mould replication, and doing so in a way that the modification is built-in to the UV roll-to-roll nanoimprinting process is a cutting-edge technology that is truly exciting. Further studies are underway to improve

performance and transfer lifetime, but the idea of gaining a permanent anti-sticking property to the surface of a type of polymer mould during formation of the mould itself is potentially groundbreaking in terms of driving efficiency gains. The approach uniquely takes advantage of entropy in dissolution of the release agent into a soluble polymer, as well as natural thermodynamic driving forces to reduce surface energy in the presence of air via migration of the low surface tension release agent to the roll-mounted mould surface. This use of natural forces to achieve desirable outcomes in lithography is quite new. Generally the tendency is for workers to fight against natural forces (esp. entropy) to achieve ordered materials, systems, and surfaces to carry out lithography. However there are now clearly situations where an increase in system disorder (higher entropy) on the molecular level can be used to obtain ordering (lower entropy) on larger length scales and to obtain desirable macro-surface properties for lithographic purposes. We look forward to continued exciting developments in this new field as well as related areas of surface science as it relates to nanoimprint lithography and roll-to-roll processing generally.

Bibliography

1 Chou, S. Y., Krauss, P. R. & Renstrom, P. J. Imprint Lithography with 25-Nanometer Resolution. *Science* **272**, 85-87, (1996).

2 Dumond, J. J. & Low, H. Y. Recent developments and design challenges in continuous roller micro- and nanoimprinting. *Journal of Vacuum Science & Technology B: Microelectronics and Nanometer Structures* **30**, 010801-010828, (2012).

3 Cattoni, A., Cambril, E., Decanini, D., Faini, G. & Haghiri-Gosnet, A. M. Soft UV-NIL at 20nm scale using flexible bi-layer stamp casted on HSQ master mold. *Microelectronic Engineering* **87**, 1015-1018, (2010).

4 Metwally, K., Queste, S., Robert, L., Salut, R. & Khan-malek, C. Hot roll embossing in thermoplastic foils using dry-etched silicon stamp and multiple passes. *Microelectronic Engineering* **88**, 2679-2682, (2011).

5 Zhou, W. *et al.* Replication of mold for UV-nanoimprint lithography using AAO membrane. *Applied Surface Science* **255**, 8019-8022, (2009).

6 Taniguchi, J. & Aratani, M. Fabrication of a seamless roll mold by direct writing with an electron beam on a rotating cylindrical substrate. *Journal of Vacuum Science & Technology B: Microelectronics and Nanometer Structures* **27**, 2841, (2009).

7 Unno, N. & Taniguchi, J. Fabrication of the metal nano pattern on plastic substrate using roll nanoimprint. *Microelectronic Engineering* **88**, 2149-2153, (2011).

8 Unno, N., Taniguchi, J. & Ishikawa, K. Fabrication of a seamless roll mold using inorganic electron beam resist with postexposure bake. *Journal of Vacuum Science & Technology B* **29**, (2011).

9 Ansari, K., Kan, J. A. v., Bettiol, A. A. & Watt, F. Stamps for nanoimprint lithography fabricated by proton beam writing and nickel electroplating. *Journal of Micromechanics and Microengineering* **16**, 1967-1974, (2006).

10 Uh, J. *et al.* Laser Engraving of Micro-patterns on Roll Surfaces. *ISIJ International* **42**, 1266-1272, (2002).

11 Chou, T.-H. *et al.* Laser interference lithography and nanoimprint techniques for lower reflection transparent conducting oxide hybrid films. *International Journal of Precision Engineering and Manufacturing* **11**, 619-622, (2010).

12 Chen, L.-S. *et al.* Longitudinal stitching of sub-micron periodic fringes on a roller. *Microelectronic Engineering* **88**, 3235-3243, (2011).

13 Wang, W., Mei, X. & Jiang, G. Control of microstructure shape and morphology in femtosecond laser ablation of imprint rollers. *Int J Adv Manuf Technol* **41**, 504-512, (2008).

14 Kim, S. L. & Kim, G. M. Micropatterning on Roll Surface Using Photo-Lithography Processes. *International Journal of Precision Engineering and Manufacturing* **12**, 763-768, (2011).

15 Huang, T.-C., Wu, J.-T., Yang, S.-Y., Huang, P.-H. & Chang, S.-H. Direct fabrication of microstructures on metal roller using stepped rotating lithography and electroless nickel plating. *Microelectronic Engineering* **86**, 615-618, (2009).

16 Idei, K., Ishizawa, N., Noda, D. & Hattori, T. *Development of Roll Metal Mold by Synchrotron Radiation*. (IEEE, 2006).

17 Jiang, L.-T. *et al.* Direct fabrication of rigid microstructures on a metallic roller using a dry film resist. *Journal of Micromechanics and Microengineering* **18**, 015004, (2008).

18 Park, H. J., Kang, M.-G. & Guo, L. J. Large Area High Density Sub-20 nm SiO2 Nanostructures Fabricated by Block Copolymer Template for Nanoimprint Lithography. *ACS Nano* **3**, 2601-2608, (2009).

19 Park, S., Lee, D. H. & Russell, T. P. Self-Assembly of Block Copolymers on Flexible Substrates. *Advanced Materials* **22**, 1882-1884, (2010).

20 Hong, S.-H., Bae, B.-J., Lee, H. & Jeong, J.-H. Fabrication of high density nano-pillar type phase change memory devices using flexible AAO shaped template. *Microelectronic Engineering* **87**, 2081-2084, (2010).

21 Park, J., Kim, N., Lee, B.-K., Lee, K.-H. & Kwon, T. Nickel stamp fabrication and hot embossing for mass-production of micro/nano combined structures using anodic aluminum oxide. *Microsystem Technologies* **14**, 1689-1694, (2008).

22 Yin, A. & et al. Fabrication of anodic aluminium oxide templates on curved surfaces. *Nanotechnology* **18**, 035304, (2007).

23 Yang, S. Y., Huang, T. C., Wu, J. T., Lai, H. C. & Chu, Y. T. (Google Patents, 2011).

24 Ge, H. *et al.* Cross-linked Polymer Replica of a Nanoimprint Mold at 30 nm Half-pitch. *Nano Letters* **5**, 179-182, (2004).

25 Jeong, D. H., Gonzalez, F., Palumbo, G., Aust, K. T. & Erb, U. The effect of grain size on the wear properties of electrodeposited nanocrystalline nickel coatings. *Scripta Materialia* **44**, 493-499, (2001).

26 Matsukawa, D., Okamura, H. & Shirai, M. Preparation of Replicated Resin Mold for UV Nanoimprint Using Reworkable Dimethacrylate. *Journal of Photopolymer Science and Technology* **23**, 781-787, (2010).

27 Schuh, C. A., Nieh, T. G. & Iwasaki, H. The effect of solid solution W additions on the mechanical properties of nanocrystalline Ni. *Acta Materialia* **51**, 431-443, (2003).

28 Tsunozaki, K. & Kawaguchi, Y. Preparation methods and characteristics of fluorinated polymers for mold replication. *Microelectronic Engineering* **86**, 694-696, (2009).

29 Yoo, P. J. *et al.* Unconventional Patterning with A Modulus-Tunable Mold: From Imprinting to Microcontact Printing. *Chemistry of Materials* **16**, 5000-5005, (2004).

30 Ahn, S., Cha, J., Myung, H., Kim, S.-m. & Kang, S. Continuous ultraviolet roll nanoimprinting process for replicating large-scale nano- and micropatterns. *Applied Physics Letters* **89**, 213101, (2006).

31 Ahn, S. *et al.* Design and Fabrication of Micro Optical Film by Ultraviolet Roll Imprinting. *Japanese Journal of Applied Physics* **46**, 5478-5484, (2007).

32 Jarrett, J. D. *et al.* High resolution UV roll-to-roll nanoimprinting of resin moulds and subsequent replication via thermal nanoimprint lithography. *Nanotechnology* **23**, 485310, (2012).

33 Ahn, S. H. & Guo, L. J. High-Speed Roll-to-Roll Nanoimprint Lithography on Flexible Plastic Substrates. *Advanced Materials* **20**, 2044-2049, (2008).

34 Ahn, S. H. & Guo, L. J. Large-Area Roll-to-Roll and Roll-to-Plate Nanoimprint Lithography: A Step toward High-Throughput Application of Continuous Nanoimprinting. *ACS Nano* **3**, 2304-2310, (2009).

35 Ahn, S. H., Kim, J.-S. & Guo, L. J. Bilayer metal wire-grid polarizer fabricated by roll-to-roll nanoimprint lithography on flexible plastic substrate. *Journal of Vacuum Science & Technology B: Microelectronics and Nanometer Structures* **25**, 2388, (2007).

36 del Campo, A. & Arzt, E. Fabrication Approaches for Generating Complex Micro- and Nanopatterns on Polymeric Surfaces. *Chemical Reviews* **108**, 911-945, (2008).

37 Matsukawa, D. *et al.* 1 edn (ed Clifford L. Henderson) 72730T-72710 (SPIE).

38 Chan-Park, M. B., Lam, Y. C., Laulia, P. & Joshi, S. C. Simulation and Investigation of Factors Affecting High Aspect Ratio UV Embossing. *Langmuir* **21**, 2000-2007, (2005).

39 Kim, K.-d., Jeong, J.-h., Sim, Y.-s. & Lee, E.-s. Minimization of residual layer thickness by using the optimized dispensing method in S-FILTM process. *Microelectronic Engineering* **83**, 847-850, (2006).

40 Jackson, W. B. *et al. Electronics produced by roll-to-roll self-aligned imprint lithography*. (IEEE, 2007).

41 Kim, H. J. *et al.* in *Imid/Idmc 2006: The 6th International Meeting on Information Display/the 5th International Display Manufacturing Conference, Digest of Technical Papers Proceedings of International Meeting on Information Display* 1539-1543 (Korean Information Display Soc, 2006).

42 Ting, C.-J., Chang, F.-Y., Chen, C.-F. & Chou, C. P. Fabrication of an antireflective polymer optical film with subwavelength structures using a roll-to-roll micro-replication process. *Journal of Micromechanics and Microengineering* **18**, 075001, (2008).

43 Lausecker, E., Huang, Y., Fromherz, T., Sturm, J. C. & Wagner, S. Self-aligned imprint lithography for top-gate amorphous silicon thin-film transistor fabrication. *Applied Physics Letters* **96**, -, (2010).

44 Taussig, C. *et al.* 77.3: Invited Paper: Roll-to-Roll Manufacturing of Backplanes for Paper-Like Displays. *SID Symposium Digest of Technical Papers* **41**, 1151-1154, (2010).

45 Chang, C. Y., Yang, S. Y. & Sheh, J. L. A roller embossing process for rapid fabrication of microlens arrays on glass substrates. *Microsystem Technologies* **12**, 754-759, (2006).

46 Chang, C., Yang, S. & Chu, M. Rapid fabrication of ultraviolet-cured polymer microlens arrays by soft roller stamping process. *Microelectronic Engineering* **84**, 355-361, (2007).

47 Yang, S.-Y., Cheng, F.-S., Xu, S.-W., Huang, P.-H. & Huang, T.-C. Fabrication of microlens arrays using UV micro-stamping with soft roller and gas-pressurized platform. *Microelectronic Engineering* **85**, 603-609, (2008).

48 Liu, S.-J. & Chang, Y.-C. A novel soft-mold roller embossing method for the rapid fabrication of micro-blocks onto glass substrates. *Journal of Micromechanics and Microengineering* **17**, 172-179, (2007).

49 Han, J., Choi, S., Lim, J., Lee, B. S. & Kang, S. Fabrication of transparent conductive tracks and patterns on flexible substrate using a continuous UV roll imprint lithography. *Journal of Physics D: Applied Physics* **42**, 115503, (2009).

50 Munson, B. R., Young, B. G. & Okiishi, T. H. *Fundamentals of Fluid Mechanics, 4th Edition*. (John Wiley & Sons Canada, Ltd., 2005).

51 Fagan, M. D., Kim, B. H. & Yao, D. A novel process for continuous thermal embossing of large-area nanopatterns onto polymer films. *Advances in Polymer Technology* **28**, 246-256, (2009).

52 Seo, S., Kim, T. & Lee, H. Simple fabrication of nanostructure by continuous rigiflex imprinting. *Microelectronic Engineering* **84**, 567-572, (2007).

53 Bird, R. B. & Hassager, O. *Dynamics of Polymeric Liquids: Fluid mechanics*. 20-22 (Wiley, 1987).

54 Heyderman, L. J., Schift, H., David, C., Gobrecht, J. & Schweizer, T. Flow behaviour of thin polymer films used for hot embossing lithography. *Microelectronic Engineering* **54**, 229-245, (2000).

55 Velten, T., Schuck, H., Haberer, W. & Bauerfeld, F. Investigations on reel-to-reel hot embossing. *International Journal of Advanced Manufacturing Technology* **47**, 73-80, (2010).

56 Yeo, L. P. *et al.* Investigation of hot roller embossing for microfluidic devices. *Journal of Micromechanics and Microengineering* **20**, 015017, (2010).

57 Guo, L. J. Recent progress in nanoimprint technology and its applications. *Journal of Physics D: Applied Physics* **37**, R123, (2004).

58 Mcmackin, I. M. A., TX, US), Stacey, Nicholas A. (Austin, TX, US), Babbs, Daniel A. (Austin, TX, US), Voth, Duane J. (Austin, TX, US), Watts, Michael P. C. (Austin, TX, US), Truskett, Van N. (Austin, TX, US), Xu, Frank Y. (Austin, TX, US), Voisin, Ronald D. (Austin, TX, US), Lad, Pankaj B. (Austin, TX, US). Single phase fluid imprint lithography method. United States patent (2006).

59 Hiroshima, H. & Komuro, M. Control of Bubble Defects in UV Nanoimprint. *Japanese Journal of Applied Physics* **46**, 6391, (2007).

60 Hiroshima, H. Quick Cavity Filling in UV Nanoimprint Using Pentafluoropropane. *Japanese Journal of Applied Physics* **47**, 5151-5155, (2008).

61 Hiroshima, H., Atobe, H., Wang, Q. & Youn, S.-W. UV Nanoimprint in Pentafluoropropane at a Minimal Imprint Pressure. *Japanese Journal of Applied Physics* **49**, 06GL01, (2010).

62 Wang, Q. & Hiroshima, H. Effects of Environmental Gas in UV Nanoimprint on the Characteristics of UV-Curable Resin. *Japanese Journal of Applied Physics* **49**, 06GL04, (2010).

63 Truffier-Boutry, D. *et al.* Chemical degradation of fluorinated antisticking treatments in UV nanoimprint lithography. *Applied Physics Letters* **94**, 044110, (2009).

64 Truffier-Boutry, D. *et al.* XPS study of the degradation mechanism of fluorinated anti-sticking treatments used in UV nanoimprint lithography. *Microelectronic Engineering* **87**, 122-124, (2010).

65 Hwang, E.-S. *et al.* Micro Pattern Roll Mold for Large Area Display by Electroforming and Wrapping Method. *Japanese Journal of Applied Physics* **48**, 050211, (2009).

66 Bender, M. *et al.* High resolution lithography with PDMS molds. *Journal of Vacuum Science & Technology B: Microelectronics and Nanometer Structures* **22**, 3229, (2004).

67 Lan, H. & Liu, H. UV-Nanoimprint Lithography: Structure, Materials and Fabrication of Flexible Molds. *Journal of Nanoscience and Nanotechnology* **13**, 3145-3172, (2013).

68 Schmid, H. & Michel, B. Siloxane polymers for high-resolution, high-accuracy soft lithography. *Macromolecules* **33**, 3042-3049, (2000).

69 Odom, T. W., Love, J. C., Wolfe, D. B., Paul, K. E. & Whitesides, G. M. Improved pattern transfer in soft lithography using composite stamps. *Langmuir* **18**, 5314-5320, (2002).

70 Verschuuren, M. A. *Substrate Conformal Imprint Lithography for Nanophotonics* Ph.D. thesis, Utrecht University, (2010).

71 Choi, D.-G. *et al.* Fluorinated Organic−Inorganic Hybrid Mold as a New Stamp for Nanoimprint and Soft Lithography. *Langmuir* **21**, 9390-9392, (2005).

72 Choi, S.-J., Yoo, P. J., Baek, S. J., Kim, T. W. & Lee, H. H. An Ultraviolet-Curable Mold for Sub-100-nm Lithography. *Journal of the American Chemical Society* **126**, 7744-7745, (2004).

73 Kim, Y. S., Lee, N. Y., Lim, J. R., Lee, M. J. & Park, S. Nanofeature-patterned polymer mold fabrication toward precisely defined nanostructure replication. *Chemistry of Materials* **17**, 5867-5870, (2005).

74 Lee, B. K., Hong, L. Y., Lee, H. Y., Kim, D. P. & Kawai, T. Replica Mold for Nanoimprint Lithography from a Novel Hybrid Resin. *Langmuir* **25**, 11768-11776, (2009).

75 Lee, M. J. *et al.* Antiadhesion Surface Treatments of Molds for High-Resolution Unconventional Lithography. *Advanced Materials* **18**, 3115-3119, (2006).

76 Garidel, S., Zelsmann, M., Voisin, P., Rochat, N. & Michallon, P. 65172C-65172C-65179.

77 Rolland, J. P., Hagberg, E. C., Denison, G. M., Carter, K. R. & DeSimone, J. M. High-resolution soft lithography: Enabling materials for nanotechnologies. *Angewandte Chemie-International Edition* **43**, 5796-5799, (2004).

78 Truong, T. T. *et al.* Soft lithography using acryloxy perfluoropolyether composite stamps. *Langmuir* **23**, 2898-2905, (2007).

79 Perumal, J., Kim, D. P. & Lee, J. J. Fluoropolymer Synthesis and Its Application as a Mold Material in UV-Nano-Imprint Lithography Process. *Journal of Nanoscience and Nanotechnology* **8**, 5341-5346, (2008).

80 Williams, S. S. *et al.* High-Resolution PFPE-based Molding Techniques for Nanofabrication of High-Pattern Density, Sub-20 nm Features: A Fundamental Materials Approach. *Nano Letters* **10**, 1421-1428, (2010).

81 Zhu, Z. D., Li, Q. Q., Zhang, L. H., Chen, M. & Fan, S. S. UV-based nanoimprinting lithography with a fluorinated flexible stamp. *Journal of Vacuum Science & Technology B* **29**, (2011).

82 Pina-Hernandez, C., Guo, L. J. & Fu, P.-F. High-Resolution Functional Epoxysilsesquioxane-Based Patterning Layers for Large-Area Nanoimprinting. *ACS Nano* **4**, 4776-4784, (2010).

83 Hougham, G. *Fluoropolymers 1*. (Springer, 1999).

84 Brewis, D. & Dahm, R. *Adhesion to Fluoropolymers*. (iSmithers Rapra Publishing, 2006).

85 Almanza-Workman, A. M., Taussig, C. P., Jeans, A. H. & Cobene, R. L. Fabrication of Three-Dimensional Imprint Lithography Templates by Colloidal Dispersions. *Journal of Materials Chemistry* **21**, 14185-14192, (2011).

86 Verschuuren, M. A., Gerlach, P., Sprang, H. A. v. & Polman, A. Improved performance of polarization-stable VCSELs by monolithic sub-wavelength gratings produced by soft nano-imprint lithography. *Nanotechnology* **22**, 505201, (2011).

87 Yang, Y., Mielczarek, K., Aryal, M., Zakhidov, A. & Hu, W. Nanoimprinted Polymer Solar Cell. *ACS Nano* **6**, 2877-2892, (2012).

88 Lee, Y. C. T., S.H. *Recent Advances in Nanofabrication Techniques and Applications*. 173 (InTech, 2011).

89 Baek, J. H., Kim, S.-M., Lee, I.-H. & Hwang, N. in *Proc. SPIE 7945, Quantum Sensing and Nanophotonic Devices VIII.* 79451B-79451B-79456.

90 Kim, J. K. *et al.* Fabrication of ZrO2 nanopatterns for biomimetic antireflection by thermal nanoimprint lithography. *Microelectronic Engineering* **100**, 12-15, (2012).

91 McPhillips, J. *et al.* Plasmonic Sensing Using Nanodome Arrays Fabricated by Soft Nanoimprint Lithography. *Journal of Physical Chemistry C* **115**, 15234-15239, (2011).

92 Paetzold, U. W. *et al.* Thin-film silicon solar cell development on imprint-textured glass substrates. *Materials Science and Engineering B-Advanced Functional Solid-State Materials* **178**, 617-622, (2013).

93 Hwang, J., Hong, S.-H. & Lee, H. Mimicking the Nanostructure of Bamboo Leaves (Backside) for Hydrophobicity Using Polydimethylsiloxane Moulding and Nano-Imprint Lithography. *Journal of Nanoscience and Nanotechnology* **9**, 3644-3647, (2009).

94 Auzelyte, V., Flauraud, V., Cadarso, V. J., Kiefer, T. & Brugger, J. Biomimetic soft lithography on curved nanostructured surfaces. *Microelectronic Engineering* **97**, 269-271, (2012).

95 Chen, Y.-P., Lee, Y.-P., Chang, J.-H. & Wang, L. A. Fabrication of concave gratings by curved surface UV-nanoimprint lithography. *Journal of Vacuum Science & Technology B* **26**, 1690-1695, (2008).

96 Li, Z. W. *et al.* Hybrid Nanoimprint-Soft Lithography with Sub-15 nm Resolution. *Nano Letters* **9**, 2306-2310, (2009).

97 Yanagishita, T., Nishio, K. & Masuda, H. Anti-Reflection Structures on Lenses by Nanoimprinting Using Ordered Anodic Porous Alumina. *Applied Physics Express* **2**, 022001, (2009).

98 Tadatomo, K. *et al.* High Output Power InGaN Ultraviolet Light-Emitting Diodes Fabricated on Patterned Substrates Using Metalorganic Vapor Phase Epitaxy. *physica status solidi (a)* **188**, 121-125, (2001).

99 Fujii, T. *et al.* Increase in the extraction efficiency of GaN-based light-emitting diodes via surface roughening. *Applied Physics Letters* **84**, 855-857, (2004).

100 Shinohara, H., Fujiwara, S., Tashiro, T., Kitahara, H. & Goto, H. Formation of Patterned Sapphire Substrate using UV Imprint Processes. *Journal of Photopolymer Science and Technology* **26**, 113-117, (2013).

101 Shinohara, H., Tashiro, T., Ookawa, T. & Nishihara, H. High-Throughput UV Nanoimprint Process Using Flexible Resin Mold for High-Brightness Light-Emitting Diodes. *IEEJ Transactions on Sensors and Micromachines* **132**, 235-239, (2012).

102 Oder, T. N., Kim, K. H., Lin, J. Y. & Jiang, H. X. III-nitride blue and ultraviolet photonic crystal light emitting diodes. *Applied Physics Letters* **84**, 466-468, (2004).

103 Tang, H., Li, H. & Xu, J. *Growth and Development of Sapphire Crystal for LED Applications*. (2013).

104 Nezuka, O., Yao, D. & Kim, B. Replication of Microstructures by Roll-to-Roll UV-Curing Embossing. *Polymer-Plastics Technology and Engineering* **47**, 865-873, (2008).

105 Barbero, D. R. *et al.* High-Resolution Nanoimprinting with a Robust and Reusable Polymer Mold. *Advanced Functional Materials* **17**, 2419-2425, (2007).

106 Saito, M. & Taniguchi, J. Electron beam direct writing of nanodot patterns on roll mold surfaces by electron beam on–off chopping control. *Microelectronic Engineering* **123**, 89-93, (2014).

107 Taniguchi, J., Unno, N. & Maruyama, H. Large-diameter roll mold fabrication method using a small-diameter quartz roll mold and UV nanoimprint lithography. *Journal of Vacuum Science & Technology B* **29**, (2011).

108 Unno, N. & Taniguchi, J. Transparent Roll Mold Fabrication Method and Transfer to Photo-curable Polymer. *Journal of Photopolymer Science and Technology* **24**, 57-62, (2011).

109 Yang, S. Y., Huang, T. C., Wu, J. T., Lai, H. C. & Chu, Y. T. Method for forming imprinting roller. United States patent (2011).

110 Khang, D.-Y., Kang, H., Kim, T.-I. & Lee, H. H. Low-Pressure Nanoimprint Lithography. *Nano Letters* **4**, 633-637, (2004).

111 Suh, D., Choi, S. J. & Lee, H. H. Rigiflex lithography for nanostructure transfer. *Advanced Materials* **17**, 1554-1560, (2005).

112 Choi, S.-J., Tahk, D. & Yoon, H. Spontaneous dewetting-induced residue-free patterning at room temperature. *Journal of Colloid and Interface Science* **340**, 74-81, (2009).

113 Rogers, J. A. & Lee, H. H. *Unconventional Nanopatterning Techniques and Applications*. (Wiley, 2009).

114 Takashi, Y., Kazuyuki, N. & Hideki, M. Nanoimprinting Using Ni Molds Prepared from Highly Ordered Anodic Porous Alumina Templates. *Japanese Journal of Applied Physics* **45**, L804, (2006).

115 Choi, J., Park, Y.-B. & Scherer, A. Fabrication of a tungsten master stamp using self-ordered porous alumina. *Nanotechnology* **16**, 1655, (2005).

116 Li, F., Zhang, L. & Metzger, R. M. On the Growth of Highly Ordered Pores in Anodized Aluminum Oxide. *Chemistry of Materials* **10**, 2470-2480, (1998).

117 Kinloch, A. J. *Adhesion and Adhesives: Science and Technology*. 33 (Chapman & Hall, 1987).

118 Park, H. J., Kang, M. G. & Guo, L. J. Large Area High Density Sub-20 nm SiO2 Nanostructures Fabricated by Block Copolymer Template for Nanoimprint Lithography. *Acs Nano* **3**, 2601-2608, (2009).

119 Huang, E., Rockford, L., Russell, T. P. & Hawker, C. J. Nanodomain control in copolymer thin films. *Nature* **395**, 757-758, (1998).

120 Hwang, S.-Y., Hong, S.-H., Jung, H.-Y. & Lee, H. Fabrication of roll imprint stamp for continuous UV roll imprinting process. *Microelectronic Engineering* **86**, 642-645, (2009).

121 Zhong, Z. W., Shan, X. C. & Wong, S. J. Roll-to-roll large-format slot die coating of photosensitive resin for UV embossing. *Microsystem Technologies* **17**, 1703-1711, (2011).

122 Rubin, I. I. *Injection molding: theory and practice*. (Wiley, 1973).

123 Chou, S. Y., Krauss, P. R. & Renstrom, P. J. Nanoimprint lithography. *Journal of Vacuum Science & Technology B: Microelectronics and Nanometer Structures* **14**, 4129-4133, (1996).

124 Iyoshi, S., Miyake, H., Nakamatsu, K.-i. & Matsui, S. UV-Curable Resins Appropriate for UV Nanoimprint. *Journal of Photopolymer Science and Technology* **21**, 573-581, (2008).

125 Tsunozaki, K. & Kawaguchi, Y. Preparation methods and characteristics of fluorinated polymers for mold replication. *Microelectronic Engineering* **86**, 694-696, (2009).

126 Jonas, M. *et al.* Microreplication in a silicon processing compatible polymer material. *Journal of Micromechanics and Microengineering* **15**, S116, (2005).

127 Hirai, Y., Yoshida, S. & Takagi, N. Defect analysis in thermal nanoimprint lithography. *Journal of Vacuum Science & Technology B: Microelectronics and Nanometer Structures* **21**, 2765-2770, (2003).

128 Ryu, I., Hong, D. & Yim, S. Effective surface oxidation of polymer replica molds for nanoimprint lithography. *Nanoscale Research Letters* **7**, 39, (2012).

129 Sbiaa, R. & Piramanayagam, S. N. Patterned Media Towards Nano-bit Magnetic Recording: Fabrication and Challenges. *Recent Patents on Nanotechnology* **1**, 29-40, (2007).

130 Usuki, K., Wakamatsu, S., Oomatsu, T., Kodama, K. & Kodama, K. Vol. 7970 (ed J. C. Herr Daniel) 79700S (SPIE, 2011).

131 Clever, H. L., Battino, R., Saylor, J. H. & Gross, P. M. The Solubility of Helium, Neon, Argon and Krypton in Some Hydrocarbon Solvents. *The Journal of Physical Chemistry* **61**, 1078-1082, (1957).

132 Schift, H. Nanoimprint lithography: An old story in modern times? A review. *Journal of Vacuum Science & Technology B* **26**, 458-480, (2008).

133 Tan, H., Kong, L., Li, M., Steere, C. & Koecher, L. 213-221.

134 Ward, I. M. & Sweeney, J. *An Introduction to the Mechanical Properties of Solid Polymers*. (Wiley, 2004).

135 Swallowe, G. M. *Mechanical Properties and Testing of Polymers: An A-Z Reference*. (Springer, 1999).

136 Howe, J. M. Bonding, structure, and properties of metal/ceramic interfaces: Part 1 Chemical bonding, chemical reaction, and interfacial structure. *International Materials Reviews* **38**, 233-256, (1993).

137 Beck, M. *et al.* Improving stamps for 10 nm level wafer scale nanoimprint lithography. *Microelectronic Engineering* **61–62**, 441-448, (2002).

138 Park, S. *et al.* Anti-adhesive layers on nickel stamps for nanoimprint lithography. *Microelectronic Engineering* **73–74**, 196-201, (2004).

139 Owen, M. J. Surface Tension of Silicone Release Paper Coatings. *Journal of Coatings Technology* **53**, 49-53, (1981).

140 Chaudhury, M. K. & Whitesides, G. M. Direct measurement of interfacial interactions between semispherical lenses and flat sheets of poly(dimethylsiloxane) and their chemical derivatives. *Langmuir* **7**, 1013-1025, (1991).

141 Merkel, T. C., Bondar, V. I., Nagai, K., Freeman, B. D. & Pinnau, I. Gas sorption, diffusion, and permeation in poly(dimethylsiloxane). *Journal of Polymer Science Part B: Polymer Physics* **38**, 415-434, (2000).

142 Sturm, P. *et al.* Permeation of atmospheric gases through polymer O-rings used in flasks for air sampling. *Journal of Geophysical Research: Atmospheres* **109**, D04309, (2004).

143 Choi, K. M. & Rogers, J. A. A photocurable poly(dimethylsiloxane) chemistry designed for soft lithographic molding and printing in the nanometer regime. **125**, 4060-4061, (2003).

144 Choi, W. M. & Park, O. O. A soft-imprint technique for submicron-scale patterns. using a PDMS mold. *Microelectronic Engineering* **73-4**, 178-183, (2004).

145 Chang, J. H. *et al.* Direct imprinting using soft mold and gas pressure for large area and curved surfaces. *Journal of Vacuum Science & Technology A* **23**, 1687-1690, (2005).

146 Weng, Y. J., Weng, Y. C., Yang, S. Y. & Wang, L. A. Fabrication of optical waveguide devices using gas-assisted UV micro/nanoimprinting with soft mold. *Polymers for Advanced Technologies* **18**, 876-882, (2007).

147 Hamouda, F., Barbillon, G., Gaucher, F. & Bartenlian, B. Sub-200 nm gap electrodes by soft UV nanoimprint lithography using polydimethylsiloxane mold without external pressure. *Journal of Vacuum Science & Technology B* **28**, 82-85, (2010).

148 Nishino, T., Sakamoto, J., Kawata, H., Mizutani, K. & Hirai, Y. Fabrication of Novel High Aspect Ratio Pillars using Fine Flexible mold by UV-NIL. *Journal of Photopolymer Science and Technology* **23**, 79-82, (2010).

149 Yang, H. *et al.* Fabrication and application of high quality poly(dimethylsiloxane) stamps by gamma ray irradiation. *Journal of Materials Chemistry* **21**, 4279-4285, (2011).

150 Lee, J. N., Park, C. & Whitesides, G. M. Solvent Compatibility of Poly(dimethylsiloxane)-Based Microfluidic Devices. *Analytical Chemistry* **75**, 6544-6554, (2003).

151 Johnston, I. D., McCluskey, D. K., Tan, C. K. L. & Tracey, M. C. Mechanical characterization of bulk Sylgard 184 for microfluidics and microengineering. *Journal of Micromechanics and Microengineering* **24**, 035017, (2014).

152 Hyewon, K., Jiyeon, L., Joonhyung, P. & Hong, H. L. An improved method of preparing composite poly(dimethylsiloxane) moulds. *Nanotechnology* **17**, 197, (2006).

153 Kim, J., Park, M., Chae, G. S. & Chung, I.-J. Influence of un-cured PDMS chains in stamp using PDMS-based lithography. *Applied Surface Science* **254**, 5266-5270, (2008).

154 Li, Z. *et al.* Surface properties of poly(dimethylsiloxane)-based inorganic/organic hybrid materials. *Polymer* **47**, 1150-1158, (2006).

155 Youn, B.-H. & Huh, C.-S. Surface analysis of plasma-treated polydimethylsiloxane by x-ray photoelectron spectroscopy and surface voltage decay. *Surface and Interface Analysis* **35**, 445-449, (2003).

156 Mark, A. E., Michael, A. J. & Bruce, K. G. Determining the optimal PDMS–PDMS bonding technique for microfluidic devices. *Journal of Micromechanics and Microengineering* **18**, 067001, (2008).

157 Isayev, A. I. & Palsule, S. *Encyclopedia of Polymer Blends, Volume 2: Processing*. (Wiley, 2011).

158 Kimble, E., Arkles, B. & Cameron, R. Symmetric Silicone Macromers. *Polymer Preprints* **50**, 859-860, (2009).

159 Pierce, E., Carmona, F. J. & Amirfazli, A. Understanding of sliding and contact angle results in tilted plate experiments. *Colloids and Surfaces A: Physicochemical and Engineering Aspects* **323**, 73-82, (2008).

160 Kovac, J. Modified Gaussian Model for Rubber Elasticity. *Macromolecules* **11**, 362-365, (1978).

161 Bauer, F., Decker, U., Naumov, S. & Riedel, C. Photoinitiator-free UV curing and matting of acrylate-based nanocomposite coatings: Part 3. *Progress in Organic Coatings* **77**, 1085-1094, (2014).

162 Scherzer, T. Photopolymerization of acrylates without photoinitiators with short-wavelength UV radiation: A study with real-time fourier transform infrared

spectroscopy. *Journal of Polymer Science Part A: Polymer Chemistry* **42**, 894-901, (2004).

163 Yoo, J. S., Kim, S. J. & Choi, J. S. Swelling Equilibria of Mixed Solvent/Poly(dimethylsiloxane) Systems. *Journal of Chemical & Engineering Data* **44**, 16-22, (1998).

164 Hedden, R. C., Wong, C. & Cohen, C. Effects of Phenyl Substituents on the Mechanical and Swelling Properties of Poly(dimethylsiloxane) Networks. *Macromolecules* **32**, 5154-5158, (1999).

165 Andrea Cattoni, Jing Chen, Dominique Decanini, Shi, J. & Haghiri-Gosnet, A.-M. in *Recent Advances in Nanofabrication Techniques and Applications* (2011).

166 Owen, M. J. & Dvornic, P. R. *Silicone Surface Science*. (Springer, 2012).

167 Lai, K. L., Leu, I. C. & Hon, M. H. Soft imprint lithography using swelling/deswelling characteristics of a polymer mold and a resist induced by a poor solvent. *Journal of Micromechanics and Microengineering* **19**, 037001, (2009).

168 Park, J. Y., Hendricks, N. R. & Carter, K. R. Solvent-Assisted Soft Nanoimprint Lithography for Structured Bilayer Heterojunction Organic Solar Cells. *Langmuir* **27**, 11251-11258, (2011).

169 Du, Y., Xue, Y. & Frisch, H. L. *Physical Properties of Polymers Handbook*. 2nd edn, 289-304 (Springer New York, 2007).

170 Abboud, J.-L. M. & Notari, R. Critical compilation of scales of solvent parameters. Part I. Pure, non-hydrogen bond donor solvents. *Pure and Applied Chemistry* **71**, 645-718, (1999).

171 Hansen, C. M. *Hansen Solubility Parameters: A User's Handbook, Second Edition*. (Taylor & Francis, 2012).

172 Barton, A. F. M. *CRC Handbook of Solubility Parameters and Other Cohesion Parameters, Second Edition*. (Taylor & Francis, 1991).

173 Barton, A. F. M. Solubility parameters. *Chemical Reviews* **75**, 731-753, (1975).

174 Nagy, J., Ferenczi-Gresz, S., Farkas, R. & Czuppon, A. Dipole moments of methylpolysiloxanes of various degrees of polymerization with monofunctional (M) and silanol (OH) and groups. *Acta chimica Hungarica: a Journal of the Hungarian Academy of Sciences* **Vol**, 351-355, (1976).

175 Green, D. & Perry, R. *Perry's Chemical Engineers' Handbook, Eighth Edition*. (McGraw-Hill Education, 2007).

176 Flory, P. J. Thermodynamics of High Polymer Solutions. *The Journal of Chemical Physics* **9**, 660-660, (1941).

177 Huggins, M. L. Solutions of Long Chain Compounds. *The Journal of Chemical Physics* **9**, 440-440, (1941).

178 Alger, M. S. M. *Polymer Science Dictionary*. (Chapman & Hall, 1997).

179 van Krevelen, D. W. & te Nijenhuis, K. *Properties of Polymers: Their Correlation with Chemical Structure; their Numerical Estimation and Prediction from Additive Group Contributions*. (Elsevier Science, 2009).

180 Sutton, C. & Mark, J. E. Dipole Moments of Dimethylsiloxane Oligomers and Poly(dimethylsiloxane). *The Journal of Chemical Physics* **54**, 5011-5014, (1971).

181 Russell, M. T., Pingree, L. S. C., Hersam, M. C. & Marks, T. J. Microscale Features and Surface Chemical Functionality Patterned by Electron Beam Lithography: A Novel Route to Poly(dimethylsiloxane) (PDMS) Stamp Fabrication. *Langmuir* **22**, 6712-6718, (2006).

182 Lindvig, T., Michelsen, M. L. & Kontogeorgis, G. M. A Flory–Huggins model based on the Hansen solubility parameters. *Fluid Phase Equilibria* **203**, 247-260, (2002).

Appendix A

A.1. Theoretical Modeling of Solubility for Monomethacryl-oxypropyl-terminated Polydimethylsiloxane in PDMS

In seeking to obtain an appropriate release agent molecule that would be soluble in a cross-linked silicone mould (see Chapter 4), available theoretical and empirical methods were approached for a means to predict solubility given a particular molecular structure of the release agent and a set of known material properties from the literature of the best known host polymer, namely Sylgard 184 polydimethylsiloxane (PDMS). Note that the roll-mounted mould employed in Chapter 4 was actually an h-PDMS/PDMS bi-layer silicone mould, however little solubility data is available in the literature for h-PDMS, so available data for PDMS was used and predictive models using PDMS as the host polymer were employed in lieu of similar data for h-PDMS. h-PDMS is very similar to PDMS in terms of its chemical structure, however, with the exception that h-PDMS monomers have a higher concentration of cross-link reaction sites relative to PDMS and are thus able to obtain a greater cross-link density after reaction with the methylhydrosilane-dimethylsiloxane copolymer cross-linker.[68] Thus the principal structure-property difference between h-PDMS and PDMS is the greater cross-link density of the former. Fortunately, knowledge of the cross-link density (or conversely, the average molar volume between cross-links, M_c) of the host polymer network is not required and does not influence the proceeding calculations to determine solvent-polymer solubility. Thus, for a general assessment of miscibility, available data for PDMS can provide useful results. Knowledge of M_c is required for the model used in the determination of the free energy change of mixing, however, thus care should be taken in approaching this calculation and the proceeding results should only be taken as a rough guide to indicate a miscible or immiscible system.

A.2. **A Brief Discussion on the Solubility Thermodynamics of Cross-linked Polymer – Solvent Systems**

A.1.1. Cohesive Energy Density and the Hildebrand Solubility Parameter

Solubility in cross-linked polymers generally is measured by the amount of solvent these materials absorb per unit mass (or volume), whereas swelling, or the swelling ratio, is the response of the material to the absorption of solvent. Many parameters have been proposed for the purpose of calculating solubilities, though perhaps the most popular is the cohesive energy density, c (J cm^{-3}), or the total energy of all attracting intermolecular interactions within a unit volume of material.[169,170] The cohesive energy density is the internal energy of the material divided by its volume, or

$$c = -E_{coh}/V \tag{A.1}$$

where E_{coh} is the molar internal energy or cohesive energy (J/mol) and V the molar volume (cm^3/mol). When two materials have similar cohesive energy density it is possible for them to be soluble in each other, since the cohesive energy must be overcome to separate solute molecules in order for solvent molecules to be introduced. The solubility parameter, or Hildebrand value for a solvent is given as

$$\delta = c^{1/2} = (-E_{coh}/V)^{1/2} \tag{A.2}$$

expressed in $MPa^{1/2}$ (also, $cal^{1/2}cm^{-3/2}$) and is a useful form for the cohesive energy density that is used to predict the mixing behaviour of, for example, a cross-linked polymer in the presence of a solvent.[169]

For two materials to be soluble in each other (or in the case of a polymer – solvent system, for the polymer to absorb the solvent) the free energy of mixing must be favorable. That is

$$\Delta G_m = \Delta H_m - T\Delta S_m \tag{A.3}$$

where $\Delta G_m < 0$. The Hildebrand-Scatchard equation relates the solubility parameters of a binary system of nonpolar liquids to the enthalpy change on mixing

$$\Delta H_m = V_m(\delta_1 - \delta_2)^2\varphi_1\varphi_2 \tag{A.4}$$

where V_m is the volume of the mixture, ∂ is the solubility parameter and φ is the volume fraction of each component in the mixture, respectively.[169] Therefore

$$\Delta H_m \propto (\delta_1 - \delta_2)^2 \tag{A.5}$$

and for a polymer – solvent system where δ_1 and δ_2 are the solubility parameters of the solvent and polymer network, respectively, ΔG_m is maximal (e.g. swelling is maximal) when $(\delta_1 - \delta_2)^2 = 0$ or when $\delta_1 = \delta_2$ such that the increase in the entropy of the system dominates.

A.1.2. Hansen Solubility Parameters

Hansen expanded on the work of Hildebrand to include other intermolecular interactions besides purely dispersive interactions.[171] Polar and hydrogen-bonding forces can be accounted for as part of the cohesive energy density as follows

$$c = -\frac{E_d + E_p + E_{hb}}{V} \quad \text{(A.6)}$$

where E_d is the molar dispersive component, E_p is the molar polar component and E_{hb} is the molar hydrogen-bonding component of the internal energy of a material. Thus

$$\delta^2 = \delta_d{}^2 + \delta_p{}^2 + \delta_{hb}{}^2 \quad \text{(A.7)}$$

where δ_d is the dispersive component, δ_p is the polar component and δ_h is the hydrogen-bonding component of the solubility parameter also with units of $MPa^{1/2}$ (or $cal^{1/2}cm^{-3/2}$). Hansen solubility parameters can be visually displayed using the three components as a 3-axis coordinate system where each material solubility parameter is represented as a vector quantity in Hansen space.[171] To determine miscibility in a polymer, for example, solvents must fall within what is called the "solubility sphere" centered around the Hansen space solubility parameter coordinates for the polymer.[171-173] The radius of this sphere, denoted as R_o is found through trial and error miscibility testing of solvents with known Hansen solubility parameters and is called the "interaction radius" of the polymer. The straight-line distance, R_a between the Hansen space coordinates of two materials was developed by Skaarup

$$R_a{}^2 = 4(\delta_{d2} - \delta_{d1})^2 + (\delta_{p2} - \delta_{p1})^2 + (\delta_{hb2} - \delta_{hb1})^2 \quad \text{(A.8)}$$

where δ_{d1}, δ_{p1}, δ_{hb1} and δ_{d2}, δ_{p2}, δ_{hb2} are the Hansen solubility parameter coordinates of the two materials, respectively.[171] The constant factor of four in front of the dispersive term has been the subject of controversy as it is not rigorously derived from the behaviour of

real systems, but it is used for practical purposes to illustrate the Hansen solubility parameters of different solvents as a sphere in Hansen space.[171] For a solvent to be miscible in a polymer, R_a should therefore be less than R_o.

Care was taken in formally explaining the various intermolecular interactions which contribute to the cohesive energy of materials and therefore to their respective solubility parameters because the solubility parameter is often only expressed as a scalar quantity in the literature and this can be misleading. Lee *et al*. cites the example of acetone and methylene chloride, which have identical solubility parameters (δ = 20.25 $MPa^{1/2}$) but entirely different swelling behaviour in PDMS.[150] This observation can be explained by the difference in the intermolecular force contributions to the overall solubility parameter. Methylene chloride swells PDMS much more than acetone because the former solvent is less polar (dipole moment, μ = 1.60 D for methylene chloride compared to 2.88 D for acetone), and more closely matches the polarity of PDMS (dipole moment per repeat unit, $\mu/n^{1/2}$= 0.6-0.7 D).[174] More formally, the partitioning of δ for a solvent that is most similar to the solute (or polymer, in our case) will result in the highest solubility. Partitioned values for δ_d, δ_p and δ_{hb} are available for common polymers (PDMS for example) and solvents in the literature.[171,175] This partitioning is useful in improving the predictive accuracy of polymer solution models.

A.1.3. Flory-Huggins Model for Polymer Solutions

Paul Flory and Maurice Huggins provided a simple, yet widely employed model to describe the thermodynamics of polymer solutions which better accounts for the large dissimilarity in the molecular sizes between the solvent and polymer network.[176,177] Their form of the Gibbs free energy change of mixing (Equation A.3) is as follows

$$\Delta G_m = RT[n_1 ln\phi_1 + n_2 ln\phi_2 + n_1\phi_2\chi_{12}] \quad (A.9)$$

Where R is the gas constant, T is the absolute temperature, n_1 and n_2 are the number of moles of solvent and polymer, respectively, while ϕ_1 and ϕ_2 are the volume fractions of the solvent and polymer, respectively. The first two terms on the right-hand side of Equation A.9 account for the favorable entropy of mixing and are negative quantities, while the third term is the enthalpy change, which can be positive, zero or negative but is generally small. The enthalpy change is equal to the total energy change across all polymer segment-solvent interactions in the mixture and contains the polymer-solvent interaction parameter *chi*, or $\chi_{12,}$ which is equal to the energy change per polymer segment-solvent interaction. χ_{12} has become known as the Flory-Huggins interaction parameter. For miscibility, the critical value for *chi* is approximately 0.5. For polymer-solvent systems where *chi* is less than 0.5, the solvent is soluble in the polymer. For systems where *chi* is greater than 0.5, the solvent is predicted to be insoluble in the polymer. χ_{12} is the only material-specific, experimentally determined parameter in the Flory-Huggins model and can be related to the Hildebrand solubility parameter for non-polar, non-hydrogen bonding mixtures as

$$\chi_{12} = \frac{V_1(\delta_1 - \delta_2)^2}{RT} \quad (A.10)$$

where V_1 is the molar volume of the solvent.[178] Thus, for regular solutions, the solubility parameters can be used to arrive at a quantitative thermodynamic description using the Flory-Huggins model. However, for solutions which contain polar or hydrogen bonding molecules, or for polymers and solvents which contain polar or hydrogen bonding

chemical groups, Equation A.10 yields poor results primarily for reasons given above. It would therefore be desirable to use Hansen partial solubility parameters (Equation A.7) as a means of accounting for polar and hydrogen bonding contributions to the interaction parameter χ_{12}.

A.1.4. Incorporation of Hansen Solubility Parameters into the Flory-Huggins Model

Hansen proposed the following empirical formula for estimating the Flory-Huggins interaction parameter in terms of dispersive, polar and hydrogen bonding partial solubility parameters

$$\chi_{12} = \alpha \frac{V_1}{RT}\left(\left(\delta_{1,d} - \delta_{2,d}\right)^2 + 0.25\left(\delta_{1,p} - \delta_{2,p}\right)^2 + 0.25\left(\delta_{1,hb} - \delta_{2,hb}\right)^2\right) \qquad \text{(A.11)}$$

where Hansen suggested $\alpha = 1$ and showed that this bridging expression performs well in predicting *chi* for real solutions, particularly for systems where polar and hydrogen contributions are relatively small compared to the dispersive component.[171] Lindvig *et al*. later proposed $\alpha = 0.6$ as a better fit to experimental and predicted solubility data.

Equation A.11 is particularly useful because it separately accounts for the different intermolecular interactions encountered in condensed matter instead of oversimplifying differences in the cohesive energy density into a single term. Large differences in any of the dispersive, polar or hydrogen bonding partial solubility parameters between the polymer and solvent will lead to a *chi* parameter larger than 0.5, while small or no difference in the partial solubility parameters will lead to a *chi* parameter of less than 0.5.

A.1.5. Group Contribution Methods for Calculating the Solubility Parameter and Partial Solubility Parameter Components

In order to model a particular polymer-solvent system using the Flory-Huggins equation by obtaining a value for χ_{12} using Equation A.11, there has to be some means of calculating the solubility parameter and the Hansen partial solubility parameter contributions. Experimental values for common polymers and solvents are available in the literature, however there are thousands of polymer-solvent combinations for which there is little or no experimental solubility data available. For the present work, in which solubility data for a set of reactive silicone oligomers in a silicone solid is needed to predict whether a given silicone solvent will dissolve in the solid, some experimental data is available, but it is not sufficient to predict miscibility purely from experimental data alone. Fortunately there are methods to estimate the partial and total solubility parameter of substances by summing group contributions to their cohesive energy.

One of the most fundamental assumptions in solubility theory is the additive nature of contributions to the solubility parameter. Each atom, segment or group comprising a molecule can be assigned a cohesive energy contribution $\boldsymbol{E}_{\mathbf{coh}}$ such that the square root of the sum of all contributions divided by the sum of the contributions to the molar volume of the molecule is defined as the solubility parameter

$$\delta = \left(\frac{-\sum \boldsymbol{E}_{coh}}{\sum \boldsymbol{V}}\right)^{1/2} \tag{A.12}$$

The underlying concept here is that there are thousands of different compounds of interest to various science and engineering disciplines, but a much smaller number of atoms, functional or structural groups, and bonding arrangements common to them all.

Such a group contribution or additive calculation method is necessarily an approximation, since atomic, functional or structural groups in a molecule will behave differently with different surroundings. Thus the validity of group contribution methods to obtain the solubility parameter is limited to situations where the behaviour of all groups with respect to neighboring groups or groups in neighboring molecules is similar. This is the case for purely dispersive chemical compounds, polymers and solvents or where polar and hydrogen bonding interactions are relatively small.[171] However, when these specific intermolecular interactions become significant, group contributions methods become inaccurate in predicting the solubility parameter and soluble systems. Van Krevelen has provided a collection of group contribution values from a variety of authors for the purpose of calculating the solubility parameter.[179]

Components of the solubility parameter can also be predicted from group contributions, using the Hoftyzer-van Krevelen formulae

$$\delta_d = \frac{\sum \mathbf{F_{di}}}{\mathbf{V}} \tag{A.13}$$

$$\delta_p = \frac{\sum \mathbf{F_{pi}}^2}{\mathbf{V}} \tag{A.14}$$

$$\delta_p = \frac{\sum \mathbf{E_{hi}}^2}{\mathbf{V}} \tag{A.15}$$

where $\mathbf{F_{di}}$, $\mathbf{F_{pi}}$, are the group contributions to the molar attraction constant for the dispersive and polar Hansen partial solubility parameters, while $\mathbf{E_{hi}}$ is the hydrogen bonding energy per structural group for the hydrogen bonding partial solubility parameter

and **V** is the molar volume of the molecule.[179] Tabulated data for group contributions to these molar attraction constants in $MJ^{1/2}\ m^{-3/2}$ and group contributions to the hydrogen bonding energy in $J\ mol^{-1}$ are also provided by van Krevelen.[179]

A.3. Calculation of the Partial and Total Solubility Parameters for Asymmetric Monomethacryloxypropyl-terminated Polydimethylsiloxane

To arrive at the most accurate value possible for the solubility parameter, experimental data was incorporated into calculations where possible and justifiable based on arguments of similarity.[171] For example, monomethacryloxypropyl-terminated poly-dimethylsiloxane (mPDMS) has a molecular weight range of 600 – 800, or a mean of 700 which is approximately a 5-mer dimethylsiloxane chain with n-butyl termination on one side and methacryloxypropyl termination on the other side (MW 687.35). Non-methacrylated dimethylsiloxane x-mer oligomers of $(CH_3)_3Si\text{-}[OSi(CH_3)_2]_xOSi(CH_3)_3$ were studied by Sutton.[180] This configuration is similar to the mPDMS structure such that if we divide the mPDMS molecule into two parts, the silicone chain and the terminal n-butyl and methacryloxypropyl groups, the partial polar solubility parameter of the former can be calculated from Sutton using the Hansen-Beerbower formula

$$\delta_p = \frac{37.4\mu}{V^{1/2}} \tag{A.16}$$

where μ is the dipole moment.[171] For the n-butyl and methacryloxypropyl terminal groups, group contribution values were used to calculate their contribution to the partial polar solubility parameter for the entire mPDMS molecule using Equation A.14 as previously discussed. Contributions from each segment of the molecule can then be

added together to arrive at an estimate of the partial polar solubility parameter. Note that this is only an approximation as the experimental dipole moment of mPDMS is not available. This approach takes advantage of the additive nature of the cohesive energy and the dispersive, polar and hydrogen bonding components thereof.

For the hydrogen bonding partial solubility parameter, Equation A.15 (Hoftyzer-van Krevelen method) was used for estimation from –O– and –COO– contributions. No values for >Si< are provided by van Krevelen,[179] however >Si< is not a polar group in itself and was thus assigned an $\mathbf{E}_{\mathbf{hi}}$ of zero, similar to >C<.

Since no values were available for >Si< for use with the Hoftyzer-van Krevelen formulae, the partial dispersive solubility parameter was calculated from Equation A.7 by subtracting the partial polar and hydrogen bonding solubility parameters from the total solubility parameter obtained by combining tabulated group contributions to $\mathbf{E}_{\mathbf{coh}}$ from Fedors and Hoftyzer-van Krevelen.[179] Table A.1 provides a summary table of relevant constants and material characteristics of the Chapter 4 solvent-polymer system, mPDMS-solid PDMS, for the proceeding calculations. Table A.2 provides all group contributions for the partial and total solubility parameters of mPDMS. Finally, Table A.3 provides the calculated total and Hansen partial solubility parameters for mPDMS, and corresponding literature values for PDMS.[175]

Table A.1 General parameters used in calculation of the solubility parameter for monomethacryloxypropyl-terminated polydimethylsiloxane (mPDMS) and the Gibbs free energy change of dissolution in PDMS.

	Symbol	Value	Units	Ref.	Remarks
Gas Constant	R	8.314	$J K^{-1} mol^{-1}$	--	--
Temperature (25 °C)	T	294.15	K	--	--
mPDMS Specific Gravity	ρ_1	0.96	$g cm^{-3}$	--	From product specification
mPDMS Molecular Weight	M	687.35	$g mol^{-1}$	--	5-mer approximation to the product specification molecular weight range (600 – 800)
Dipole Moment of mPDMS	μ	1.2	Daltons	[180]	For a non-reactive 5-mer, see text
PDMS Specific Gravity	ρ_2	1.03	$g cm^{-3}$	[181]	--
PDMS Mean Molar Mass per Cross-link	M_c	1957	$g mol^{-1}$	[149]	--

Table A.2 Group contributions to the cohesive energy, molar attraction constants and the hydrogen bonding energy for calculation of the total solubility parameter and Hansen partial solubility parameters for mPDMS. The number of each group is given where mPDMS is approximated as a 5-mer silicone oligomer. Tabulated values are given by Hoftyzer-van Krevelen except values marked by †, which are given by Fedors.[179]

Groups	No.	E_{coh} (J mol^{-1})	Σ E_{coh} (J mol^{-1})	F_{di} (J/cm^3)$^{1/2}$ mol^{-1}	F_{pi} (J/cm^3)$^{1/2}$ mol^{-1}	E_{hb} J mol^{-1}
>Si<	7	3390†	23730	--	--	--
-O-	6	6290	37740	100	400	3000
$-CH_3$	16	9640	154240	420	0	0
$-CH_2-$	6	4190	25140	270	0	0
=C<	1	4860	4860	70	0	0
-COO	1	3410	3410	390	390	7000
$=CH_2$	1	4310†	4310	400	0	0

Table A.3 Total and partial solubility parameters for mPDMS and PDMS. mPDMS values were calculated using available experimental data from the literature in combination with group contribution methods. Values for PDMS were obtained from the literature.[175] Units are in $MPa^{1/2}$.

	mPDMS	PDMS
δ	18.0	16.6
δ_d	16.9	15.9
δ_p	1.8	0.1
δ_{hb}	5.9	4.7

A.4. Calculation of the Flory-Huggins Interaction Parameter from Hansen Partial Solubility Parameters and Derivation of the Free Energy Change of Mixing mPDMS in PDMS

Plugging the calculated values from Table A.3 into Equation A.11, where we adopt Lindvig's correction to α such that $\alpha = 0.6$,[182] we obtain a value for the Flory-Huggins interaction parameter, χ_{12} of ~0.36 for the PDMS-mPDMS system. Below ~0.5, χ_{12} implies a miscible polymer-solvent system, whereas for χ_{12} greater than ~0.5 the model indicates the system is immiscible.

With a χ_{12} of ~0.36, the Flory-Huggins model (Equation A.9) can be solved to obtain the free energy change of mixing. The mixing of one mole of mPDMS in one mole of PDMS results in a free energy change $\Delta G = -2.71$ kJ which is typical for soluble polymer-solvent systems.

A.5. **Extension of Flory-Huggins Interaction Parameter Calculation to x-mer Monomethacryloxypropyl-terminated Polydimethylsiloxanes for Prediction of Solubility**

The previous calculations can be extended more generally to x-mer monomethacryl-oxypropyl terminated polydimethylsiloxanes where data, such as a molecular weight range and specific gravity of the substance, is available to obtain the molar volume. Data is available for oligomers with approximately 8 (MCR-M11), 63 (MCR-M17) and 131 (MCR-M22) repeat units in addition to the 5-mer mPDMS (MCR-M07, Gelest) used extensively in the present work. This calculation was very useful in the early development stages of the present work in order to predict in advance which release agent would be the most likely to dissolve in solid silicones. There was some controversy over whether the increasing molar volume or the increasing "likeness" of the molecule to PDMS would dominate the solubility. At some point the release agent molecule would become so large that the Flory-Huggins *chi* parameter would predict insolubility. On the other hand, as the chain lengthens, the terminal methacryloxypropyl group becomes less dominant over the intermolecular interactions with the cross-linked PDMS network as the network becomes more likely to interact with the main silicone backbone. Thus longer x-mer mPDMS chains become more "like" PDMS, and potentially more soluble. This would be reflected in the Hansen partial solubility parameters being more similar to solid PDMS, and would lower the *chi* parameter derived from Equation A.11.

Calculations for *chi* from available data quickly showed, however, that the molar volume of the solvent, V_1 of Equation A.11, dominates the behaviour of *chi* for x-mer chain lengths of 8 or greater as can be observed from Figure A.1 and the plotted free energy change of mixing for 1 mole of solvent in 1 mole of polymer in Figure A.2. At first glance, the smallest possible mPDMS molecule appears to have the best solubility in

solid PDMS according to the Flory-Huggins model using Hansen partial solubility parameters to obtain *chi*. However, a further exploration of small x-mers, for x ranging from 1 – 8 would be worthwhile if molar volumes can be obtained for these reactive silicone oligomers. This range may contain a *chi* minimum due to similarity arguments as discussed.

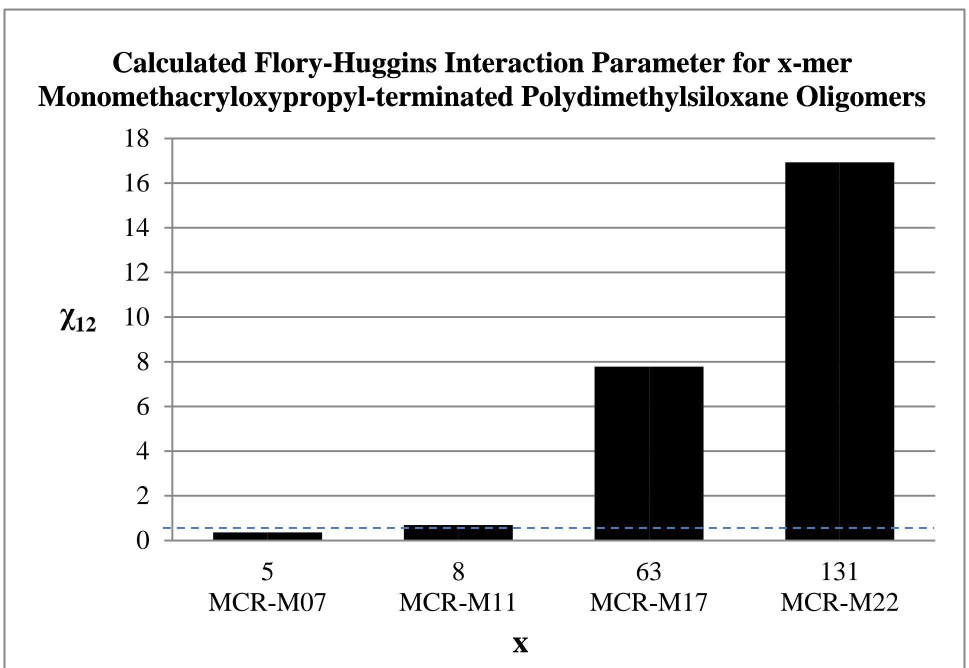

Figure A.1 Bar chart of calculated Flory-Huggins interaction parameter (dimensionless) for various x-mers of monomethacryloxypropyl-terminated polydimethylsiloxane. The dotted line indicates an interaction parameter (χ_{12}) of 0.5, which demarcates a soluble from an insoluble polymer-solvent system.

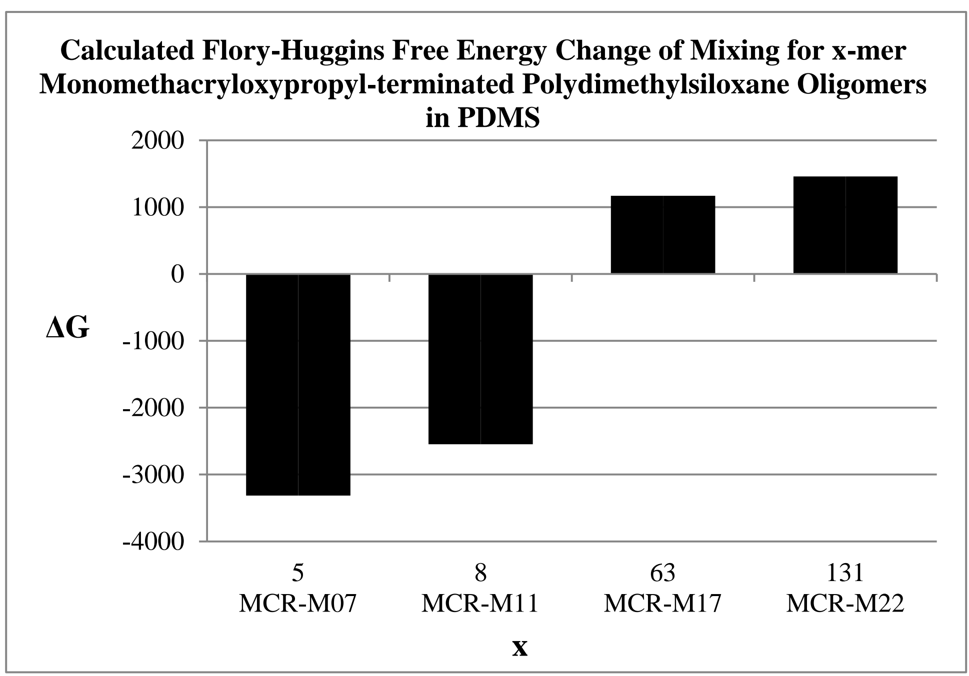

Figure A.2 Bar chart of calculated Flory-Huggins free energy change of mixing in Joules for x-mers of monomethacryloxypropyl-terminated polydimethylsiloxane in PDMS.

A *chi* minimum would also have to be considered against the diffusion kinetics of the mPDMS x-mer, as higher values for x and higher molecular weight chains will generally take longer to dissolve into the polymer network. More importantly, migration rates to the surface of the PDMS solid would tend to decline with increasing molecular weight, which could negatively impact transfer of mPDMS from a given silicone mould to other contacting surfaces such as resin moulds, particularly with repeated usage. This is especially important when considering that the preferred means of exposing mPDMS for absorption by the silicone mould, as discussed in Chapter 4, is to pool the mPDMS exclusively on the h-PDMS patterned face of the h-PDMS/PDMS bi-layer silicone mould. h-PDMS is known to have a much higher cross-link density than PDMS, or conversely a much lower average molar mass between cross-links.[68,149] Therefore the size in terms of the molar mass of the mPDMS molecule must also be small enough to diffuse and migrate within h-PDMS at reasonable rates, along with the requirement of solubility implied by *chi*.

MCR-M07 was thus selected for use especially in Chapter 4 of the present work from these solubility calculations, as it had the smallest *chi* parameter of all commercially available reactive silicones with simple linear chemistry. Moreover, it was also the smallest (lowest molecular weight) version of mPDMS and would thus benefit from having fast migration rates to the surface of silicone moulds.

Appendix B

B. Detailed Process Steps & Parameters

Table B.1 Process steps used for UV roll-to-roll nanoimprinting of resin moulds in Chapter 3.

	Material / Processing Parameters
Mould	2nd generation nickel shim (nickel-on-nickel electroforming)
Resin	YNIL-R2-2 (Young Chang Chemical)
Web	Lexan 8010 Polycarbonate Reel (100 m length, 200 mm width, 125 µm thickness)
Dispense Parameters	10 KHz Dispense Head Frequency, 30 pL droplet volume, 65 mm width
Resin Spreading Pressure	400 kPa via 2 Rubber Pressure Rollers
UV Exposure	Mercury-Arc Lamp (405 nm h-line peak) 80 W cm^{-1} peak output
Separation	Unguided peel separation by rewind tension applied across deflection roller

Table B.2 Process parameters for batch mode thermal NIL using segmented UV roll-to-roll nanoimprinted resin moulds in Chapter 3.

	Material / Processing Parameters
Mould	YNIL-R2-2 / Polycarbonate Bilayer Resin Mould (5cm x 5cm square cut-out)
Resist	200 nm thick PMMA film (Mn 25,000)
Substrate	4” DSP silicon wafer
Temperature	150° C
Pressure	40 bars
Dwell Time	5 minutes

Table B.3 h-PDMS Formulation used in h-PDMS/PDMS bi-layer silicone mould fabrication for Chapter 4.

	VDT-731 (g)	Platinum divinyl-tetramethyl-disiloxane catalyst (uL)	2,4,6,8 tetra methyl-tetravinyl cyclotetra-siloxane inhibitor (g)	HMS-301 (g)	Young's Modulus (MPa)
Modified h-PDMS Formulation	3.7 (77.4% wt.)	50 (~1% wt.)	0.05 (1% wt.)	1 (20.6% wt.)	~6 Mpa STDev ±0.4

Table B.4 Process steps used for fabrication of h-PDMS/PDMS bi-layer silicone mould and exposure to mPDMS for Chapter 4.

	Material / Processing Parameters
Mould	Silicon master moulds with vapour deposited 1H,1H,2H,2H, Perfluorodecyltricholorosilane anti-stick coating as provided in Table 4.1.
Casting h-PDMS	Spincoat h-PDMS on Si master at 6000 RPM for 30 seconds. Coating thickness is approx. 13.5 µm. Allow h-PDMS to gel at room temperature for 2 hours
Application of Sylgard 184 PDMS	Mix 10:1 Prepolymer-to-Crosslinker, Sylgard 184, vacuum degas, and pour onto h-PDMS coated Si master
Bake	Bake casted h-PDMS/PDMS at 60° C overnight
Peel & Trim	Cut out and trim h-PDMS/PDMS mould using sharp X-ACTO knife
mPDMS Exposure	Immerse patterned face only for ~5 – 15 minutes (15 minutes was used for the work presented herein)
Removal of Excess mPDMS	Removal of excess mPDMS was accomplished by use of a filtered N_2 gas gun

Table B.5 Process steps used for UV roll-to-roll nanoimprinting of resin moulds using mPDMS exposed h-PDMS/PDMS roll-mounted moulds in Chapter 4.

	Material / Processing Parameters
Mould	2nd generation h-PDMS/PDMS mould after 15 min patterned-face exposure to mPDMS
Resin	59% 1,6-hexanediol diacrylate (monomer) 39% neopentyl glycol diacrylate (cross-linker) 2% Diphenyl(2,4,6 trimethylbenzoyl)phosphine oxide (photoinitiator)
Web	Lexan 8010 Polycarbonate Reel (100 m length, 300 mm width, 125 μm thickness)
Dispense Parameters	10 KHz dispense head frequency, 30 pL droplet volume, 65 mm width
Resin Spreading Pressure	400 kPa via 2 rubber pressure rollers
UV Exposure	395 nm UV LED array 8 W cm^{-2}
Separation	Unguided peel separation by rewind tension applied across deflection roller

List of Publications

Dumond, J. J. & Low, H. Y. Recent developments and design challenges in continuous roller micro- and nanoimprinting. *Journal of Vacuum Science & Technology B: Microelectronics and Nanometer Structures* **30**, 010801-010828, doi:10.1116/1.3661355 (2012).

Dumond, J. J., Mahabadi, K.A., Yew, S.Y., Tan, C., Fuh, Y.H. Lee, H.P. & Low, H.Y. High resolution UV roll-to-roll nanoimprinting of resin moulds and subsequent replication via thermal nanoimprint lithography. *Nanotechnology* **23**, 485310 (2012).

Dumond, J. J., Fuh, Y.H., Lee, H.P. & Low, H.Y. Surface Delivery of Reactive Release Agents onto UV Roll-to-Roll Nanoimprinted Resin Moulds. *Manuscript in Preparation.*